2018

Redox Reactions at Oil-Water Interface by Particle Collision Electroanalysis

Dilip K. Paul

Redox Reactions at Oil-Water Interface by Particle Collision Electroanalysis

A dissertation submitted in partial fulfillment of the requirements for the degree of Doctor of Philosophy at Virginia Commonwealth University

by

Dilip Kumar Paul

Advisor: Julio C. Alvarez

Associate Professor, Department of Chemistry

Virginia Commonwealth University

Richmond, Virginia, 23284

United States

Acknowledgements

During my PhD journey, I received exceptional support, help and advice from numerous people. First of all, I would like to thank my parents, without their blessed and support it would have been difficult to complete my degree. Words will be never enough to express just how thankful I am to my beloved wife, Lamia Nahar. Without her continuous support, I could not finish this journey. She makes my life colorful in every direction. I would also like to give thanks to my family members and special thanks to my older sister and her husband.

I would like to express my deepest gratitude to my advisor, Dr. Julio C. Alvarez for giving me the opportunity to pursue my PhD under his supervision. His support helped me to be successful in numerous ways. His valuable advice, encouragement and patient helped me to accomplish my academic goals. I am also grateful to the members of my committee, Dr. Maryanne M. Collinson, Dr. Matthew C. T. Hartman and Dr. Joseph Reiner.

I would like to thank God for providing me this honor to achieve my goals in my life. I truly believe God was always there to show me the right path not only during last five years, but in every step in my life.

TABLE OF CONTENTS

LIST OF FIGURES

LIST OF SCHEMES

LIST OF TABLES

Abstract

Redox Reactions at Oil-Water Interface by Particle Collision Electroanalysis

by

Dilip Kumar Paul

A dissertation submitted in partial fulfillment of the requirements for the degree of Doctor of Philosophy at Virginia Commonwealth University

Advisor: Julio C. Alvarez

Associate Professor, Department of Chemistry

Particle Collision Electrochemistry (PCE) has gained considerable attention in heterogeneous catalysis, petroleum chemistry and pharmaceutical fields. The PCE refers to a phenomenon in which a particle strikes on an inert electrode surface as a consequence of its Brownian motion and produces a spike of current for the direct oxidation/reduction of the individual particle. This method allows us characterization of individual particles and in-situ study of electrochemical reactions coupled to the particle.

Herein, emulsion droplets were studied by PCE where toluene droplets contained hydrophobic tetrachloro-1,4-benzoquinone (Q). This was investigated as a model system to study the molecular effects that arise due to hydrogen bonding reagents (oleic acid, acetic acid) inside and outside of the droplets. The emulsions were prepared by sonicating toluene-quinone solution with the water phase containing an ionic liquid to

provide conductivity to the droplet. Each droplet produced a current spike while colliding with the electrode surface that was held at a potential to reduce tetrachoro-1,4-benzoquinone. In bulk acetonitrile and toluene, tetrachoro-1,4-benzoquinone undergoes a two electron reduction process to form the tetrachloro phenolate di-anion (Q^{2-}). It was shown that the hydrogen bonding affinity of Q^{2-} for acetic acid (pKa = 4.8) was higher than for oleic acid (pKa = 9.9) for both bulk systems (as acetic acid is stronger hydrogen bonding donor than oleic acid). However, the reversed trend was observed in emulsified toluene droplets when studied by PCE. This was attributed to the preferential partition of the carboxylic acids between the two phases in the emulsion. Oleic acid stays inside the droplets due its hydrophobic nature and hydrogen bonding with Q^{2-} takes place inside the droplet. In contrast, solvation of acetic acid by the surrounding water, causes the hydrogen bonding with Q^{2-} to occur significantly less inside the droplet.

Another redox system studied by PCE was hydrophobic ferrocene (Fc) trapped in the toluene droplet to determine the effect of surfactant on the particle size. The diameter determined electrochemically was compared with Dynamic Light Scattering (DSL) measurements. The presence of nonionic surfactant (triton X-100) was observed to affect the droplet's size easily monitored by PCE. The mediated oxidation of cysteine by the oxidized Fc inside the droplet was investigated at different concentrations of cysteine.

Chapter 1

Introduction

1.1 "In Water" and "On Water" Organic Reaction

Generally, organic reactions have been performed in polar or nonpolar organic solvents. For many years, it was believed that conventional solvents had no effect on the rate of the reactions. For example, the rate of dimerization of cyclopentadiene only differs by a factor of maximally four in different organic solvents.[1] But Breslow and coworkers in 1980 first reported significant rate acceleration of Diels-Alder reactions[2] using water as a reaction medium (Scheme 1.1). These reactions are called "in water" reactions because the reactants are well solubilized in water, forming a homogeneous phase. Later on, substantial rate enhancements were also observed for other types of organic reactions such as Aldol condensations[3] and Claisen rearrangements[4] when carried out in water. The rate accelerations were ascribed to the hydrophobic effect that aggregates the organic reactants to minimize the contact area with water molecules [5,6]

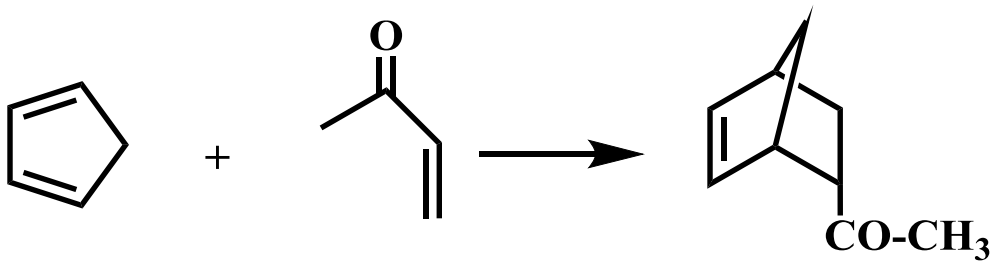

Cyclopentadiene Butenone Endo product

Scheme 1.1 Diels –Alder reactions of cyclopentadiene with butanone.

Previously Sharpless[7] et. al. observed significant rate enhancements for a variety of reactions where water-insoluble reactants were stirred vigorously in water for

short period of times. These reactions were named “on water” reactions and because reactants are water-insoluble, a heterogeneous interface is always present. An organic-water interface is formed in an emulsion (liquid-liquid) or a suspension (solid-liquid) during mixing the reactants in these reactions. In such cases, the apparent reaction rate was enhanced significantly. For instance, the cycloaddition of quadricyclane to dimethyl azodicarboxylate (Scheme 1.2 and Table 1.1)[7] was completed in a few minutes when these liquid reactants were stirred intensely on water. In contrast, it took two days to complete the reaction when performing in neat (solvent free) condition. This implies that other factors were involved besides higher concentration of the reactants.

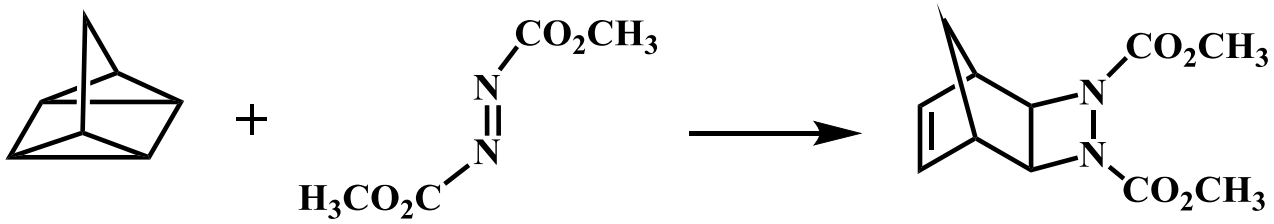

Quadricyclane Dimethyl azodicarboxylate 1,2-diazetidines

Scheme 1.2 Reaction of quadricyclane with dimethyl azodicarboxylate.

To date, several labs have reported on the rate-enhancing effect of water as a solvent medium for various organic reactions with insoluble reactants.[8-18] The investigations suggest that several factors account for the observed rate accelerations.[7,11] First, heterogeneity is important in the reaction mixture so that an interface is developed between two phases. Second, the interface must be with an aqueous phase because emulsions of reactants prepared in perfluorohexane showed only slightly higher rate than the neat reaction (Table 1.1).Third, there was a solvent

isotope effect on the reaction rate when the reaction was carried out in D_2O instead of H_2O. Finally, the intrinsic charge that develops at the interface needs to be considered.

Table 1.1 Reaction of quadricyclane with dimethyl azodicarboxylate in various solvents.

Solvent	**Concentration (M)**	**Time to completion**
Toluene	2	> 120 h
EtOAC	2	> 120 h
CH_3CN	2	84 h
CH_2Cl_2	2	72 h
DMSO	2	36 h
MeOH	2	18 h
neat	4.53	48 h
On D_2O	4.53	45 min
On C_6F_{14}	4.53	36 min
On H_2O	4.53	10 min

Although extensive theoretical studies have been performed regarding “on water” reactions, still a variety of explanations are associated with experimental results of these reactions.[19-21] Jung and Marcus[19] have proposed that free (dangling) OH groups of interfacial water molecules forming H-bonding with the transition state (TS) of the reaction. This phenomenon stabilizes TS by lowering the activation barrier. Marcus’s

assumption was matched with the experimental results where dangling OH bonds observed at macroscopic oil-water interface.[22] Conversely, Jorgensen's theoretical[21] work contradicted with Marcus's Model and reported certain organic reactions are accelerated less on the surface of the water than in bulk water. Experimental kinetic studies by Kumar[14] as well as from Huck[12] and Zhen[16] also agreed with Marcus' assumption. However, none of these researchers considered the isotopic effects that were observed in Sharpless' experiments. Beattie[11] and McErlean[13] have provided convincing evidence for the strong D_2O /H_2O isotopic effects in "on-water" reactions. They proposed an acid-base catalysis that involves a proton transfer (PT) across the organic-water interface. Butler and Coyne[17] also observed PT at the organic–water interface depending on the pK_a of the reactants. In addition, H-bonding formed between the dangling OH groups and H-bond acceptor species on the reactants, even though non-reacting competitors for H-bond acceptors were present in the organic phase. Additionally, the water solubility of the organic reactants and the presence of organic cosolvents also have an impact on "on-water" reactions, as indicated by Zou and coworkers[15], who emphasized that a degree of water solubility of the reactants is crucial to achieve the "on water" effect, unless small amounts of organic solvents are added while maintaining the heterogeneity.

Despite, all the factors mentioned, the "on-water" effect is highly susceptible to hydrogen bonding and/or proton transfer(s). This dissertation describes the study of electrochemical reduction of quinones inside droplets of toluene dispersed in water, as quinone electrochemistry is highly sensitive to those factors.

1.2 Quinone

Quinones are one of the important and prototypical examples of organic redox couples. They play a crucial role in biological electron transport processes and have also wide applications in industry and chemical synthesis.[23-25] All of which have led to detailed investigations of how PT and hydrogen bonding affect the thermodynamic and kinetics of these electrochemical quinone-hydroquinone systems.

1.2.1 Electrochemical Reactions of Quinones

It is well known that in an aqueous buffer solution, quinones (Q) undergo reduction accepting two electrons (e^-) and two protons (H^+) to form the hydroquinone (QH_2) as the final product in a single voltammetric peak at a specific potential (Scheme1.3 a).[26] The reduction of quinones in aqueous unbuffered solution leads to a slightly different mechanism[26] because in the absence of buffer, the effective pH near the electrode surface changes as H^+ are being consumed locally during reduction. Consequentially, the reduction potential shifts to more negative values as the local pH increases. For the unbuffered conditions when the concentration of H^+ is less than the concentration of the quinone, then the reduction leads to the nonprotonated dianion (Q^{2-}) that binds water molecules via hydrogen (H) bonding (Scheme 1.3 b), however the reduction still occurs in a single voltammetric peak at a particular potential. On the other hand, in nonaqueous aprotic media, quinones show two cathodic peaks comprising the two single-electron reductions and form the radical monoanion ($Q^{\bullet-}$) and dianion (Q^{2-}) (Scheme 1.3 c).[27] In this case, the two reduction (cathodic) peaks are generally separated by about 0.7 V. Gupta and Linschitz [27] reported that the ratio of the cathodic peak current to the anodic peak current for the first redox process is close to

unity for different quinones (e.g. tetrachloro benzoquinone, 2,5-dichloro benzoquinone, 2,5-dimethoxy benzoquinone). But the height of the second cathodic peak is less than the first one for all studied quinones, which was explained by the complexation a quinone molecule and its dianion (equation 1.1)

$$Q + Q^{2-} = [QQ]^{2-} \ldots\ldots\ldots\ldots\ldots\ldots (1.1)$$

(a) Buffered H_2O or unbuffered with $[H^+] > [Q]$

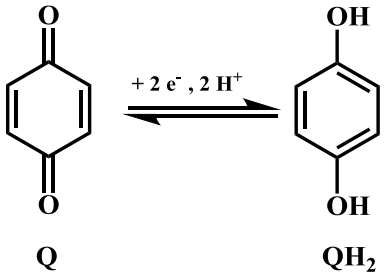

(b) Unbuffered H_2O with $[H^+] < [Q]$

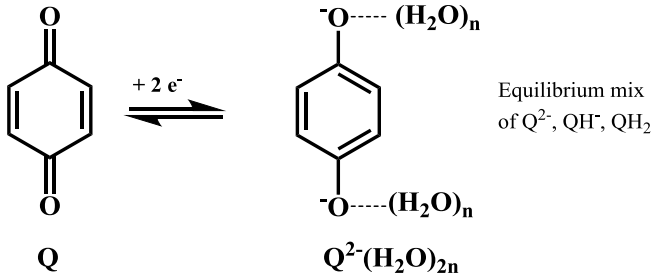

(c) Aprotic Solvents

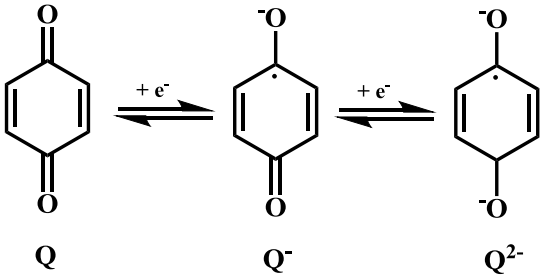

Scheme 1.3 Quinone redox reactions.

1.2.2 Factors Affecting the Reduction of Quinone

The redox potential of the quinones depends on the stability of the products of their reduction reactions. The stabilization is determined by several factors such as polarity of the solvent, nature of the supporting electrolyte, inter or intramolecular H-bonding, the presence of acidic or basic additives, ion paring and protonation equilibrium.[27-29] Generally the cation of the supporting electrolyte forms an ion pair with $Q^{\bullet-}$ and Q^{2-} while acidic additives form hydrogen bond complexes or transfer protons to the $Q^{\bullet-}$ and Q^{2-} , all of which may stabilize those species. H-bonding or protonation depends on the pK_a of acid additives and basicity of reduced forms $Q^{\bullet-}$ and Q^{2-} . The effect of hydrogen-bonding interactions can be clearly differentiated from protonation by consideration of appropriate pK_a values and characteristics of cyclic voltammogram (CV) of quinones.[27] Typically, H-bonding is revealed by continuous shifts in potential with no change in peak height, reversibility and absence of new peaks in the CV. However, increasing first peak's height at the expense of the second can be an indication of a disproportionation mechanism assisted by H-bonding.[27] Weber[30] reported four important criteria to study hydrogen bond systems by electrochemical techniques. First, either the donor and/or acceptor must be electroactive. Second, their oxidized and reduced forms should be chemically long-lived with electron transfer kinetics reasonably fast during the experimental time scale. Third, the redox couple must be able to significantly influence the binding between the donor and the acceptor. In many cases, the effects of hydrogen bonding can be distinguished from those of proton-transfer.

The reduction mechanism of quinones can include a nine-member square scheme as shown in Scheme 1.4, with all the species that can be bound by hydrogen

bonding. This describes the series of electron transfers (horizontal arrow) and hydrogen-bonding interactions (vertically arrow) between a quinone (Q) species and the hydrogen-donor (D). In Scheme 1.4, $E_{obs}^{(Q/\ Q^{\bullet -})}$ and $E_{obs}^{(QD/QD^{\bullet -})}$ are the observed half-wave ($E_{1/2}$) or peak potentials of the Q/Q•- and the hydrogen-bonded QD/QD•- redox couple, respectively.

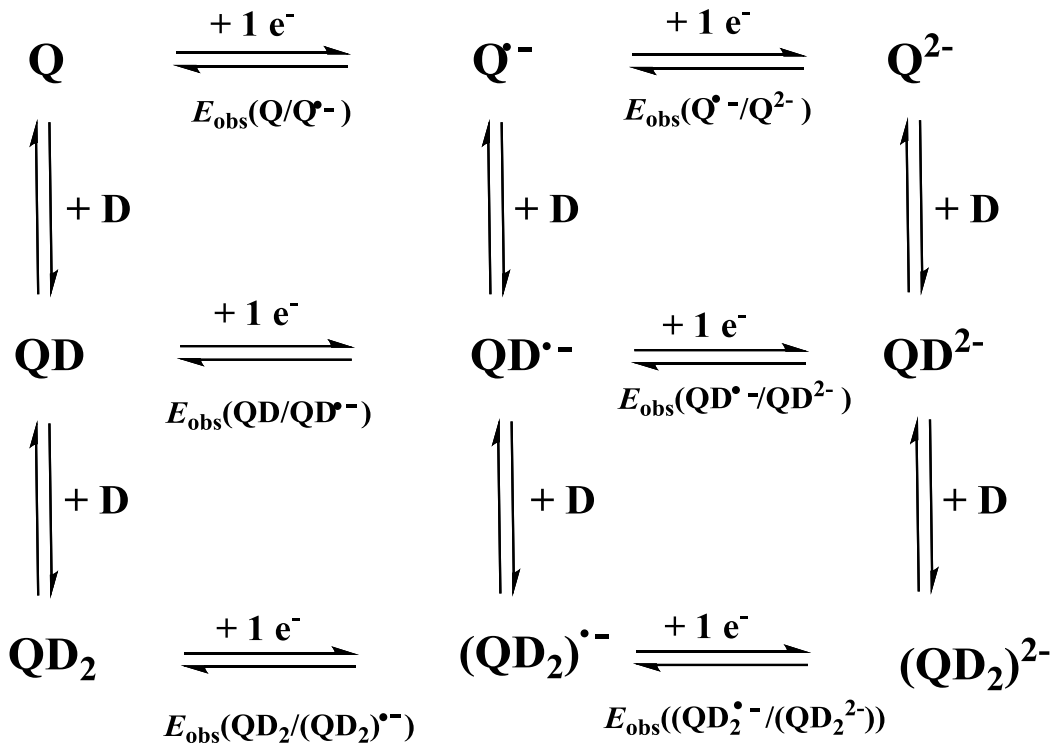

Scheme 1.4 Series of electron transfers and hydrogen-bonding interactions with quinone.

The 3 x 3 diagram for PT is analogous to Scheme 1.4, but D is replaced by a acid that can transfer a proton to the quinone species. In this work the main focus will be on hydrogen bonding and PT effects on the electrochemistry of quinones. An overview of previous literature regarding these factors are discussed in section 1.2.3.

1.2.3 Binding Studies of Quinones to Hydrogen Donor Additives

Hydrogen-bonding and proton transfer are the fundamental factors for controlling the potentials and reaction paths in the reduction of quinones. The neutral quinone exhibits electron acceptor properties and the reduced dianions have strong affinity to hydrogen bonding donor to form complexes.

Linsehitz[27] systematically studied the above two factors and their corresponding effect on quinone reductions. This investigation surveyed a series of quinones of increasing basicity (chloranil to duroquinone, Scheme 1.5) with a broad range of reduction potentials, and examined the effect of different hydrogen donor additives on their electrochemistry in polar aprotic solvents.

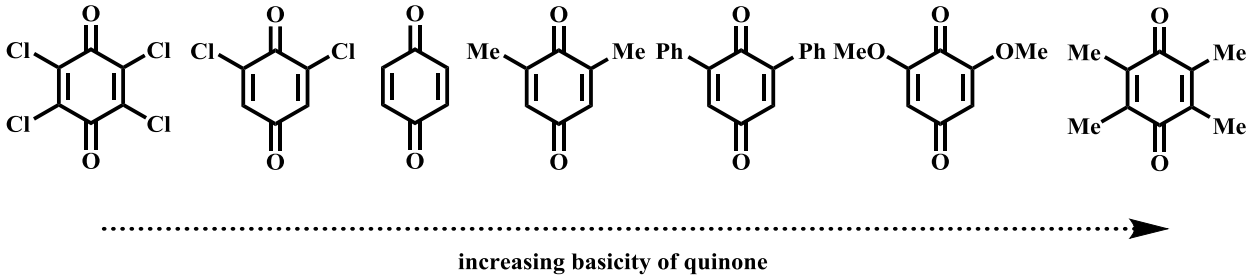

Scheme 1.5 Quinones examined by Linschitz.[27]

Weak hydrogen bonding agents (HBAs) (such as ethanol, 2-propanol and tert-butyl alcohol) had marginal effect on the first electron transfer but had a substantial impact on the second electron transfer. In such cases, both cathodic peaks shifted positively with no loss of reversibility but the second peak shifted in greater extent and the relative heights of the waves remained constant. Determination of K_{eq} for this association was not straight forward as multiple molecules of alcohol can associate with

the quinones and this number varies depending on the basicity of the quinone and size of the alcohol molecule. However, the largest effects are observed for the most basic quinone, duroquinone.

When stronger HBAs, such as trifluoroethanol, were used with the same quinones, different types of effects are observed in the CVs. An electron-deficient quinone like dichlorobezoquionone, showed a shift in $E_{1/2}$ corresponding to hydrogen-bonding mainly with Q^{2-}. On the other hand, the more basic quinone (duroquinone) displayed irreversibility in CV trace which was attributed to disproportionation mechanism of the radical monoanion ($Q^{\bullet-}$) facilitated due to strong H-bonding of Q^{2-}. While stronger H-bond donors like hexafluoroisopropanol were used, different mechanisms were involved based on quinone basicity. Finally, strongly acidic donors like trifluoroacetic acid showed unambiguous protonation effects on different quinones. In a closely related study, this work was extended to even more basic quinones, and similar effects were observed. [31]

In 2003, Gonzalez's[32] group also reported the electrochemical reduction of several quinones in the presence of different alcohols. They observed that H-bonding between quinone dianion and the different alcohols governed by quinone basicity, steric effects, and by the number of α-hydrogen atoms present in the quinone nucleus.

Several studies done by Smith[26] and Alligrant[33-34] show that the voltammetry of quinones and hydroquinone is very sensitive to the type of proton acceptors available in solution. Those studies highlight the importance of hydrogen bonding interactions between hydroquinone/quinone and the solvent molecules (in the case of water) and basic species present in the solution. Smith's work mainly demonstrated the importance

of studying quinone's electrochemical behavior in buffered and unbuffered conditions, that produced a comprehensive view of the roles of proton transfer and H-bonding on the electrochemical mechanism of these redox molecules.[26] Similar investigation was carried out by Bunjo and coworker[35] where the reduction of 9,10-anthraquinone in presence of strong acid (Benzoic acid) showed the increase of first cathodic peak height at the expense of second cathodic peak without keeping the reversibility. This attributed to the well-known sequence, fast protonation of $Q^{\bullet-}$, and reduction of the more easily reduced $HQ^{\bullet}$ radical at the same potential. Peover and Ansnagar studied the redox behavior of different quinone derivatives and reported the similar reduction mechanism in the presence of strong acids such as 2,4,6-trichlorophenol and benzoic acid. [36,37]

In chapter 2 of this dissertation below, our focus is to study the electrochemical reduction of tetrachlorobezoquinone in toluene-water emulsion in the presence of hydrogen donor additives such as oleic acid and acetic acid. This could help to understand the role of water on the rate enhancements observed in "on water" reactions. In chapter 3, redox mediation reactions were monitored across the toluene-water interface.

1.3 Mediation or Catalytic Reactions

Electrochemical detection of biological species is complicated by direct oxidation on conventional electrodes e.g. glassy carbon and gold electrodes. Therefore, alternative approaches have been investigated in order to decrease the overpotentials for oxidation as well as minimize the surface fouling effect. One method is the indirect or mediated oxidation of these species by metal complexes in solution.

Stanbury[38-39] studied the oxidation of thiols like cysteine and thioglycolic acid (TGA) by oxidant metal ions. The metal complexes used were $[Fe(bpy)_2(CN)_2]^+$ and $[Fe(bpy)(CN)_4]^-$ to oxidize cysteine, and $[IrCl_6]^{2-}$ to oxidize TGA. Ferrocene and its derivatives were widely applied as catalysts to mediate electron transfer with species that show slow electron transfer, such as ascorbic acid,[40] hydrogen peroxide,[41] and sulfide[42] species. Different amines[43] were also investigated by the electrochemically generated ferrocenium ions as the catalyst (Scheme 1.6).[43]

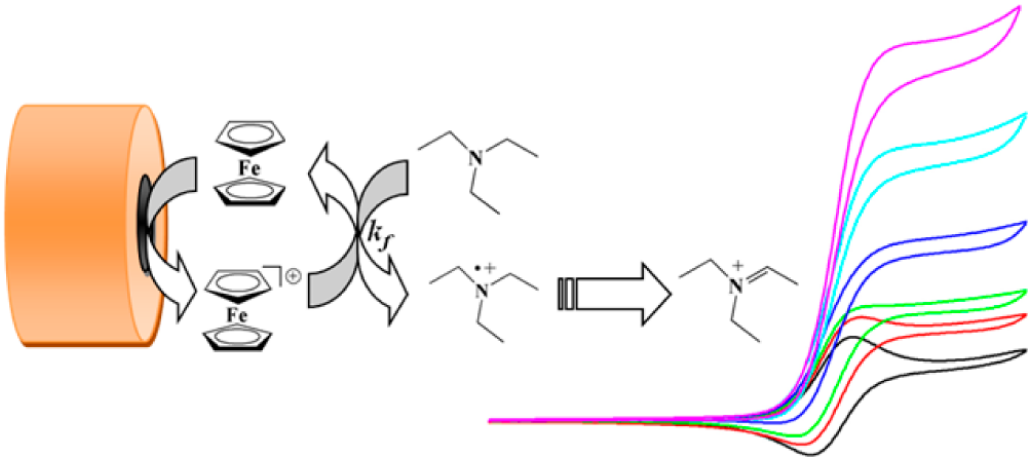

Scheme 1.6 Catalytic oxidation of amine by electrochemically generated ferrocenium ions. (Adapted from reference 43)

In this dissertation, we investigated redox mediation in toluene-water emulsions for L-cysteine oxidation with ferrocenium ion as mediator using the particle collision electrochemistry.

1.4 Emulsions

An emulsion is a metastable system consisting of two immiscible liquids in which droplets of one liquid is dispersed in the other, also called continuous phase. Milk is a common example of emulsion where fat globules are dispersed in water. The size and

nature of the boundary between the dispersed and a continuous phase, that the "interface", plays an important role in the stability of the emulsion.

1.4.1 Classification of Emulsions

Emulsions are classified based on the nature of the dispersed phase[44]as oil-in-water or water-in-oil (Scheme 1.7)

Oil-in-water emulsions (O/W): These are emulsions in which oil is present as the dispersed phase and water as the continuous phase. For example mayonnaise, vinaigrette and vanishing cream etc.

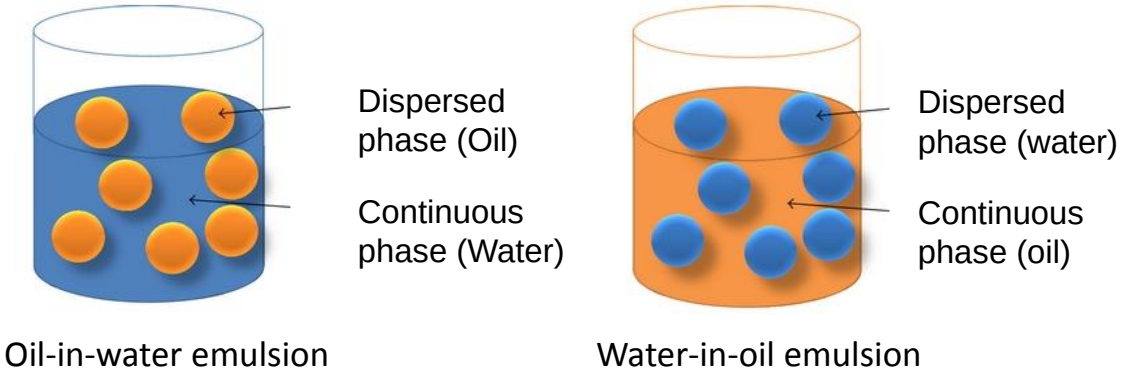

Scheme 1.7 Classification of emulsion.

Water-in-oil emulsion (W/O): These are emulsions in which water forms the dispersed phase, and the oil acts as the dispersion medium, for instance butter and cold cream.

Based on the size of the liquid droplets, emulsions can be categorized as:[44]

i) Macroemulsions: These are kinetically stabilized emulsions with a size range of droplets from 0.1 μm to 5 μm, which tend to be white or milky in color because the

droplet size is larger than the wavelength of light. Consequently, macroemulsions scatter light effectively.

ii) **Nanoemulsions**: These usually have a size range between 20-100 nm and they are kinetically stable emulsions. These are transparent.

iii) **Microemulsions**: These are thermodynamically stable emulsions that have size range between 5-50 nm and because the droplet size is less than the wavelength of visible light, they are transparent.

1.4.2 Mechanism of Emulsion Destabilization

From the thermodynamic point of view, emulsions are unstable because they have a natural tendency to separate into their liquid/liquid phases in order to reduce the interfacial area and minimize interfacial energy. Therefore, several complicated breakdown processes (Scheme 1.8) may happen during storage of emulsions like sedimentation or creaming, flocculation, Ostwald ripening, coalescence, and phase inversion.[44]

Sedimentation or Creaming

Sedimentation is the process where droplets are settled at the bottom because of the density difference between the droplet and the continuous phase. When the density of dispersed phase is higher than that of the medium, sedimentation occurs. Whereas in creaming process, droplets are settled at the top because the density of dispersed phase is lower than that of the medium.

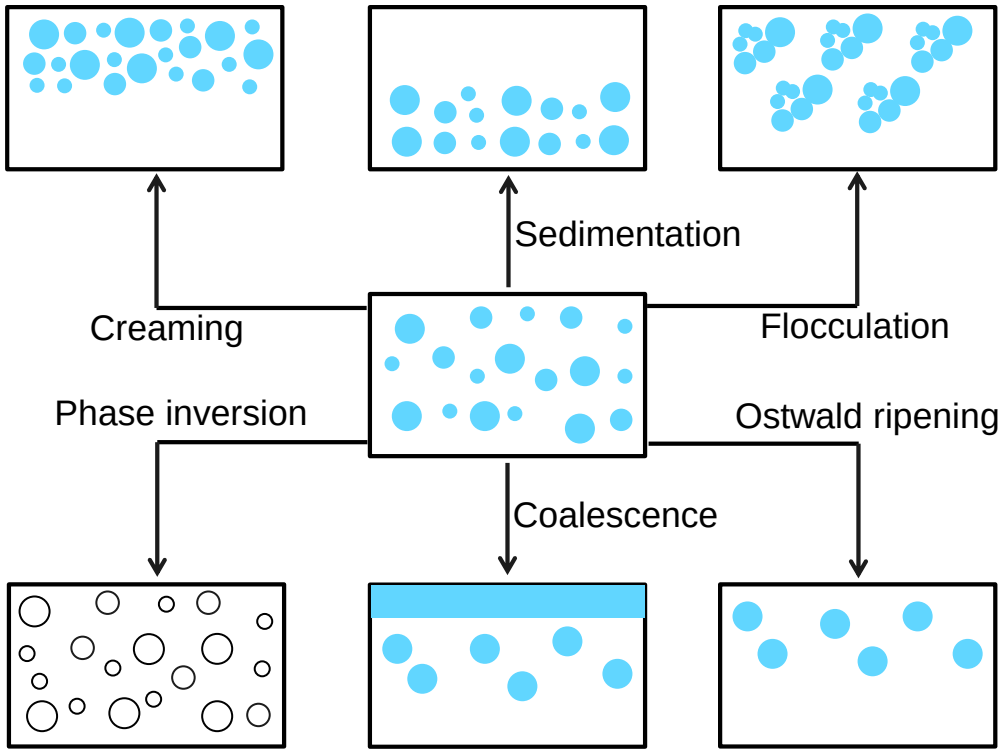

Scheme 1.8 Schematic representation of the various breakdown processes in emulsions.

Flocculation

Aggregation of the droplets into large units without any change in droplets size is referred to flocculation. This process occurs when the attractive forces (van der Waals) between the droplets exceeds that of the repulsive forces resulting in a small separation distance between the droplets. Flocculation may be strong or weak, depending on the magnitude of the attractive forces involved.

Coalescence

Coalescence is the fusion of two or more droplets to form larger drops with reduced total surface area. This process significantly changes the droplet size distribution, which shifts to larger sizes. Emulsions can be separated into two distinct

liquid phases in this destabilization mechanism. To minimize this type of destabilization process, the repulsive forces must exceed the van der Waals interactions.

Ostwald ripening

In emulsions, the formation of large droplets at the expense of smaller droplets is known as Ostwald ripening. The smaller droplets solubilize into larger one due to the finite solubility of liquid phases in emulsions. As a result, the smaller droplets disappear with time and size distribution of droplets moves to large values.

Phase inversion

This is a process where disperse phase becomes the continuous phase. For example, in time an O/W emulsion may change to a W/O emulsion. In many cases, this phase inversion process proceeds through a transition state.

1.4.3 Stability of emulsions

Emulsion stability mainly depends on the balance between the attractive and repulsive forces of the droplets. According to the DLVO theory, the dispersed particles are subjected to two independent forces: the van der Waals forces of attraction and the electrostatic forces of repulsion arising from the presence of electrical double-layers at the particle surfaces.[45] Stable emulsions are formed when the repulsive forces predominate over the attractive forces and keep the droplets separated. This situation can be achieved by adding a stabilizing agent otherwise known as surfactant or emulsifier. When a small quantity of surfactant is added to the solution, surfactants generally start to accumulate in the interfacial region thus reducing interfacial tension.[46] The structure of this interfacial layer depends not only on the composition of the

surfactants but also on the concentration of the surfactants and/or polymers employed. The selection of emulsifier is complicated and affect the formation of long-term stable emulsions, which is governed by the nature of emulsifier as well as the hydrophobic – lipophilic balance (HLB) number.[44] There are three types of emulsifiers: anionic, cationic and amphoteric. The surface charge of the droplets is determined by the types of emulsifier used during emulsion preparation. On the other hand, the HLB is a system parameter that determines how the oil phase interacts with the surfactant. The higher the HLB value of a surfactant, the more hydrophilic (water soluble) it is, whereas the lower the HLB number, the more lipophilic (oil soluble) the surfactant. Table 1.2 gives the required HLB numbers to emulsify various oils.

Table 1.2 Different HLB numbers for various oils.

Oil	W/O emulsion	O/W emulsion
Paraffin oil	**4**	**10**
Beeswax	**5**	**9**
Cyclohexane	**-**	**15**
Toluene	**-**	**15**

1.5 Single Particle Collision Electrochemistry

Single particle collision electrochemistry is a powerful method that allows characterization of the electrochemical reactivity of individual nanoparticles (NPs) in a solution. Research on this method has been increasing significantly over the last

decade because of its applicability in different fields, such as medical science,[47] food technology,[48] pharmaceutics,[48] and electrocatalysis.[49-50] The discrete collision of NPs on an electrode surface due to their random motion results in oxidation or reduction of a single particle or electrocatalysis by the individual NP. This phenomenon is known as “nano-impacts” or “single particle collision”. Detection of single particles has gained interest to obtain a deeper insight about the behavior and the processes that are not available from traditional ensemble measurement techniques. Information that can be extracted from these experiments range from size, stability and electrocatalytic properties, to any electrochemical reaction that can be coupled to the collision event. Particles both hard (metal NPs, oxides, semiconductor) or soft (liposome, micelle, emulsion droplets) are amenable to being studied by this method.

1.5.1 Type of Collisions

In the “nano-impact” chronoamperometric method, an electrochemical current in the form of a spike is recorded when a single particle strikes the electrode while is held at a specific potential. To date, various types of measurement approaches have been reported in the literature, however the most common is direct and indirect electrolysis with or without electrocatalytic amplification. Other methods include, electrode area blocking[52] and open-circuit potential measurements[53].

1.5.1.1 Direct Faradic Impacts

In direct mode, a redox reaction occurs during the collision of a single particle on the electrode surface provided an appropriate potential is applied. Consequently, a spike of faradic current is observed for an individual collision when recording a chronoamperometric response (Scheme 1.9). For example, silver NPs can be detected

in citrate solution through direct electro-oxidation of the particles during collisions at the electrode surface (equation 1.2).[49] Particle size is determined by calculating the charge passed per current spike.

$$\mathrm{Ag\,(nanoparticle)} - \mathrm{e^-} \rightarrow \mathrm{Ag^+} \quad \ldots\ldots\ldots\ldots\ldots\ldots\ (1.2)$$

1.5.1.2 Indirect Faradic impacts

In indirect electrolysis mode, an electroactive species that shows sluggish electron-transfer kinetics at a suitable potential produces a small current transient. But the enhancement of current may occur if a nanoparticle interacts with the electrode allows oxidation or reduction of the particular electroactive species via electro-catalysis (Scheme 1.9 B). In 2007, Bard and co-workers took advantage of electrocatalytic amplification while individual platinum NPs in aqueous solution collided at an ultramicroelectrode (UME) and observed the amplified current as Pt NPs catalyzed the reduction of H^+ and H_2O_2.[54] They reported that the resulting current-time profile is directly related to particle size, residence time of particle at electrode and the nature of particle interaction with the electrode surface.

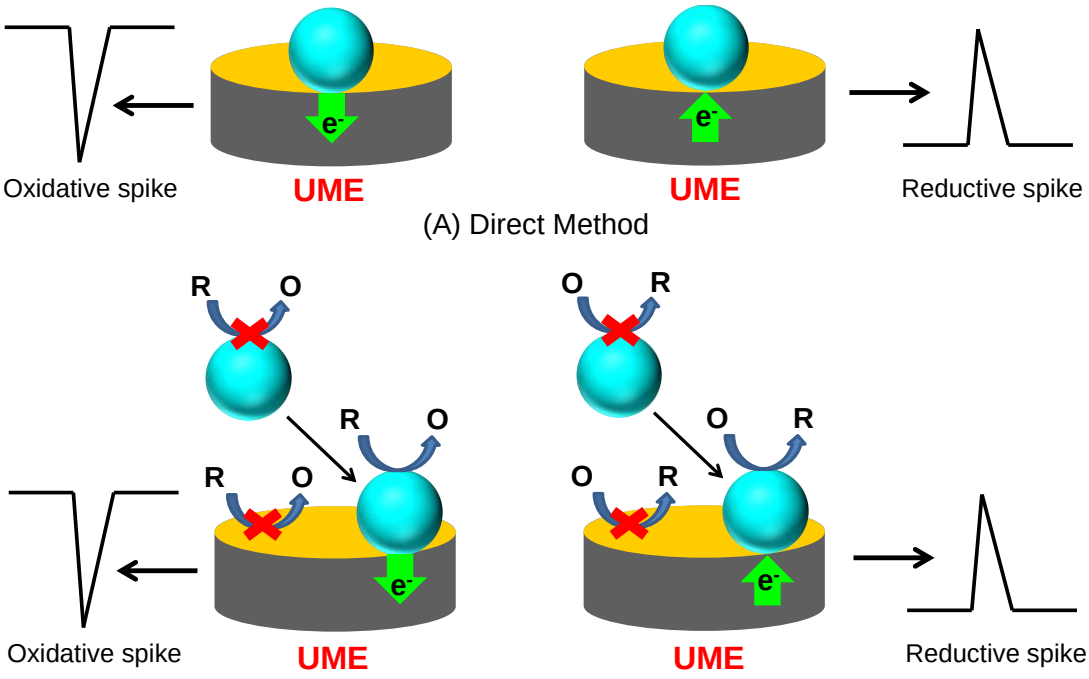

Scheme 1.9 Basic form of nano-impact collision. (A) Direct method and (b) Indirect method.

1.6 Nano-Impact Collision to Emulsions

Collisions of colloidal semiconductor particles e.g. SnO_2 and TiO_2 on the surface of electrodes were first reported by Heyrovsky in 1995.[55,56] Later on, a large number of publications came out primarily on hard particles based on particle-impact electrochemistry. Recently the Compton group and several others have investigated the collision of various types of metallic NPs (Au,[57] Ni,[58] Cu[59]), oxides (IrO_2,[60] CeO_2,[61] SiO_2[62]) and organic hard particles (polystyrene,[63] indigo[64]) by utilizing the same basic concepts, that is, the direct or indirect method.

Up to now, most single particle collision experiments have been concentrated on hard particles. Last couple of years, some researchers extended this approach to soft

particles such as liposomes[50], vesicles[65,66] and emulsions.[52] Like hard particles, it is possible to study soft particles and more specifically the redox active components trapped inside these particles by “nano-impact” collision electrochemistry. Recently, Compton and co-workers investigated the direct collision of vitamin C encapsulated liposome in neutral buffer solution.[50] Single liposome components were characterized by the current spikes in real time as it collides with an electrode. Thereafter, Ewing’s group examined the electrochemistry of nanometer-sized vesicles containing catecholamine hormone.[65] A peak or spike is attributed to oxidation of catecholamine when each vesicle bursts on the electrode surface. However, it was found by Bard and coworkers, that redox contents (potassium ferrocyanide) inside the vesicle were not oxidized during the collision unless a nonionic surfactant like triton X-100 was present inside the vesicle.[66] In addition to this, a cetyltrimethylammonium bromide (CTAB) micelle was detected via oxidation of bromide by Toh and Compton in 2015.[67] They observed that the concentration of CTAB plays a significant role on the number of spikes observed in a “nano-impact” experiment. More recently, Bard’s group studied emulsion oil droplets (e.g., toluene,[52] benzene,[68] cyclohexane[68]) as electrochemical reactors containing hydrophobic molecules such as ferrocene (Fc), decamethyl-ferrocene, rubrene and others. These oil droplets dispersed in an aqueous phase strike on the surface of electrode because of Brownian motion. As a result, the redox molecules inside each droplet undergo an oxidation or reduction reaction at a specific potential and each collision produces a current spike. In addition, Cheng and Compton used Vitamin B_{12} nanodroplets to mediate the reduction of dioxygen and proposed a mechanism for dioxygen reduction.[69] Nowadays, it is assumed that soft particles like

emulsion droplets could be an alternative for hard particle because of their wide applications and environmental friendliness.

1.7 Emulsions Preparation

Typically oil in water emulsions (O/W) can be prepared by homogenizing an oil phase and an aqueous phase together in the presence of a surfactant or an emulsifier (e.g., triton X-100, sodium lauryl sulfate and span 80).[70,71] To prepare a stable emulsion system, different types of homogenizers can be used, including high shear mixers, high pressure homogenizers, colloid mills and ultrasonic homogenizers depending on the characteristics of the materials being homogenized (e.g., product viscosity, interfacial tension, shear sensitivity) and the desired emulsion properties such as droplet concentration, droplet size distribution. The desired droplet characteristics can be tuned by careful selection of homogenizer type, homogenizer operating conditions, and surfactants. For instance, droplet size of emulsions produced by high-pressure homogenizers can be decreased by increasing the pressure of the homogenization. The electrical charge on the droplets surface can be also controlled by choosing an appropriately charged emulsifier, which may be positive, neutral or negative.

In this thesis, the toluene/water emulsions were prepared[52] by following the literature method with slight modification. In a typical preparation, 5 mM of tetrachlorobezoquionone (TCBQ) was added to 355 µL of toluene in a vial, followed by the addition of 145 µL of ionic liquid (400 mM) to form a homogeneous mixture. Afterward, 100 µL of this toluene mixture was added to 5 mL of degassed deionized Milli pure water. Finally, the content of the vial was mixed vigorously for 20 s in a vortex mixer and sonicated for 5 min at room temperature. An emulsion was formed (Scheme

1.10) and showed stability up to 6 h. Here, the ionic liquid (IL) served as both supporting electrolyte and emulsifier.

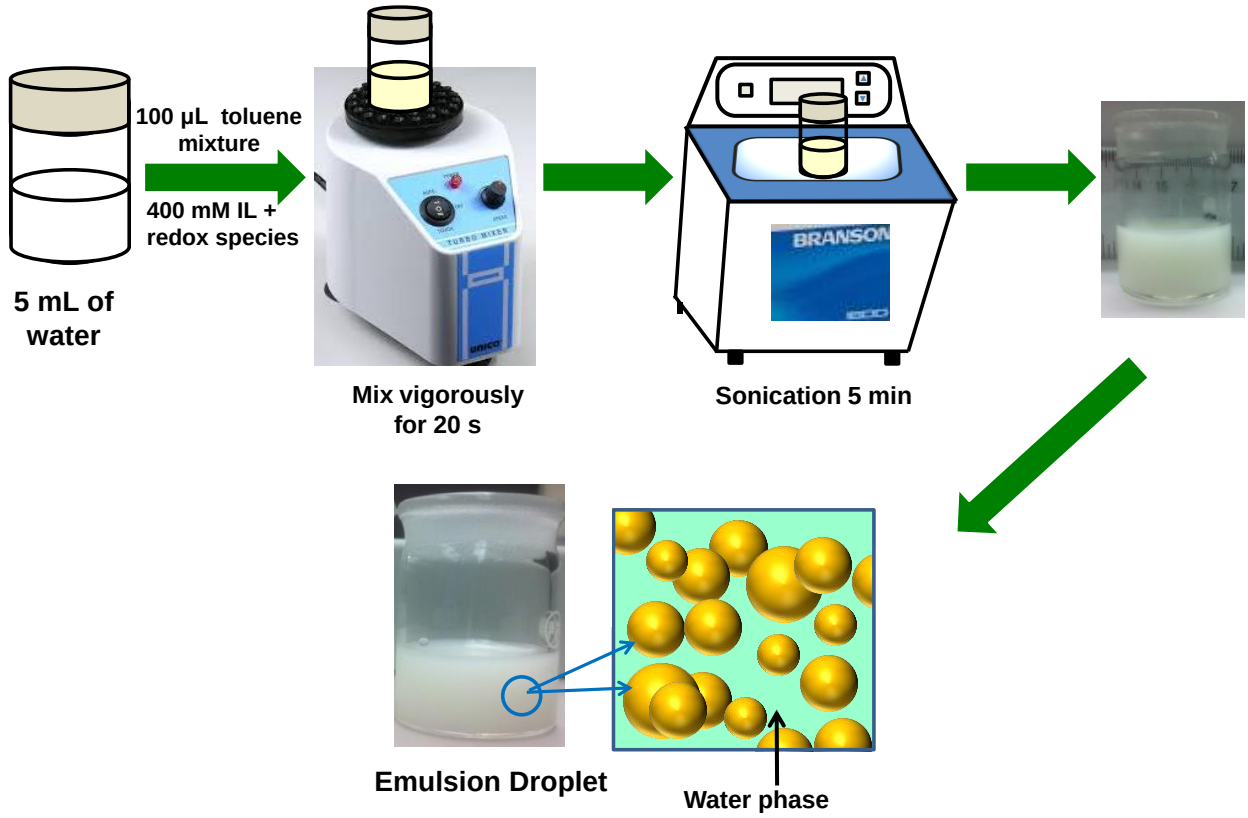

Scheme 1.10 Preparation of toluene-water emulsion.

The size of emulsion droplets was characterized by Dynamic Light Scattering (DLS) measurements. The concentration of the toluene (TCBQ + IL) emulsion droplets was calculated from the total toluene (TCBQ + IL) volume (0.1 mL) divided by the average emulsion droplet (diameter 1439 nm) volume (1.56 fL). Accordingly, the molar concentration of emulsion droplets used for collision experiments was 21.2 pM. All particle collisions measurements were finished within 1 h.

Other toluene emulsions were prepared following the same procedure including oleic acid, acetic acid and ferrocene. More details are discussed in chapter 2 and chapter 3.

1.8 Preparation of Ultramicroelectrodes (UMEs)

Ultramicroelectrodes are defined as electrodes whose critical dimension is in the micrometer range typically smaller than 25 μm.[72,73] They have several advantages, including small size, high sensitivity, small current (pA to nA), steady state response, low double layer charging current and small ohmic resistance.[72,73] The fabrication of high quality UMEs is a challenging and time consuming process that requires experimental skill and patience.

UMEs were prepared based on the general procedure developed in our laboratory based on previous literature. The fabrication involves several steps as shown in Scheme 1.11. First, borosilicate glass capillaries (around 15 cm long) with a conical shape at one end were cleaned by sonication in ethanol followed by water and dried in an oven (100 ºC) for 2 h. About 1 cm length of electroactive materials (Au, Pt and C fiber) wire was connected to a large copper wire using conductive Ag epoxy (epo-teck H20E, parts A and parts B). The epoxy was cured around 100 ºC overnight in an oven. Next, the micrometer wire (electrode) was inserted carefully into a clean capillary by using a tweezer. The capillary is slowly sealed on the metal wire (Au and Pt) using a Nickel – Chromium resistor at 800 ºC. A DC power supply is applied with 7.56 A and 8.77 V to increase the temperature up to 800 ºC. The other end of the electrode was sealed with Torr Seal epoxy (1:2 ratio) and dried in the oven for 10 minutes. The

electrode was then gently wet polished for 10 to 30 seconds on 600 grit sandpaper and then polished with 0.05 µm alumina with distilled water on micro-cloth pads.

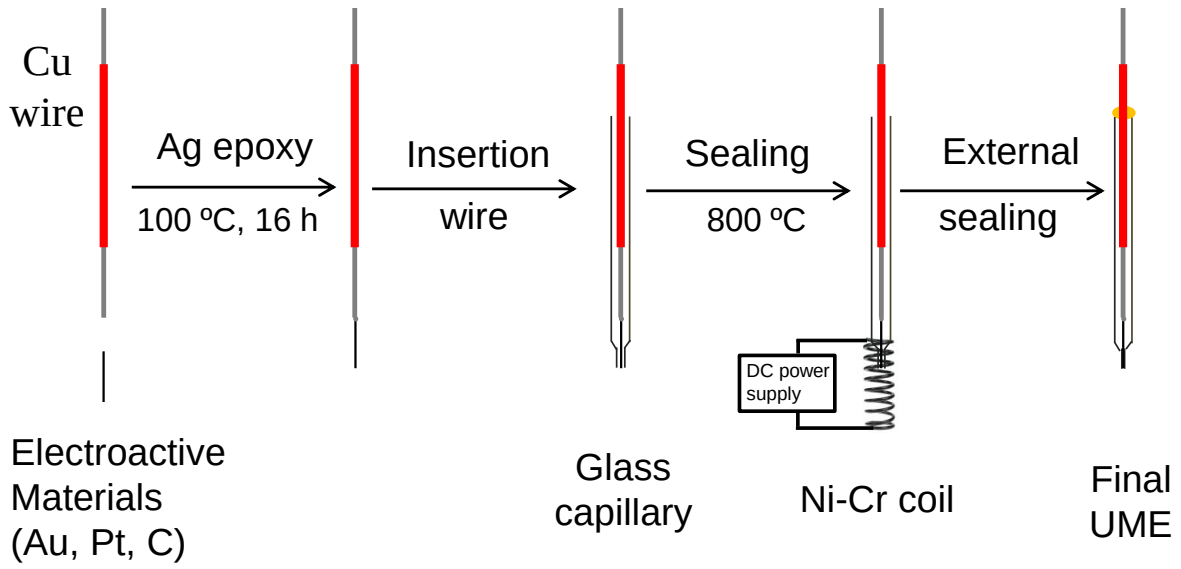

Scheme 1.11 Different steps for the preparation of UME.

A similar procedure was employed to prepare the C-fiber electrode except for the sealing step. This electrode was sealed by using a mixture of epoxy and hardener instead of a heated coil. During sealing process, the capillary with C-fiber was placed into a mixture of 15% (w/w) m-Phenylenediamine in epon^{TM} resin 820 at 75 ºC for 1 min. Next, the capillary was kept in an oven at 140 ºC for 12 h for complete sealing.

Cyclic voltammetry and chronoamperometry were the electrochemical methods applied in all the studies discussed herein. DLS and zeta potential measurements were performed to determine size and charge of the emulsions respectively. The next section of this section describes the fundamentals of cyclic voltammetry, chronoamperometry, DLS and zeta potential measurements.

1.9 Experimental Methods

1.9.1 Cyclic Voltammetry (CV)

Cyclic Voltammetry has been widely applied in nearly every branch of science to study a broad range of reactions. This is a simple and very popular electroanalytical technique used in the study of the electroactive species such as organometallic complexes (e.g. ferrocene), organic complexes (e.g. quinone, trolox), biomolecules (proteins), metals and semiconductors. This method has proven very useful in obtaining information about the redox potential of analytes, the number of electrons involved in an electrochemical reaction, reversibility of a charge transfer reaction and finally the rate of the electron transfer between the redox species in solution and a working electrode.

Cyclic voltammetry studies were carried out using a potentiostat (CH Instruments, Austin, TX) equipped with a standard three-electrode cell placed in a faradic cage as shown in Scheme 1.12**.** The cell contains the analyte solution and the charge transfer reactions take place at the surface of a working electrode. In CV, a working electrode immersed in a quiescent solution is subjected to a linear sweep of potential in a cyclic manner while measuring the resulting current. During the voltammetric scan, the potential of the working electrode is measured with respect to the reference electrode and the current is measured with respect to the counter or auxiliary electrode. Indeed, the counter electrode completes a circuit with the working electrode and maintain the flow the electrons (current) generated by the applied potential to the working electrode.

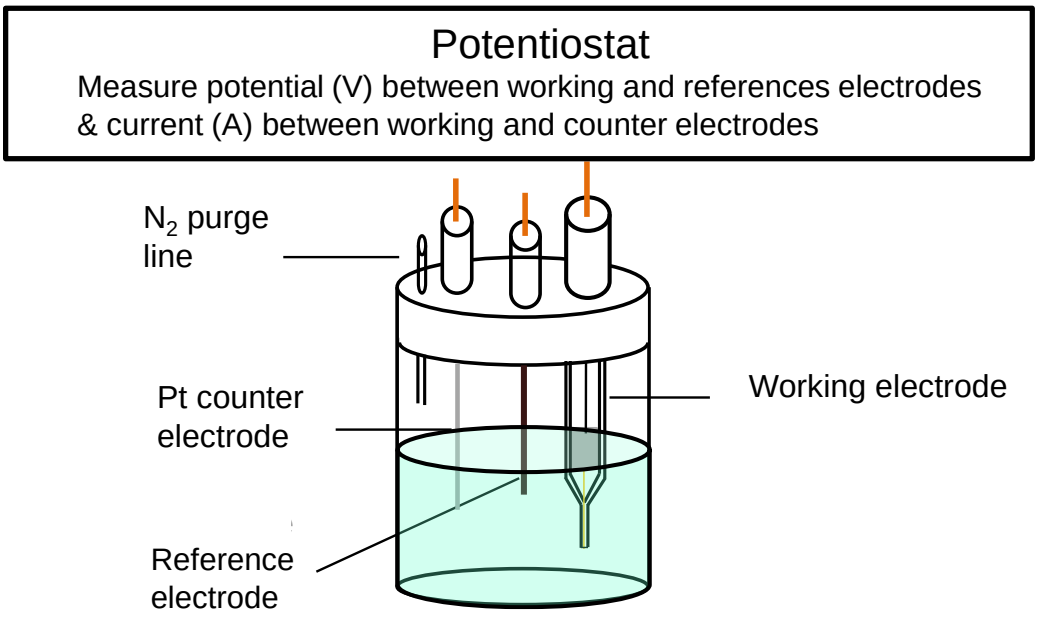

Scheme 1.12 Typical three electrode cell.

Figure 1.1 shows a typical cyclic voltammogram of 1.0 mM $Ru(NH_3)_6^{3+}$ in an aqueous solution of 0.1 M KCl and the arrows represent the direction of the forward and reverse scans. In CV, there is no faradic current observed from 0.2 V (vs Ag/AgCl) to around 0.05 V (vs Ag/AgCl) as no electron transfer occurs between the glassy carbon working electrode and $Ru(NH_3)_6^{3+}$ in solution. Any measured current within this region is known as nonfaradaic or charging current. In the forward scan (+0.20 V → -0.50 V), the peak at -0.203 V is called cathodic peak, due to the one electron reduction of $Ru(NH_3)_6^{3+}$ to $Ru(NH_3)_6^{2+}$ at the electrode surface. The decrease of the reduction current past -0.203 V occurs because the concentration of $Ru(NH_3)_6^{3+}$ species at the electrode surface approaches zero and the reduction process becomes limited by diffusion of this species from the bulk of the solution. The peak potential in the reverse scan, at -0.136 V referred to as the anodic peak corresponds to the oxidation of $Ru(NH_3)_6^{2+}$ to $Ru(NH_3)_6^{3+}$. Similar to the reduction process, the oxidation current of

$Ru(NH_3)_6^{2+}$ reaches to a maximum when the concentration of $Ru(NH_3)_6^{2+}$ near the electrode is depleted and the oxidation process becomes limited by diffusion of $Ru(NH_3)_6^{2+}$ towards the electrode surface.

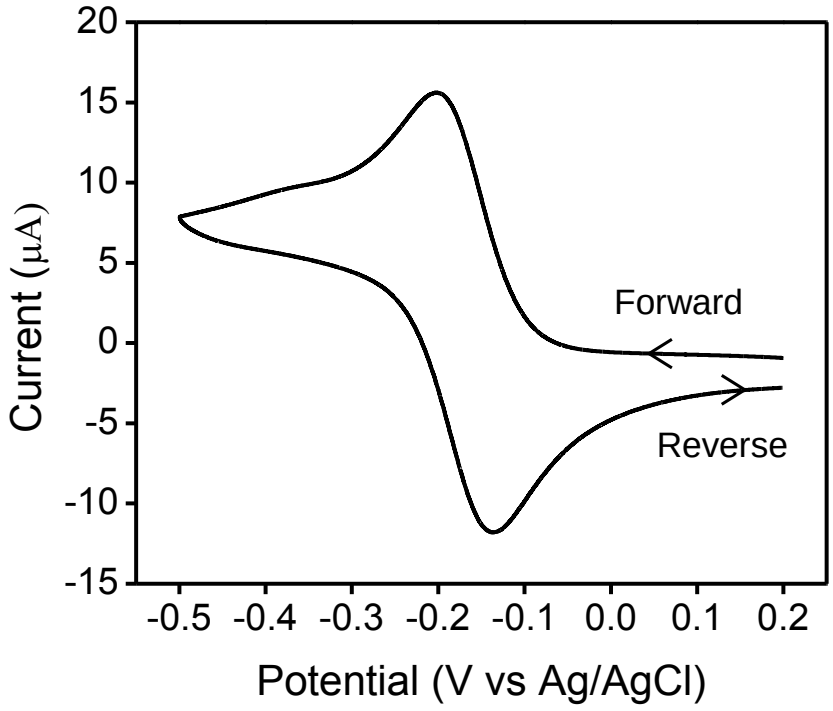

Figure 1.1 Cyclic voltammogram of 1.0 mM $Ru(NH_3)_6^{3+}$ in 0.1 M KCl at 0.1 V/s. Voltammetry performed at a glassy carbon electrode and Ag/ AgCl/ 1.0 M KCl was the reference electrode.

In summary, from the above voltammogram several remarks can be made about the redox couple $Ru(NH_3)_6^{3+}$/ $Ru(NH_3)_6^{2+}$: (1) the ratio between the cathodic current and anodic current is almost 1, (2) the cathodic and anodic peak separation is about 60 mV, that indicates electron transfer is first and the redox couple is electrochemically reversible.

A steady-state voltammogram was recorded to examine the radius of prepared electrodes in 0.1 M KCl aqueous solution of 1.0 mM ferocenemethanol (FcMeOH) at

scan rate 10 mV/s. Figure 1.2 shows the voltammogram of prepared C-fiber electrode. The radius of the electrode was calculated by using equation 1.3.

$$i_{ss} = 4nFDrC \ldots\ldots\ldots\ldots\ldots\ldots (1.3)$$

Where, the following abbreviations are used: i_{ss} = steady-state current in Ampere, n = number of electrons, F = Faraday's constant (96487 C/mole e^-), D = diffusion coefficient of ferocenemethanol (7.8 x 10^{-6} cm^2/s),[74] C = concentration in mole/cm^3, r = radius of the C- fiber UME (μm).

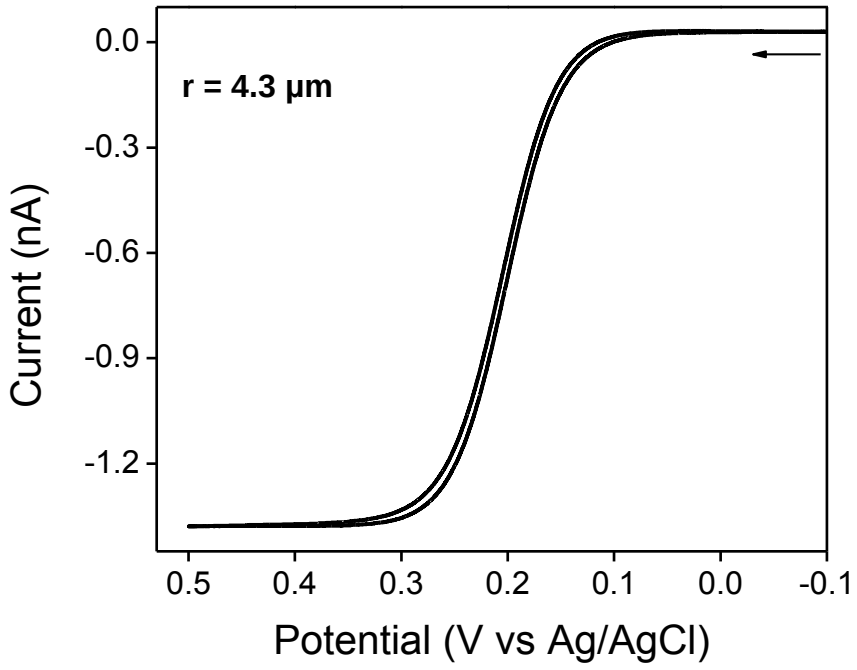

Figure 1.2 Steady-state voltammogram of 1.0 mM FcMeOH in 0.1 M KCl at 10 mV/s. Voltammetry performed at C-fiber electrode and Ag/AgCl was the reference electrode.

1.9.2 Cyclic Voltammetry of Ultramicroelectrode

Cyclic voltammograms obtained with ultramicroelectrode differ significantly from those of conventional macroelectrodes in normal experimental time scales. For an ultramicroelectrode, the shape of CV is sigmoidal which is almost similar to the S-shaped voltammograms obtained rotating disk electrodes. The voltammograms are controlled by the rate of mass transport (diffusion).[72,75] Mass transport at an UME takes place in a hemispherical fashion (radial diffusion) at lower scan rates. Indeed, the radial diffusion increases the mass transport at UME surface. Consequently, current density is increased at UME surface compared to macroelectrodes experiencing planer diffusion. As a result, it produces a steady state S-shaped voltammograms. However, at higher scan rates, the peak shaped voltammograms are obtained. For a spherical electrode, current is given by[75]

$$i = \frac{nFACD^{1/2}}{t^{1/2}\pi^{1/2}} + \frac{nFADC}{r} \ldots\ldots\ldots\ldots\ldots\ldots (1.4)$$

Where n = number of electron transferred, F = Faraday's constant, A = geometric electrode area, D = diffusion coefficient and C = concentration of redox species.

In equation 1.4, the first term dominates at short times, whereas second term dominates at long times.

(i) Short times: At short times, the diffusion layer is thin compared to electrode radius and the spherical electrode seems to be planer to a redox molecule at the edge of diffusion layer. As a result, mass transport is carried out by mainly by planer diffusion.[75]

At short times, the term in equations 1.4 becomes significantly larger than the second one. The current response follows the Cottrell equation.

$$i = \frac{nFACD^{1/2}}{t^{1/2}\pi^{1/2}} \ldots\ldots\ldots\ldots\ldots\ldots\ldots (1.5)$$

(ii) Long times: At longer times, the diffusion layer becomes much larger than electrode radius. The spherical electrode seems to be radial or spherical to a redox molecule at the edge of diffusion layer. As a result, mass transport process is dominated by radial or spherical diffusion process.[75] At longer time scales, the contribution from the first term in equation 1.4 appears to a very negligible at a certain point. Consequently time independent steady state current is achieved which is given equation 1.6. At long experimental timescales, the steady state response is developed as the rate of electrolysis is equal to diffusion rate of the redox molecules to the electrode surface.

$$i = \frac{nFADC}{r} \ldots\ldots\ldots\ldots\ldots\ldots (1.6)$$

The steady state currents response generated at ultramicroelectrode are also dependent on their geometry. For example, the steady state current for a disk UME is given by

$$i = 4nFDCr \ldots\ldots\ldots\ldots\ldots\ldots (1.7)$$

1.9.3 Chronoamperometry (CA) and Amperometric i-t curve (*i-t*)

Chronoamperometry is an electrochemical technique where a potential pulse is applied to the working electrode while current is measured versus time. During CA experiments, either single potential step or multiple potential steps are used based on experimental design. A typical double potential step chronoamperometry is shown in Scheme 1.13 ((a) potential waveform and (b) current response). In double step experiments, there generally is a potential (E_1) chosen where no faradic process occurs. The potential is then moved to a particular value (E_2) that certain enough to oxidize or reduce a redox species at the electrode surface and held that potential for certain time period which is called as pulse width (Scheme 1.13). After completing the first step, the potential is returned to its initial applied potential at a specific pulse width to complete the second step.

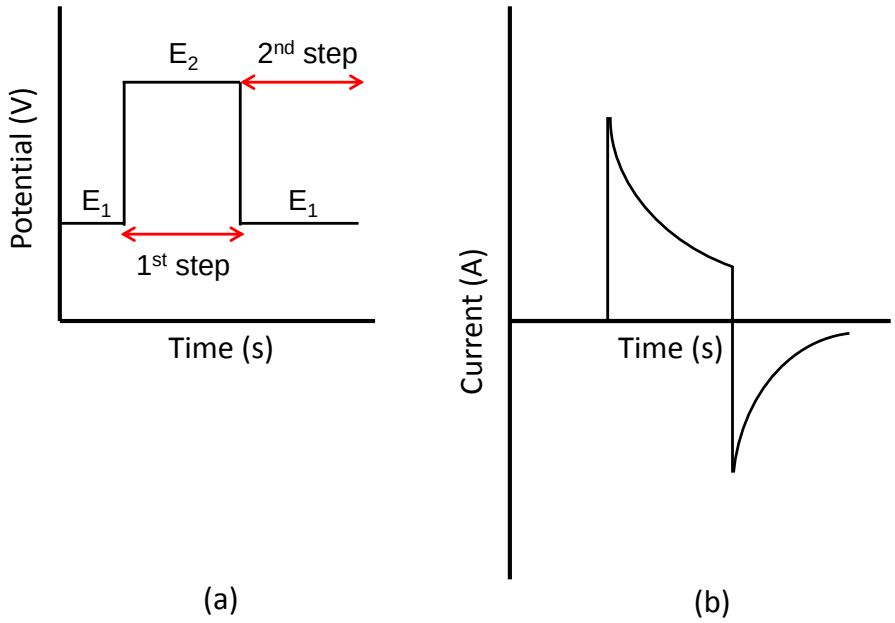

Scheme 1.13 Double potential step chronoamperometry. (a) Typical waveform and (b) Current response.

On the other hand, chronoamperometry relies on recording the current (i) as a function of time (t) after setting the potential at a selected value. The resulting response is sometimes called an amperometric i-t curve. The Scheme 1.14 represents the potential waveform applied as a function of time and the current sampling interval.

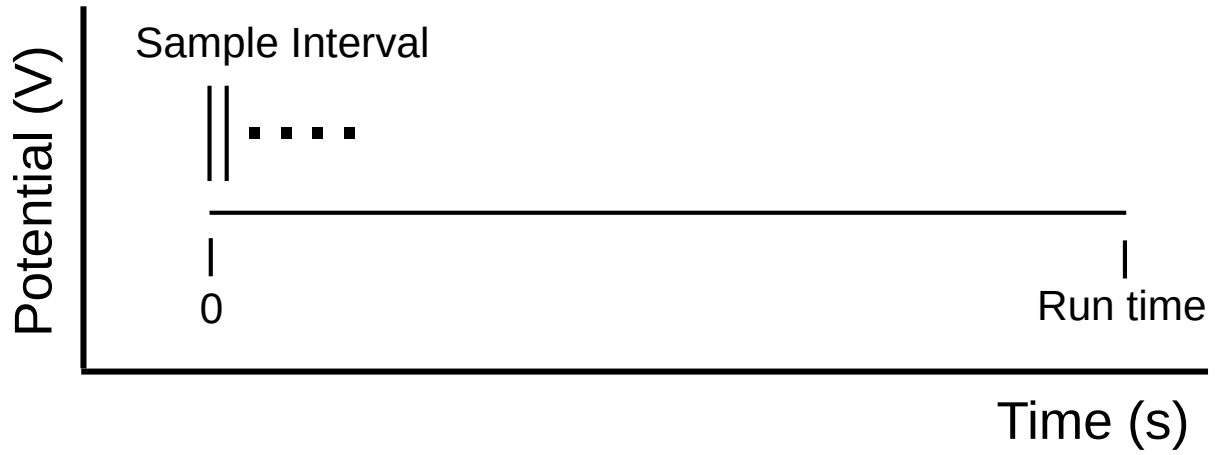

Scheme 1.14 A typical waveform of amperometric i-t curve technique.

In amperometric i-t technique, the data sampling is determined according to the length of the experiment. The longer the experiment, the longer the sampling interval should be. Consequently, a longer sampling interval results in more signal averaging and less noise. In both techniques, the current response is followed by Cottrell equation[75] shown below-

$$i(t) = \frac{nFAD^{1/2}\,C}{\pi^{1/2}t^{1/2}} \ldots\ldots\ldots\ldots\ldots\ldots (1.8)$$

1.9.4 Single Counter Software

The “Signal Counter” program (Center for Marine and Environmental Research, Zagreb, Croatia) was used for spike identification, spike height determination and spike area integration. The integration results charge in coulombs for individual spike. The average charge was calculated at a certain potential by the summation of the charge for all spike divided by total spikes. The current was also determined at a specific potential from the height of the individual spike. The average current was calculated by adding the charge for all spike divided by total number of spike. At each potential, sample was analyzed three times and all three electrochemical data were was used to calculate both average charge and current. During data analysis, the electrochemical date file (bin) was uploaded to the software for analysis and the software usually detects the spike automatically. OriginPro8.5.1 was applied for electrochemical data analysis. Figure 1.3 shows the spikes in single counter software.

Assuming diffusion as dominant mode of mass transport, the droplet collision frequency (f_d) was calculated by using equation 1.9 where D_d = the droplet’s diffusion coefficient, C_d = droplet concentration, r_e = electrode radius and (r_e) N_A = Avogadro’s number. Around 200 spikes were considered to measure the experimental collision frequency.

$$f_d = 4D_d C_d r_e N_A \qquad \ldots\ldots\ldots\ldots\ldots\ldots (1.9)$$

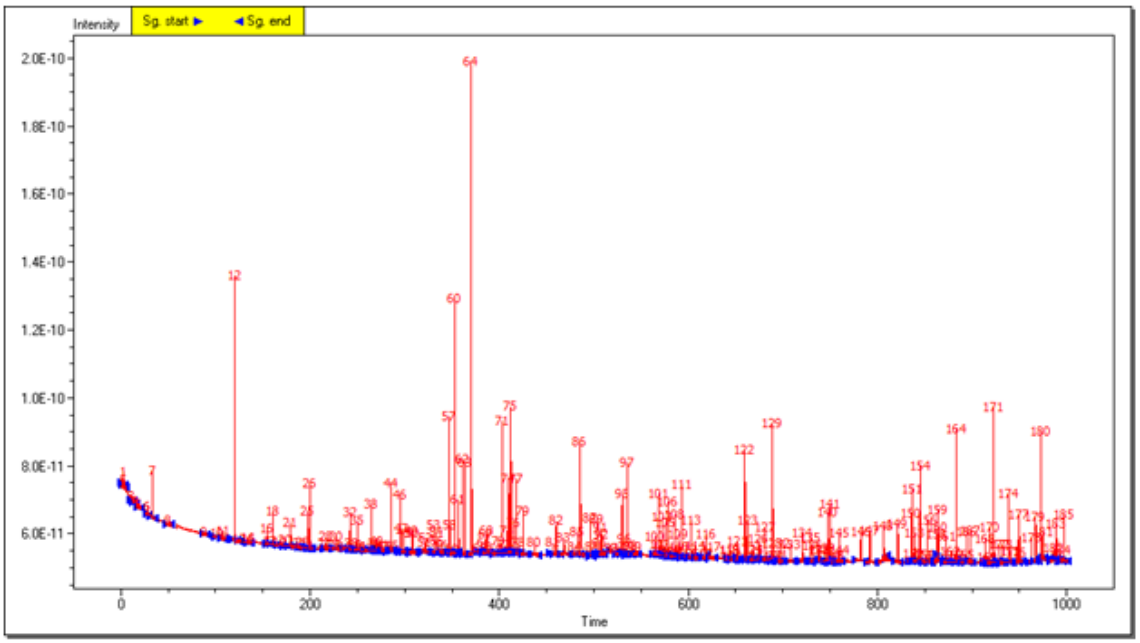

Figure 1.3 *i-t curve* of toluene water emulsion with tetrachlorobenzoquinone in the toluene phase at potential -0.5 V vs Ag/AgCl. The 185 spikes shown during 100 ms interval were detected using Signal Counter software.

1.9.5 Dynamic Light Scattering (DLS)

DLS is a technique that can be used to assess useful information about hydrodynamic size, size distribution and diffusion coefficients of emulsion droplets or nanoparticle without destroying the structure of emulsion droplets or NPs.[76,77] A stable emulsion system or NPs is required for best results during measurements in a DLS instrument. DLS utilizes a monochromatic light source to probe the emulsion droplets and records the time variation of the intensity of the light scattered by diffusing the droplets or particles into a continuous phase as that shown in Scheme 1.15.[76,77] In a DLS measurement, the time analysis is carried out with a correlator which constructs

the time autocorrelation function, G(τ) of the scattered intensity according to equation 1.10, where I = intensity, t = the time and τ = the delay time or lag time.

$$\mathrm{G}(\tau) = \frac{\langle I(t).I(t+\tau)\rangle}{\langle I(t)^2\rangle} \ldots\ldots\ldots\ldots\ldots\ldots (1.10)$$

This function is then used to measure the diffusion coefficient of the droplets. The intensity of scattered light at certain angles over time is related to the diffusion of the droplets in dispersion medium. Therefore, it is necessary to know the viscosity, refractive index, and temperature of the system being analyzed to effectively characterize droplets or particles using DLS. The hydrodynamic diameter and size distribution in terms of polydispersity index (PDI) values are calculated from the measured diffusion coefficients.[77] In equation 1.11, the magnitude of the scattering wave (q) is calculated using the range of scattering angles (θ), wavelength of the incident light (λ), and refractive index of the dispersant (n).

$$q = \left(\frac{4\pi n}{\lambda}\right) sin\left(\frac{\theta}{2}\right) \ldots\ldots\ldots\ldots\ldots\ldots (1.11)$$

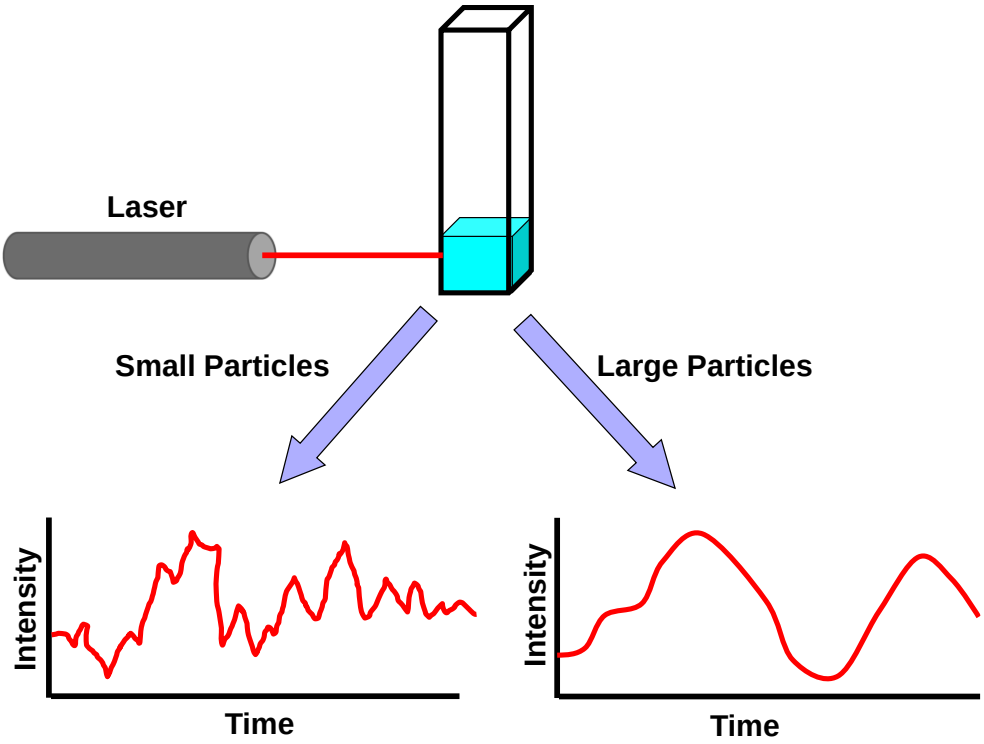

Scheme 1.15 Variation of intensity of different particles in DLS.

The hydrodynamic radius (r) is calculated using the Stokes-Einstein equation shown in equation 1.12 where the following abbreviations are used: k_B = Boltzmann constant, T = temperature in kelvin, η = viscosity of the medium and r = hydrodynamic radius of an emulsion droplet. Thus it can be seen that the hydrodynamic radius is directly related to the diffusion coefficient (D).

$$D = \frac{TK_B}{6\pi\eta r} \dots\dots\dots\dots\dots\dots (1.12)$$

Next, the size distribution is calculated, in terms of the PDI, using the average decay rate ($\langle \Gamma \rangle$) and the variance of the decay rate distribution (μ_2) (equation 1.13).[76]

$$PDI = \frac{\mu_2}{\langle \Gamma \rangle^2} \dots\dots\dots\dots\dots\dots (1.13)$$

An absolute monodisperse sample is highly improbable, therefore the correlation function calculated ⟨Γ⟩ and q values can be used to obtain an average hydrodynamic radius (equation 1.14).[76] which is known as Z-average value. Depending on the instrument used, a weighted function can be used to calculate the summation of all possible decay rates for each droplet to determine a size distribution. The DLS data can be presented based on the number, volume, or intensity of droplets.

$$r = \frac{k_B T}{6\pi n \langle \Gamma \rangle} q^2 \ldots\ldots\ldots\ldots\ldots\ldots (1.14)$$

In this study, A Malvern Zetasizer Nano-ZS (Malvern Instruments, U.K.) equipped with He-Ne laser (wavelength = 633 nm) was used to record the hydrodynamic diameter, polydispersity index of all emulsion samples. As an example, Figure 1.4 shows a DLS measurement data of the toluene droplets loaded tetrachlorobezoquinone in water. The measurements data of other emulsions studied are given in chapter 2 and 3. All measurements were carried out into disposal plastic cuvettes at 20 ºC without any dilution of prepared emulsions. Instrument was calibrated by 200 nm polystyrene standard sample before every measurement. To measure the size of the droplets, 2.5 mL volume of each sample was transferred to a plastic cuvette and DLS was run 5 times with each run containing 12 measurements. Three different samples of each emulsion were run for the size measurement studies.

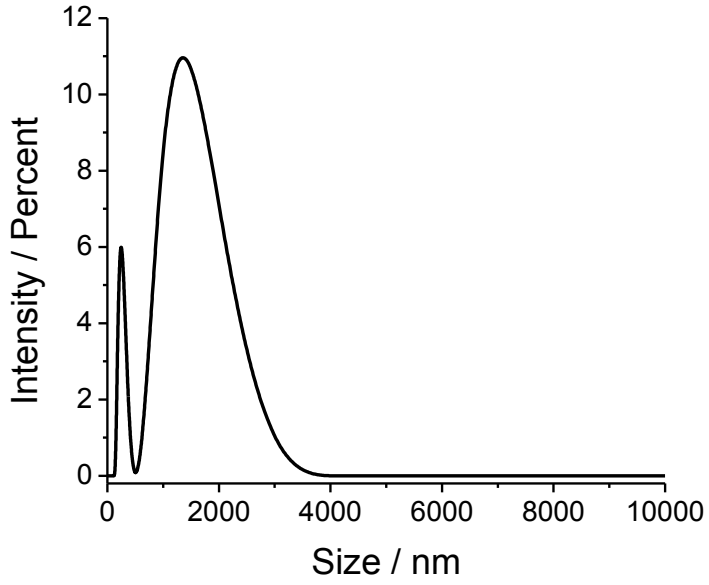

Figure 1.4 Size distributions of toluene droplets emulsion from DLS.

1.9.6 Zeta Potential

Zeta potential (ZP) is one of the basic characterization tools to identify and measure the charge of colloidal dispersions such as NPs and emulsions. The magnitude of the zeta potential gives an indication of the stability of the colloidal system. Particles or emulsions with ZP values of ± 0-10 mV, ± 10-20 mV, ± 20-30 mV and ± 30 mV are considered as unstable, relatively stable, moderately stable and highly stable respectively.[77]

The ZP, also known as electrokinetic potential is a potential that exists very near the surface of colloidal particles moving in a liquid under an electric field (electrophoresis). When a charged particle is dispersed in a liquid, two layers are developed on its surface (Scheme 1.16). The inner region called the Stern layer, where the counter ions are strongly bound and an outer region (diffuse layer) consists of both negative and positives charges which are less firmly attached. Within this diffuse layer,

there is a plane which acts as a boundary between the moving particles and the layer of dispersant medium around it while electrophoresis happens. This plane is known as slipping plane and the potential exits at this plane is called the zeta potential (ζ) (Scheme 1.16).

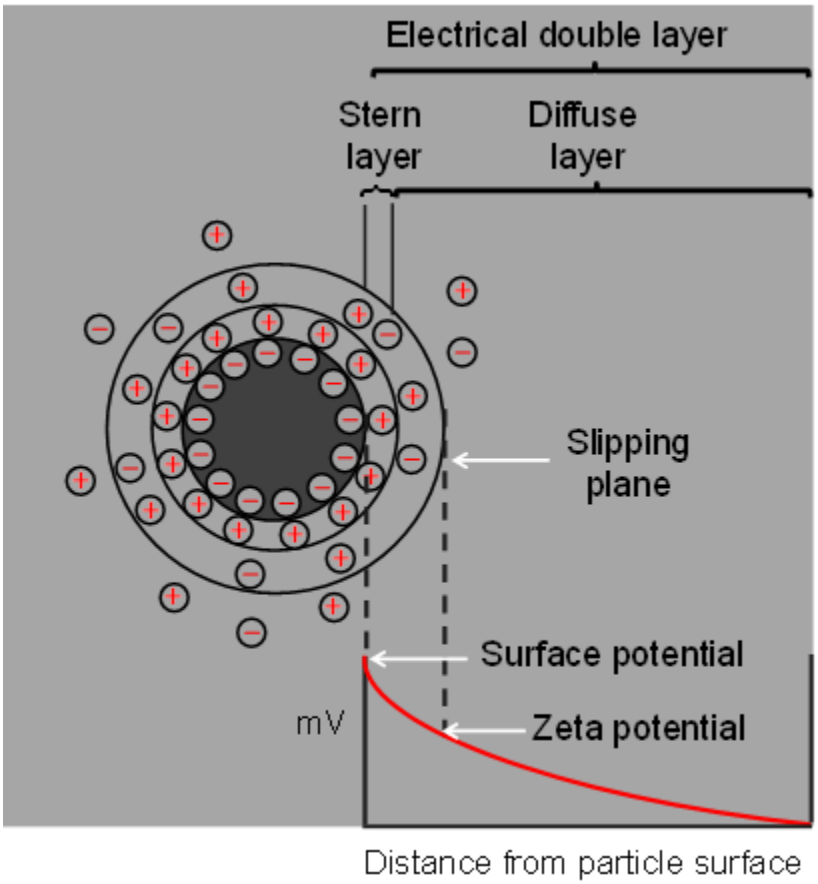

Scheme 1.16 A negatively charged particle suspended in a liquid with various notional regions around it.

This measurement is not a direct process. It is determined by measuring the electrophoretic mobility of charged particles under an external applied electrical field and then substituting into the Henry's equation. The electrophoretic mobility (μ_e)[77] is calculated as-

$$\mu_e = \frac{V}{E} \dots\dots\dots\dots\dots\dots (1.15)$$

where, V = particle velocity (μm/s), E = electric field strength (Volt/cm). Then the ZP of the particles can be obtained by using Henry's[77] equation 1.16.

$$\mu_e = \frac{2\varepsilon\zeta f(Ka)}{3\eta} \ldots\ldots\ldots\ldots\ldots\ldots (1.16)$$

where, ζ = zeta potential, ε = dielectric constant, η = viscosity and f(*K*a) = Henry's function. Two values are generally used as approximations for the *f(Ka)* determination - either 1.5 or 1.0 depending on the size of the particles and concentration of salts in aqueous solution.

During this work, zeta potential analyses were performed with a Malvern Zetasizer Nano-ZS instrument. Scheme 1.17 illustrates a typical set up of ZP measurements by electrophoretic light scattering. Like the typical DLS system, ZP measurement system comprises six main components. For ZP measurements, this light source (laser beam) is split to provide incident and reference beam. The incident beam is directed towards the sample cell and the reference beam is modulated to determine the Doppler effect. When an external electric field is applied to the cell, movement of the colloidal particles in measurement volume changes the frequency of the incident light that is proportional to the particle speed. A detector sends this information to a digital signal processor (correlator). This information is then passed to a computer, where the Zetasizer software creates a frequency spectrum from which the electrophoretic mobility and finally the zeta potential information is calculated. An attenuator is used to control the intensity of scattered light from the particles. In addition, compensation optics is installed within the scattering beam path to maintain the alignment of the scattering beams.

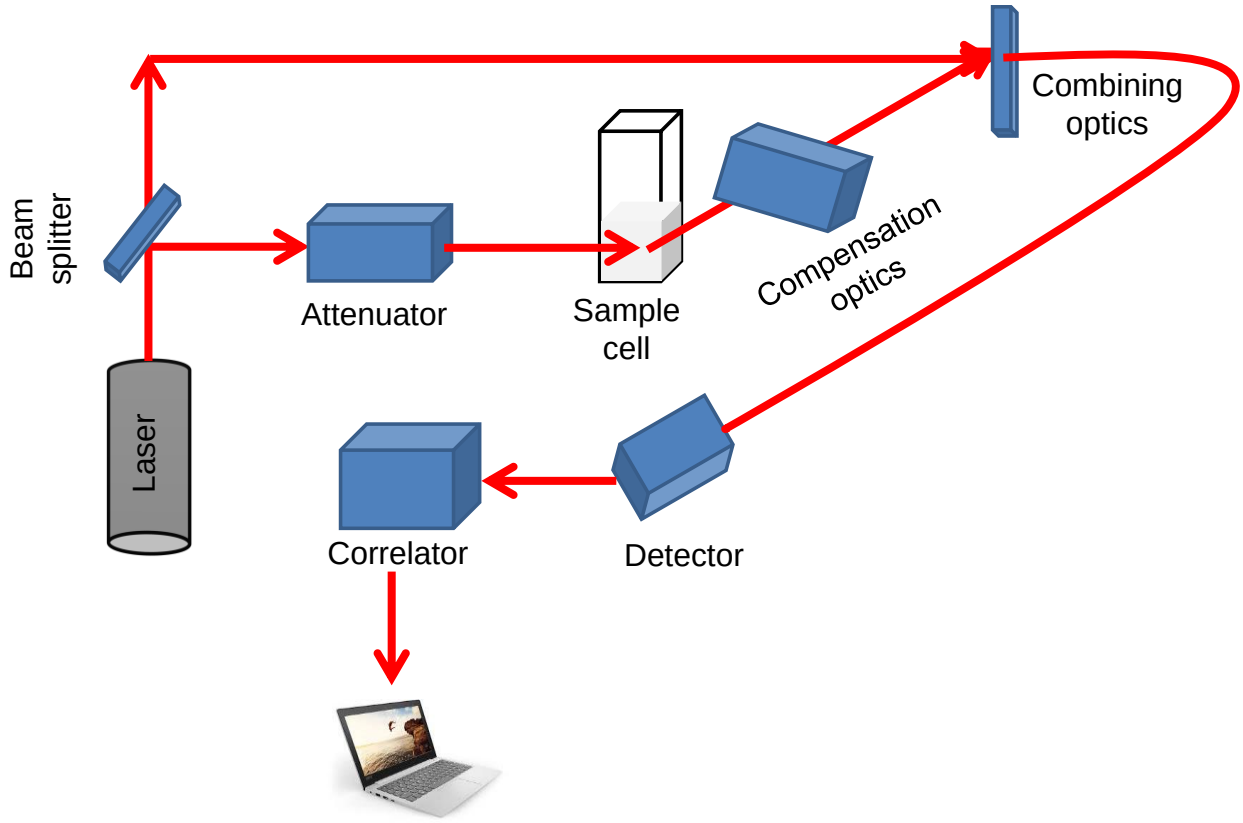

Scheme 1.17 A schematic diagram of the instrumentation of zeta potential measurement by electrophoretic light scattering.

In this thesis, plastic zeta cells were used for the ZP measurements of the emulsions. The zeta cell had inbuilt gold plated copper electrode and cell was loaded with around 1 mL of emulsion sample to conduct the measurement for every run. Before every measurement, the cell was prewashed with ethanol and water to remove any contaminants.

1.10 Thesis Goal

Two different aims are pursued in this dissertation: the first one entails investigating factors that control chemical reactivity for reactions occurring in organic-water heterogeneous systems like emulsions and suspensions, that mimic the

conditions in which “on-water” catalysis has been observed. The second aim is to demonstrate that mechanistic information can be extracted for reactions occurring at the organic-water interface in emulsions, using particle collision electrochemistry. To address these aims, the quinone tetrachlorobezoquinone was selected as a model compound because its susceptibility to hydrogen bonding and proton transfer can be monitored electrochemically by adding hydrogen bonding donors and acids that partition selectively between the phases of emulsions. Another system investigated in this work is the electrochemical mediated oxidation of water-soluble cysteine with ferrocene trapped inside organic droplets.

The long term goal of this project is to use Particle Collision Electrochemistry for ascertaining mechanistic cues of organic reactions occurring in microheterogeneous systems (emulsions, suspensions and heterogeneous catalysts) that can be useful in designing better catalysts and improving chemical reactivity. The main advantage of this newly developed electrochemical technique is the ability to obtain single and ensemble average information under in-situ conditions if the collision event is judiciously coupled to a chemical reaction of interest.

1.11 References

1. Reichardt, C. *Solvents and Solvent Effects in Organic Chemistry*, 4th ed., VCH, Weinheim, **2011**, pp207.

2. Rideout, D. C.; Breslow, R. Hydrophobic Acceleration of Diels-Alder Reaction. *J. Am. Chem. Soc.* **1980***, 102,* 7817-7818.

3. Lubineau, A. Water-Promoted Organic Reactions: Aldol Reaction under Neutral Conditions. *J. Org. Chem.* **1986**, *51*, 2144-2145.

4. Gajewski, J. J. The Claisen Rearrangement. Response to Solvents and Substituents: The Case for Both Hydrophobic and Hydrogen Bond Acceleration in Water and for a Variable Transition State. *Acc. Chem. Res.* **1997**, *30*, 219-225.

5. Breslow, R. Hydrophobic Effects on Simple Organic Reactions in Water. *Acc. Chem. Res*. **1991**, *24*, 159-164.

6. Butler, R. N.; Coyne, A. G. Water: Nature's Reaction Enforcers Comparative Effects for Organic Synthesis "In-Water" and "On-Water". *Chem. Rev.* **2010**, *110,* 6302-6337.

7. Narayan, S.; Muldoon, J.; Finn, M. G.; Fokin, V.V.; Kolb, H. C.; Sharpless, K. B. "On Water": Unique Reactivity of Organic Compounds in Aqueous Suspension. *Angew. Chem. Int. Ed.* **2005**, *44*, 3275-3279.

8. Zhang, H.–B.; Liu, L.; Chen, Y.-J.; Wang, D.; Li, C.-J. "On Water"-Promoted Direct Coupling of Indoles with 1,4-Benzoquinones without Catalyst. *Eur. J. Org. Chem.* **2006**, *2006,* 869-873.

9. Shapiro, N.; Vigalok, A. Highly Efficient Organic Reactions "on Water", "in Water", and Both. *Angew. Chem. Int. Ed.* **2008**, *47*, 2849-2852.

10. Tiwari, S.; Kumar, A. Interfacial Reactivity of "on Water" Reactions in the Presence of Alcoholic Cosolvents. *J. Phys. Chem. A* **2009**, *113,* 13685-13693.

11. Beattie, J. K.; McErlean, C. S. P.; Phippen, C. B. W. The Mechanism of On-Water Catalysis. *Chem. Eur. J.* **2010**, *16,* 8972-8974.

12. Mellouli, S.; Bousekkine, L.; Theerge, A. B.; Huck, W. T. S. Investigation of “On Water” Conditions Using a Biphasic Fluidic Platform. *Angew. Chem. Int. Ed.* **2012**, *51*, 7981-7984.

13. McErlean, C. S. P.; Beare, K. D. Revitalizing the Aromatic Aza-Claisen Rearrangement: Implications for the Mechanism of ‘On-Water’ Catalysis. *Org. Biomol. Chem.* **2013**, *11*, 2452-2459.

14. Manna, A.; Kumar, A. Why Does Water Accelerate Organic Reactions under Heterogeneous Condition?.*J. Phys. Chem. A* **2013**, *117*, 2446-2454.

15. Zuo, Y.-J.; Qu, J. How Does Aqueous Solubility of Organic Reactant Affect a Water-Promoted Reaction? *J. Org. Chem.* **2014**, *79*, 6832-6839.

16. Guo, D.; Zhu, D.; Zhou, X.; Zhen, Bo. Accelerating the “On Water” Reaction: By Organic−Water Interfaceor By Hydrodynamic Effects?. *Langmuir* **2015**, *31*, 13759-13763.

17. Butler, R. N.; Coyne, A. G. Understanding “On-Water” Catalysis of Organic Reactions. Effects of H^+ and Li^+ Ions in the Aqueous Phase and Nonreacting Competitor H-Bond Acceptors in the Organic Phase: On H_2O versus on D_2O for Huisgen Cycloadditions. *J. Org. Chem.* **2015**, *80*, 1809-1817.

18. Chandra, A,; Fokin, V. V. Organic Synthesis “On Water”. *Chem. Rev***. 2009**, *109,* 725-748.

19. Jung, J.; Marcus, R. A. On the Theory of Organic Catalysis “On Water”. *J. Am. Chem. Soc.* **2007***, 129,* 5492-5502.

20. Acevedo, Q.; Armacost, K. Claisen Rearrangements: Insight into Solvent Effects and “On Water” Reactivity from QM/MM Simulations. *J. Am. Chem. Soc.* **2010***, 132,* 1966-1975.

21. Thomas, L.L.; Tirado-Rives, J.; Jorgensen, W. Quantum Mechanical/Molecular Mechanical Modeling Finds Diels-Alder Reactions Are Accelerated Less on the Surface of Water Than in Water. *J. Am. Chem. Soc.* **2010***, 132,* 3097-3104.

22. Pereraa, P. N.; Fegaa, K. R.; Lawrenceb, C. Sundstroma, E. J.; Tomlinson-Phillipsa, J.; Ben-Amotza, D. Observation of Water Dangling OH Bonds around Dissolved Nonpolar Groups. *PNAS.* **2009**, *106*, 12230-12234.

23. Garrett, R. H.; Grisham, C. M. *Biochemistry*, 3rd ed.; Thomson Brooks/Cole: Belmont, CA, **2005**, pp 681-685.

24. Goor, G.; Glenneberg, J.; Jacobi, S. "*Hydrogen Peroxide" in Ullmann's Encyclopedia of Industrial Chemistry*, Wiley-VCH, Weinheim, **2007**.

25. Jerry, M. *Advanced Organic Chemistry: Reactions, Mechanisms, and Structure. 3rd ed. Willy, NewYork,* **1985.**

26. Quan, M.; Sanchez, D.; WasylKim, M. F.; Smith, D. K. Voltammetry of Quinones in Unbuffered Aqueous Solution: Reassessing the Roles of Proton Transfer and Hydrogen Bonding in the Aqueous Electrochemistry of Quinones. *J. Am. Chem. Soc.* **2007***, 129*, 12847-12856.

27. Gupta, N.; Linschitz, H. Hydrogen-Bonding and Protonation Effects in Electrochemistry of Quinones in Aprotic Solvents. *J. Am. Chem. Soc.* **1997***, 119*, 6384-6391.

28. Wilford, J. H.; Archer, M. D. Solvents Effects on the Redox Potentials Benzoquinone. *J. Electroanal. Chem.* **1985**, *190*, 271-277.

29. Peover, M. E.; Davis, J. D. The Influence of Ion-Association on the Polarograpgy of Quinones Dimethylformamide. *J. Electroanal. Chem.* **1963**, *6*, 46-53.

30. Tessensohn, M. E. Webster, R. D. Using Voltammetry to Measure Hydrogen-Bonding Interactions in Non-Aqueous Solvents: A Mini-Review. *Electrochem. Commun.* **2016**, *62*, 38-43.

31. Macı´as-Ruvalcaba, N. A.; Gonza´lez, I.; Aguilar-Martı´nez, M. Evolution from Hydrogen Bond to Proton Transfer Pathways in the Electroreduction of α-NH-Quinones in Acetonitrile. *J. Electrochem. Soc***. 2004**, *151*, E110-E118.

32. Go´mez, M.; Gonza´lez, F. J.; Gonza´lez, I. Effect of Host and Guest Structures on Hydrogen Bonding Association Influence on Stoichiometry and Equilibrium Constants. *J. Electrochem. Soc*. **2003**, *150*, E527-E534.

33. Alligrant, T. M.; Hackett, J. C.; Alvarez, J. C. Acid/Base and Hydrogen Bonding Effects on the Proton-Coupled Electron Transfer of Quinones and Hydroquinones in Acetonitrile: Mechanistic Investigation by Voltammetry, ^{1}H NMR and Computation. *Electrochim. Acta* **2010**, *55,* 6507-6516.

34. Alligrant, T. M.; Alvarez, J. C. The Role of Intermolecular Hydrogen Bonding and Proton Transfer in Proton-Coupled Electron Transfer. *J. Phys. Chem. C* **2011**, *115*, 10797-10805.

35. Katsumi, J., Nakayama, T.; Esaka, Y.; Uno, B. Mechanistic Study on the Electrochemical Reduction of 9,10-Anthraquinone in the Presence of Hydrogen-bond and Proton Donating Additives. *Anal. Sci.* **2012**, *28*, 257-265.

36. Given, P. H.; Peover, M. E. Polarographic Reduction of Aromatic Hydrocarbons and Carbonyl Compounds in Dimethylformamide in the Presence of Proton-Donors. *J. Chem. Soc.* **1960**, 385-393.

37. Ashnagar, A.; Bruce, J. M.; Dutton, P. L.; Prince, R. C. One- and Two-Electron Reduction of Hydroxy-1,4-Naphthoquinones and Hydroxy-9,10-Anthraquinones. The Role of Internal Hydrogen Bonding and Its Bearing on the Redox Chemistry of the Anthracycline Antitumour Quinones. *Biochim. Biophys. Acta* **1984**, *801*, 351-359.

38.Hung, M.; Stanbury, D. M. Catalytic and Direct Oxidation of Cysteine by Octacyanomolybdate(V). *Inorg. Chem.* **2005**, *44*, 3541-3550.

39. Sun, S.; Stanbury, D. M. Kinetics and Mechanism of Oxidation of Thioglycolic Acid by Hexachloroiridate(IV). *Dalton Trans.* **2002**, 785-791.

40. Casado, C. M.; Cuadrado, I.; Morán, M.; Alonso, B.; Barranco, M.; Losada, J. Cyclic Siloxanes and Silsesquioxanes as Cores and Frameworks for the Construction of Ferrocenyl Dendrimers and Polymers. *Appl. Organomet. Chem.* **1999**, *13*, 245−259.

41. Fomin, F. M.; Zaitseva, K.S. Mechanism of the Oxidation of Ferrocene and Its Derivatives with Hydrogen Peroxide: A New Effect. *Zhurnal Fizicheskoi Khimii,* **2014**, *88*, 468-472.

42. Lawrence, N. S.; Tustin, G. J.; Faulkner, M.; Jones, T. G. J. Ferrocene Sulfonates as Electrocatalysts for Sulfide Detection. *Electrochim. Acta* **2006**, *52*, 499−503.

43. Torriero, A. A. J.; Shiddiky, M. J. A.; Burgar, I.; Bond, A. M. Homogeneous Electron-Transfer Reaction between Electrochemically Generated Ferrocenium Ions and Amine-Containing Compounds. *Organometallics* **2013**, *32*, 5731−5739.

44. Tadros, T. F. *Emulsions Formation, Stability, Industrial Applications*. Walter de Gruyter GmbH, Berlin, 2016, pp 1-5, 76-77.

45. Salou, M.; Siffert, B.; Jada, A. Study of the Stability of Bitumen Emulsions by Application of DLVO Theory. *Colloids Surf. A* **1998**, *142*, 9-16.

46. Poce-Fatou, J. A. A Superficial Overview of Detergency. *J. Chem. Educ.* **2006**, *83*, 1147-1151.

47. Sepunaru, L.; Plowman, B. J.; Sokolo, S. V.; Young, N.P.; Compton, R. G. Rapid Electrochemical Detection of Single Influenza Viruses Tagged with Silver Nanoparticles. *Chem. Sci.* **2016**, *7*, 3892-3299.

48. Calzolai, L.; Gilliland, D.; Rossi, F. Measuring Nanoparticles Size Distribution in Food and Consumer Products: A Review. *Food Addit. Contam.* **2012,** *29*, 1183-1193.

49. Zhou, Y. G.; Rees, N. V.; Compton, R. G. The Electrochemical Detection and Characterization of Silver Nanoparticles in Aqueous Solution. *Angew. Chem. Int. Ed.* **2011,** *50*, 4219-4221.

50. Cheng, W.; Compton, R. G. Investigation of Single-Drug-Encapsulating Liposomes Using the Nano-Impact Method. *Angew. Chem. Int. Ed.* **2014**, *53*, 13928-13930.

51. Rees, N. V. Electrochemical Insight from Nanoparticle Collisions with Electrodes: A mini-review. *Electrochem. Commun.* **2014**, *43*, 83-86.

52. Kim, B. K.; Boika, A.; Kim, J.; Dick, J. E.; Bard, A. J. Characterizing Emulsions by Observation of Single Droplet Collisions-Attoliter Electrochemical Reactors. *J. Am. Chem. Soc.* **2014,** *136*, 4849−4852.

53. Zhou, H.; Park, J. H.; Fan, F. R. F.; Bard, A. J. Observation of Single Metal Nanoparticle Collisions by Open Circuit (Mixed) Potential Changes at an Ultramicroelectrode. *J. Am. Chem. Soc.* **2012**, *134*, 13212-13215.

54. Xiao, X.; Bard, A. J. Observing Single Nanoparticle Collisions at an Ultramicroelectrode by Electrocatalytic Amplification. *J. Am. Chem. Soc.* **2007**, *129*, 9610-9612.

55. Heyrovsky, M.; Jirkovsky, J. Mueller, B. R., Polarography and Voltammetry of Aqueous Colloidal SnO_2 Solutions. *Langmuir* **1995**, *11*, 4293-4299.

56. Heyrovsky, M.; Jirkovsky, J. Polarography and Voltammetry of Ultrasmall Colloids: Introduction to a New Field. *Langmuir* **1995**, *11*, 4288-4292.

57. Zhou, H.; Fan, F. R. F.; Bard, A. J. Observation of Discrete Au Nanoparticle Collisions by Electrocatalytic Amplification Using Pt Ultramicroelectrode Surface Modification. *J. Phys. Chem. Lett.* **2010**, *1*, 2671-2674.

58. Zhou, Y. G.; Haddou, B.; Rees, N. V.; Compton, R. G. The Charge Transfer Kinetics of the Oxidation of Silver and Nickel Nanoparticles via Particle–Electrode Impact Electrochemistry. *Phys. Chem. Chem. Phys.* **2012**, *14*, 14354-14357.

59. Haddou, B.; Rees, N. V.; Compton, R. G. Nanoparticle–Elctrode Impacts: the Oxidation of Copper Nanoparticles has Slow Kinetics. *Phys. Chem. Chem. Phys.* **2012**, *14*, 13612-13617.

60. Kwon, S. J.; Fan, F. R. F.; Bard, A. J. Observing Iridium Oxide (IrOx) Single Nanoparticle Collisions at Ultramicroelectrodes. *J. Am. Chem. Soc.* **2010**, *132*, 9610-9612.

61. Sardesai, N. P.; Andreescu, D.; Andreescu, S. Electroanalytical Evaluation of Antioxidant Activity of Cerium Oxide Nanoparticles by Nanoparticle Collisions at Microelectrodes. *J. Am. Chem. Soc.* **2013**, *135*, 16770-16773.

62. Boika, A.; Thorgaard, S. N.; Bard, A. J. Monitoring the Electrophoretic Migration and Adsorption of Single Insulating Nanoparticles at Ultramicroelectrodes. *J. Phys. Chem. B* **2013**, *117*, 4371−4380.

63. Quinn, B. M.; van 't Hof, P. G.; Lemay, S. G. Time-Resolved Electrochemical Detection of Discrete Adsorption Events. *J. Am. Chem. Soc.* **2004**, *126*, 8360-8361.

64. Cheng, W.; Zhou, X.-F.; Compton, R. G. Electrochemical Sizing of Organic Nanoparticles. *Angew. Chem. Int. Ed.* **2013**, *52*, 12980-12982.

65. Omiatek, D. M.; Dong, Y.; Heien, M. L.; Ewing, A. G. Only a Fraction of Quantal Content is Released During Exocytosis as Revealed by Electrochemical Cytometry of Secretory Vesicles. *ACS Chem. Neurosci.* **2010**, *1*, 234-245.

66. Lebègue, E.; Anderson, C. M.; Dick, J. E.; Webb, L. J.; Bard, A. J. Electrochemical Detection of Single Phospholipid Vesicle Collisions at a Pt Ultramicroelectrode. *Langmuir* **2015**, *31*, 11734-11739.

67. Toh, H. S.; Compton, R. G. Electrochemical Detection of Single Micelles through 'Nano-Impacts. *Chem. Sci.* **2015**, *6*, 5053-5058.

68. Li, Y.; Deng, H.; Dick, J. E.; Bard, A. J. Analyzing Benzene and Cyclohexane Emulsion Droplet Collisions on Ultramicroelectrodes. *Anal. Chem.* **2015**, *87*, 11013-11021.

69. Cheng, W.; Compton, R. G. Oxygen Reduction Mediated by Single Nanodroplets Containing Attomoles of Vitamin B_{12}: Electrocatalytic Nano-Impacts Method. *Angew. Chem. Int. Ed.* **2015,** *54*, 7082-7085.

70. Kulichenko, S. A.; Shevchenko, G. M**.** Triton X-100 Stabilized “Oil-in-Water” Emulsions as Suitable Media for Alkalimetric Determination of Hydrophobic Organic Acids. *Anal. Bioanal. Chem.* **2003**, *375*, 255-258.

71. Opawale, F. O.; Burgess, J. D., Influence of Interfacial Properties of Lipophilic Surfactants on Water-in-Oil Emulsion Stability. *J. Colloid Interface Sci.* **1998,** *197*, 142-150.

72. Foster, J. R. Microelectrodes: New Dimensions in Electrochemistry. *Chem. Soc. Rev*. **1994**, *23*, 289-297.

73. Wightman, R. M. Microvoltammetric Electrodes. *Anal. Chem.*, **1981**, *53*, 1125A-1134A.

74. Danis, L.; Polcari, D.; Kwan, A.; Michelle, S.; Mauzeroll, J. Fabrication of Carbon, Gold, Platinum, Silver, and Mercury Ultramicroelectrodes with Controlled Geometry. *Anal. Chem.* **2015**, *87*, 2565-2569

75. Bard, A. J.; Faulkner, L.R. *Electrochemical Methods: Fundamentals and Applications*. 2nd ed.; Willy, New York, 2001, pp 156-163.

76. Lim, J.; Yeap, S. P.; Che, H. X.; Low, S. C. Characterization of Magnetic Nanoparticle by Dynamic Light Scattering. *Nanoscale Res. Lett.* **2013***, 8*, 381-384.

77. Bhattacharjee, S. DLS and zeta potential – What they are and what they are not? *J. Controlled Release* **2016**, *235*, 337-351.

Chapter 2

Reversal of Hydrogen Bonding Equilibria due to Micro-Confinement of Immiscible Phases in Toluene-Water Emulsions Studied by Particle Collision Electrochemistry

Abstract: This work describes a reversal of hydrogen bonding affinity driven by micro-compartmentalization of polydisperse toluene droplets (0.4 to 4.0 μm) in water. When no heterogeneous water phase is present in toluene, the phenolate dianion ($TCBQ^{2-}$) generated electrochemically by reduction of tetrachloro-1,4-benzoquinone (TCBQ), shows higher degree of hydrogen bonding with acetic acid (pK_a = 4.8) than oleic acid (pK_a = 9.9). Such result, which was easily confirmed by monitoring the positive shift (easier to reduce) on the redox potential of TCBQ, is consistent with previous literature and the pK_a of the mono- (8.0) and di-protonated (5.8) hydroquinone ($TCBQH_2$). In contrast, when the reduction takes place inside toluene droplets dispersed in water, the reverse scenario is observed. That is, the weak H-donor, oleic acid produces a larger positive potential shift than acetic acid, because of their opposite preference to partition between toluene and water. This outcome is revealed by studying the electrochemical response of the toluene droplets loaded with TCBQ using Particle Collision Electrochemistry (PCE). The effect could play a role in aqueous micro-heterogenous systems involving other chemical reactions. PCE is an approach that allows interrogation of single microscopic particles in Brownian motion colliding with an ultramicroelectrode, and can render unique information if the collision encounter is judiciously coupled to a chemical event. This work aims to illustrate a subtle, yet consequential effect that emerges from micro-confinement of immiscible phases, as well

as the mechanistic information that can be extracted at the organic-water interface by using PCE.

2.1 Introduction

In some cases, the role of water in increasing the rate of organic chemical reactions has been demonstrated as to be caused by the hydrophobic effect,[1,2] but in others, it has defied unified consensus.[3] For instance, the term “on-water” catalysis was coined to describe the remarkable rate enhancement observed for reactions of insoluble organic compounds in aqueous suspensions and emulsions.[3] Such an effect, seemingly originated from the organic-water phase boundary, has been confirmed in succeeding reports, even though a variety of explanations have been put forward.[4-17] For example, trans-phase hydrogen bonding with water dangling OH groups to stabilize organic transition states,[8,13] proton transfer across the interface coupled with acid-base catalysis,[4,14] water and cosolvent solubility,[11,15] and finally, hydrodynamic effects.[7] Similarly, in heterogeneous catalysis, despite elusive mechanistic understanding, the crucial role of water has been collectively recognized[18-22] in technologically relevant reactions like carbon monoxide oxidation,[20] alcohol oxidation,[21] Fischer-Tropsch,[22] and others.[18] These examples show that the role of water in organic reactions is highly nuanced and complex. Herein, we report a case of hydrogen bonding affinity driven by the phase immiscibility in aqueous emulsions of toluene droplets, that is completely reversed in homogeneous toluene when only adventitious water is present. The effect is uncovered by studying the electrochemical reduction of tetrachloro-1,4-benzoquinone (TCBQ) to $TCBQ^{2-}$ inside the droplets (Scheme 2.1) employing Particle Collision

Electrochemistry (PCE).[23-31] This latter is a methodology recently developed for characterization of microscopic particles in solution as they collide with the surface of an ultramicroelectrode (UME) by virtue of Brownian motion.[32] The quality of PCE to interrogate discrete collisions of particles, providing single particle information, have inspired fundamental studies leading to the sub-field *single entity electrochemistry*,[32-33] which now has compiled investigations on a wide variety of particles[34-38] including DNA,[34] viruses,[35] blood cells,[36] cancer cells,[37] nanoparticles,[38] vesicles[39] and emulsion droplets.[25] The goal of this work is two-fold, first, to uncover chemical effects derived from micro-confinement of organic immiscible phases in water, and second, to show how PCE can be used to characterize such effects.

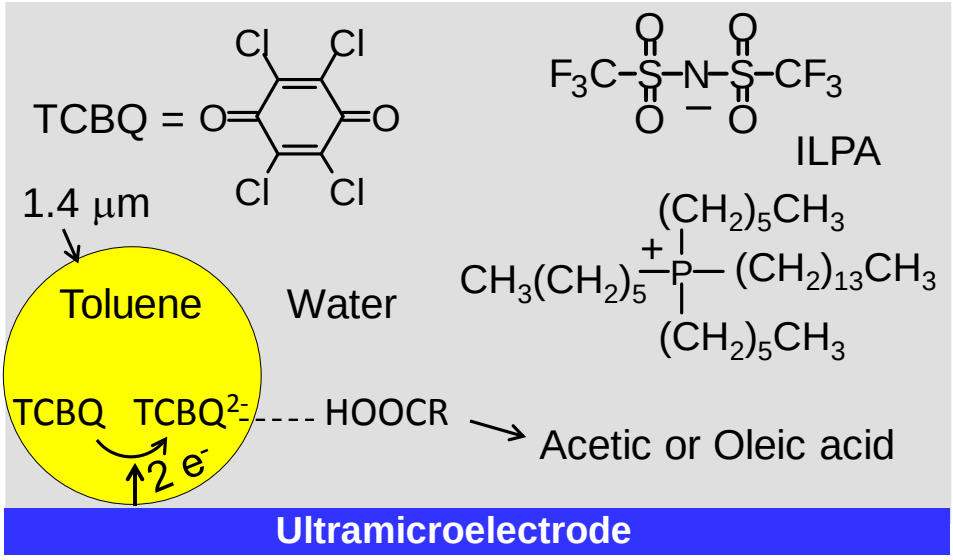

Scheme 2.1 PCE of toluene droplets in water.

Given the low polarity of toluene, for this work, the ionic liquid trihexyltetradecylphosphonium bis(trifluoromethylsulfonyl)amide (ILPA) was added to improve ion conduction and emulsification of the droplets (Scheme 2.1).[25] The study also included size and zeta potential (η) measurements by Dynamic Light Scattering

(DLS), as well as cyclic voltammetry of TCBQ in homogeneous toluene. Considering the well-documented affinity of quinone anions for hydrogen bonding in aprotic solvents,[40-48] particularly with alcohols,[40] water,[41,42] and carboxylic acids,[45,47] we selected acetic and oleic acid (RCOOH) as hydrogen bonding donors (HD) because they display contrasting levels of hydrophobicity. Likewise, TCBQ was chosen because its hydrogen bonding with alcohols and acids has been electrochemically characterized in several aprotic solvents.[40]

Electrochemistry is one of the best methods to determine hydrogen bonding because it offers better sensitivity than UV-Vis spectroscopy,[44,48] it can handle both paramagnetic and diamagnetic species, unlike NMR spectroscopy;[45,46] and at high concentration (>> 1 mM), the signal is not overwhelmed by a large excess of H or OH, as it would be for ^{1}H NMR and IR spectroscopy. Typically, in aprotic media, a neutral quinone like TCBQ undergoes two consecutive one-electron transfers, to yield the radical anion $TCBQ^{\bullet-}$ at potential E_1, succeeded by the dianion $TCBQ^{2-}$ produced at a more negative potential E_2. Incremental addition of HD species prompts a shift in E_1 and/or E_2 towards less negative potentials (easier to reduce), depending on the pK_a of the conjugate acids $TCBQH^{\bullet}$ and $TCBQH_2$ with respect to HD.[40] The separation $\triangle E_{1\text{-}2}$ is also determined by the polarity of the solvent [40] and the supporting.[49]

2.2 Experimental Section

2.2.1 Reagents and Materials

Tetrachloro-1,4-benzoquinone (TCBQ, Aldrich, 99.0%), trihexyltetradecylphosphonium bis(trifluoromethylsulfonyl)amide (ILPA, Sigma-Aldrich,

≥95.0%), tetrabutylammonium perchlorate (TBAP, Fluka, ≥99.0%), oleic acid (Alfa Aesar, 90.0%), acetic acid (Sigma-Aldrich, ≥97.7%), ferrocenemethanol (Fisher, 97.0%), potassium chloride (KCl, Fisher, 99.99%), Silver (Ag) Epoxy (Epoxy technology), Epon^{TM} resin 820 (Miller-stephenson), *m*-phenylenediamine (Aldrich, 99.0%), acetonitrile (Acros, 99.9%), ethanol (Fisher, 99.5%) and 2-propanol (Sigma-Aldrich, ≥99.7%) were all used as received. Toluene (Fisher, ≥99.9%) was distilled prior to use. Carbon fiber was generously donated by Prof. Maryanne M Collinson. Borosilicate glass capillary was obtained from Kansas State University, (Manhattan, KS). Millipore water (18.2 MΩ.cm) was used throughout the experiments.

2.2.2 Instrumentation

All electrochemical measurements were carried out using a potentiostat CHI model 660C (CH Instruments, Austin, TX) equipped with a standard three-electrode cell placed in a faradic cage. For voltrammetric measurements experiment in acetonitrile, a glassy carbon macroelectrode (3 mm diameter) was used as the working electrode, a Pt wire as the counter electrode and a silver (Ag) wire coated with silver chloride served as the quasi-reference electrode (QRE). Before each voltammetric experiment, the glassy carbon macroelectrode was polished with 0.05 μm alumina mixed with water and rinsed with acetonitrile followed by drying with nitrogen. In Particle Collision experiments, the working electrode was a 4.3 μm radius carbon fiber-UME. A 0.5 mm diameter Pt - wire was used as the counter electrode and the reference electrode was Ag/AgCl/1 M KCl. All working solutions were deaerated by bubbling nitrogen for 15 mins prior to performing the experiments and nitrogen atmosphere was maintained inside the cell during the experimental period. A vortex model Genie 2 (Fisher, Waltham MA) and an

ultrasonic bath model Branson 1510 were employed to prepare the emulsions. The dynamic light scattering (DLS) experiments were performed into a disposal plastic cuvette using a Zetasizer Nano ZS instrument (Malvern, Westborough, MA). Zeta potential measurements were also carried out in the same instrument. Three different samples were run for the measurement of both size and zeta potential. The "Signal Counter" program (Center for Marine and Environmental Research, Zagreb, Coroatia) was used for spike identification and individual spike area calculation.

2.2.3 Preparation of Carbon Fiber Ultramicroelectrode (C-UME)

C-UME was prepared based on the general procedure developed in our laboratory according to the previous literature.[50] At the beginning, glass capillaries were cleaned by sonication in ethanol followed by water and dried in an oven (100 ºC) for 2 h. 1 cm length of carbon fiber was connected to a copper wire using conductive Ag epoxy (epo-teck H20E, parts A and parts B), which was subsequently cured around 100 ºC overnight in an oven. Epon^{TM} resin 820 was mixed 15% (w/w) *m*-phenylenediamine hardener and heated upto 75 ºC. The fiber was then inserted carefully into a clean capillary and dipped into the mixture for 1 min. Next, the capillary was kept in an oven at 140 ºC for 12 h for complete sealing. The other end of the electrode was sealed with Torr Seal epoxy (1:2 ratio) and dried in oven for 10 minutes. Finally the electrode was then gently wet polished for 10 to 30 seconds on 600 grit sandpaper and then polished with 0.05 μm alumina with distilled water on microcloth pads. A steady-state voltammogram was recorded to examine the radius of prepared electrodes in 0.1 M KCl aqueous solution of 1.0 mM ferocenemethanol at scan rate 10 mV/s. The radius of the

electrode was calculated by using equation 2.1. The calculated radius of the prepared C-UME was 4.3 µm.

$$i_{ss} = 4nFDrC \ldots\ldots\ldots\ldots\ldots\ldots (2.1)$$

where i_{ss} = steady-state current in ampere, n = number of electrons, F = Faraday's constant (96487 C/mole e^-), D = diffusion coefficient of ferrocenemethanol (7.8 x 10^{-6} cm^2/s)[50], C = concentration in mole/cm^3, r = radius of the C- fiber UME (µm).

2.2.4 Emulsions Preparation

The toluene/water emulsions were prepared[25] by following the literature method with slight modification. In a typical preparation, 5 mM of TCBQ was added to 355 µL of toluene in a vial, followed by the addition of 145 µL of ILPA (0.4 M) to form a homogeneous mixture. Afterwards, 100 µL of this toluene mixture were added to 5 mL of degassed deionized Milli pure water. Finally the content of the vial was mixed vigorously for 20 s in a vortex mixer and sonicated for 5 min at room temperature. An emulsion was formed and showed stability up to 6 h. Here, ionic liquid served as both supporting electrolyte and emulsifier. Two different sizes of emulsion droplets (diameter 257.6 nm and 1439 nm) were observed at DLS measurement. The concentration of the toluene (TCBQ + ILPA) emulsion droplets was calculated from the total toluene (TCBQ + ILPA) volume (0.1 mL) divided by the average emulsion droplet (diameter 1439 nm) volume (1.56 fL). Accordingly, the molar concentration of the emulsion droplets was 21.2 pM as used for the electrochemical collisions experiments. Details calculation is shown in supporting information. All particle collisions measurements were finished within 1 h.

Other toluene emulsions were prepared following the same procedure including oleic acid and acetic acid. In both cases, DLS data showed two different sizes of emulsion droplets (264.5 nm, 1478 nm with oleic acid and 286.3 nm, 1485 nm with acetic acid). The concentration of the toluene (TCBQ + ILPA) emulsion droplets with oleic acid and acetic acid were also calculated from the total toluene (TCBQ + ILPA) volume (0.1 mL) divided by the average emulsion droplet and concentrations were 19.6 pM and 19.3 pM respectively. Emulsions with additives (acetic and oleic acid) were also stable up to 6 h (Scheme 2.2)

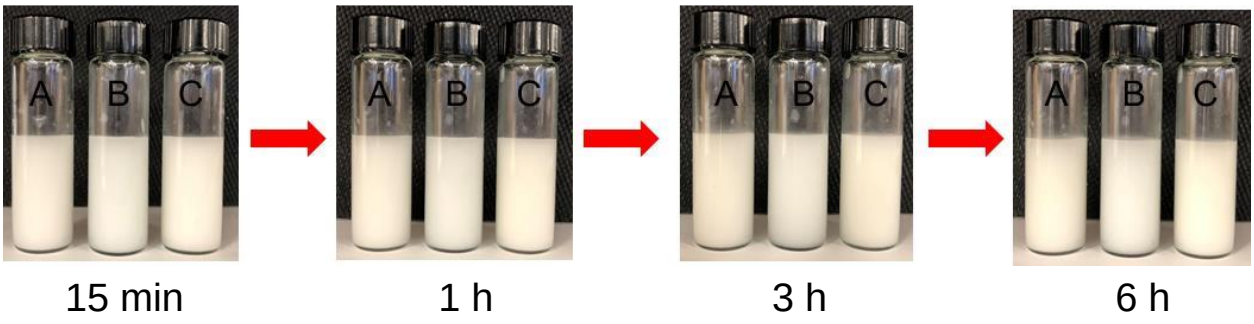

Scheme 2.2 Photograph of emulsions at different time intervals. (A) toluene (5 mM TCBQ + 400 mM ILPA)/water emulsion, (B) toluene (5 mM TCBQ + 400 mM ILPA)/water emulsion with 50 mM oleic acid and (C) toluene (5 mM TCBQ + 400 mM ILPA)/water emulsion with 50 mM acetic acid.

2.3 Results and Discussion

2.3.1 Effect of Hydrogen bonding on Reduction of TCBQ in Bulk Toluene

Figure 2.1 shows the cyclic voltammograms (CV) for 5 mM of TCBQ and 0.4 M of ILPA in homogenous toluene, and in the presence of equal concentration of the HD molecules. The three CVs show the typical response for a UME of radius 4.3 µm, with a current that initially rises at 0.2 V and reaches a plateau at ~-0.3 V when the current becomes limited by diffusion.[51] Despite the aprotic character of toluene, the reduction of pristine TCBQ appears as a single $2e^-$-wave equation 2.2 centered at E ≈ -0.18 V.

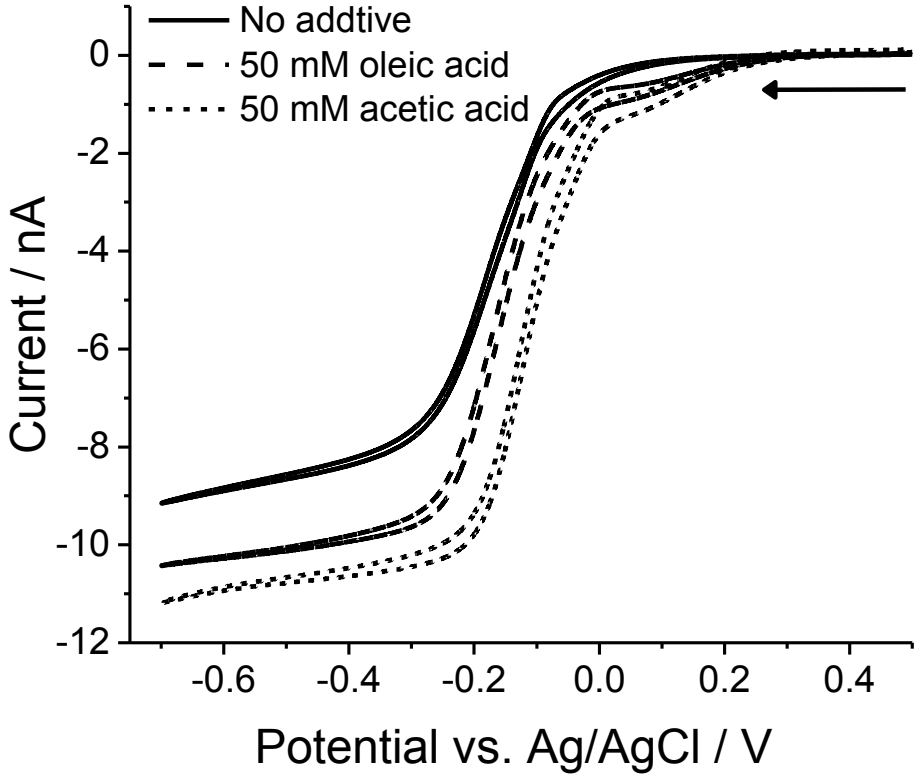

Figure 2.1 CV response for 5.0mM TCBQ and 0.4 M ILPA in toluene with a C-UME (4.5 µm radius). Scan rate 20 mV/s.

This is attributed to the low polarity[40] of toluene as well as the preferential stabilization of the dianion $TCBQ^{2-}$ by ion pairing with the cation of ILPA.[49] Both HD additives display higher current plateaus than TCBQ alone and a displacement of E towards positive potentials (easier reduction), due to hydrogen bonding (equation 2.3) and/or protonation of the dianion.[10] The small current shoulder between 0.2 and 0.0 V is ascribed to the first electron reduction that produces the radical monoanion $TCBQ^{\bullet-}$, which now appears marginally, due to hydrogen bonding. This assignment is congruent with the two $1e^-$-waves observed upon incremental additions of ethanol as hydrogen bonding kicks in and polarity of the toluene mixture increases (Figure 2.2). Accordingly, the hydrogen

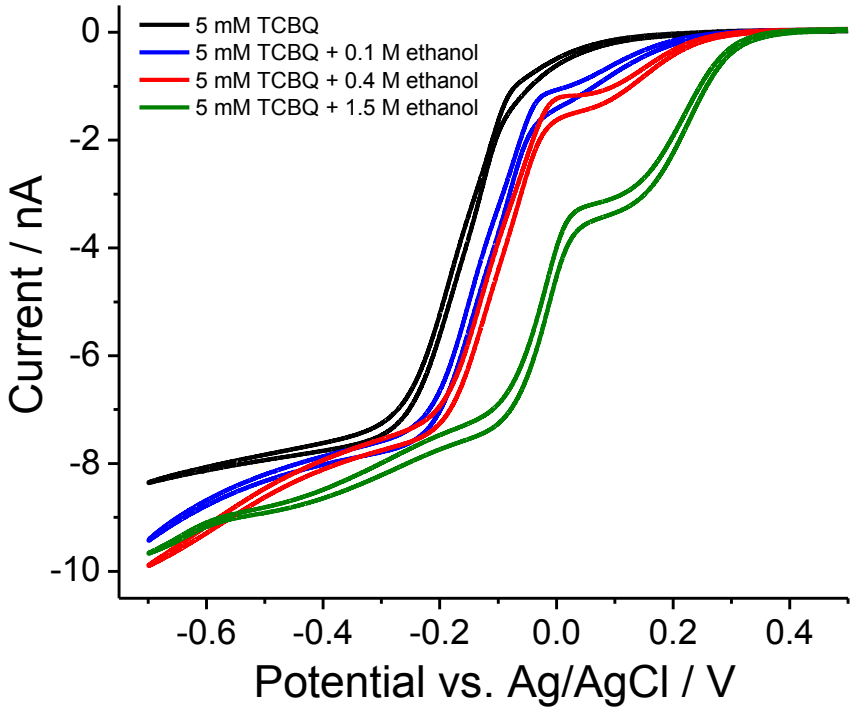

Figure 2.2 Cyclic voltammograms of TCBQ and 0.4 M ILPA at different concentrations of ethanol in toluene on C UME (radius 4.3 μm). Scan rate = 20 mV/s.

bonding equilibrium of ethanol with $TCBQ^{2-}$ (K_{HB} = 6.3 x 10^3) and $TCBQ^{\bullet-}$ in acetonitrile has been reported previously.[40] In any case however, for homogeneous toluene, acetic acid furnishes a larger positive shift of E and a higher current than oleic acid. The latter effect is attributed to disproportionation of the radical monoanion, $2TCBQ^{\bullet-} = TCBQ + TCBQ^{2-}$, assisted by hydrogen bonding of $TCBQ^{2-}$, so that the more $TCBQ^{2-}(HD)_x$ complex is produced, the more TCBQ is available to reduce.[40]

$$TCBQ + 2\,e^- \rightleftharpoons TCBQ^{2-} \quad \ldots\ldots\ldots\ldots\ldots\ldots\ldots \quad (2.2)$$

$$TCBQ^{2-} + xHD \rightleftharpoons TCBQ^{2-}(HD)_x \quad K_{HB} >> 1 \ldots\ldots\ldots \quad (2.3)$$

$$E = E_f + \frac{0.059}{2}\left(logK_{HB} + log[HD]^x - log\frac{[TCBQ^{2-}(HD)_x]}{[TCBQ]}\right) \ldots\ldots\ldots \quad (2.4)$$

The shift of E in Figure 2.1 can be qualitatively explained by substituting the hydrogen boding equilibrium, K_{HB}, into the Nernst expression for equation 2.2 to obtain equation 2.4,[51] where E_f is the formal potential for reaction 2.2. Despite the oversimplified description, equation 2.4 shows that, by increasing the concentration of HD or the equilibrium constant K_{HB}, a positive shift in E is expected. The same rationale can be applied to a protonation equilibrium provided it occurs subsequent to the electron transfer.[40] Accordingly, protonation and hydrogen bonding of quinones in aprotic media, produce similar effects on CVs and can be distinguished when considering pK_a values[40] and/or using ^1H NMR[45,46].

Table 2.1 Aqueous pK_a values for species in this work.

Species	$TCBQH_2$[a]	$TCBQH^-$[a]	Acetic	Oleic[b]
pK_a	5.8	8.0	4.8	9.9

[a] Ref 52, [b] Ref 53

Given the pK_a values for TCBQ[52] and oleic acid[53] (Table 2.1), the dominant contribution for this pair, should be hydrogen bonding because proton transfer (PT) to $TCBQ^{2-}$ and $TCBQ^{\bullet-}$, is disfavored thermodynamically. The measured pK_a of long-chain carboxylic acids has been found to vary from 6.5 to 9.0 as the chain length increases from C_8 to C_{16}.[54] This effect, which is due to inter-chain interactions, favors chain aggregation thus reducing ionization of the COOH group to render a relative high pK_a of oleic acid.[53] For the pair acetic-TCBQ, some level of PT is expected, yet, experimentally it is found that protonation of quinone mono and dianions is significantly hindered as solvent polarity decreases.[40] Consequentially, we attribute the effects in Figure 2.1, mostly to hydrogen bonding with some contribution of protonation in the case of acetic acid. This would explain the similarity in the magnitude of the shift observed with both acids at the same concentration. Cyclic voltammograms were also performed for 5 mM of TCBQ in acetonitrile and toluene in the presence of different concentrations of acetic acid, oleic acid (Appendix). Shifting of E was observed to positive direction (easy to reduce) as increasing the concentration of both acetic acid and oleic acid.

2.3.2 Particle Collision Electrochemistry of the Toluene/water Emulsion Droplets

The toluene droplets were studied using PCE by stepping the potential of a carbon UME to a value negative enough to drive the reduction of TCBQ. At this point, electron transfer between the droplet contents and the UME can occur through the point of contact during random collisions.[25,26] Such stochastic encounters appear as current (*i*) spikes (see below) superimposed on the charging baseline of the UME recorded as a function of time (*t*). Assuming diffusion as dominant mode of mass transport, the droplet collision frequency (f_d) depends on the droplet's diffusion coefficient (D_d), its concentration (C_d) and the electrode radius (r_e) in accordance to equation 2.5, where N_A = Avogadro's number. [25,26]

$$f_d = 4D_d C_d r_e N_A \quad \ldots\ldots\ldots\ldots\ldots\ldots (2.5)$$

The size of the droplet exerts its influence on f_d through D_d conforming to the Stokes-Einstein equation 2.6.[25,26]

$$D_d = \frac{k_B T}{6\pi\eta r_d} \ldots\ldots\ldots\ldots\ldots\ldots (2.6)$$

where k_B is the Boltzmann constant, T is the absolute temperature, η is the viscosity of water at 25 ºC and r_d is the radius of the droplet.

The dwell time of the collisions, which is also affected by droplet size, determines the width and height of the current spikes, also controlled by the concentration of TCBQ. However, if solubility precludes ion partition to maintain neutrality within the droplet in response to electrolysis, the spike height may be partially or totally curtailed.[23,31] That is, despite collisions, spikes will not appear if the interphase crossing of ions to balance electron transfer in the droplet is blocked.[23,31] Notwithstanding this caveat, each spike

has a time-dependent current response, $i_{spike}(t)$, with a peak current (i_p) that decays exponentially following the bulk electrolysis model of a femto or zeptoliter reactor (equation 2.7).[25,26] This equation presupposes that the electron transfer from inside the droplet at the imposed potential occurs at such a rate that is limited by diffusion. In this case, r_{ef} is the effective contact radius in the collision, D_{TCBQ} is the diffusion coefficient of TCBQ in toluene and V is the droplet volume.[25,26]

$$i_{spike}(t) = i_p e^{-\left(\frac{4 r_{ef} D_{TCBQ}}{V}\right) t} \quad \ldots\ldots\ldots\ldots\ldots\ldots \quad (2.7)$$

Figure 2.3 displays *i-t* curves recorded for 1000 s at -0.5 V vs Ag/AgCl of aqueous emulsions of toluene droplets loaded with TCBQ and ILPA in the same conditions of Figure 2.1: no additive, 50 mM of acetic acid, and 50 mM of oleic acid. In the presence of the latter, i_{spike} shows on average the highest values, whereas droplets with no additive have the smallest spikes. Control experiments without TCBQ in the toluene droplets show no spikes in Figure 2.4.

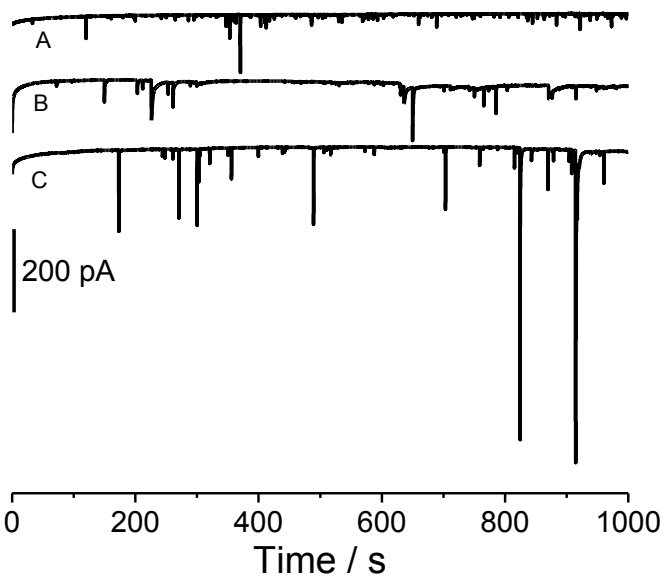

Figure 2.3 *i-t* curves for toluene droplets (5.0 mM TCBQ, 0.4 M ILPA) in water. A) No additive, B) 50 mM acetic acid, C) 50 mM oleic acid.

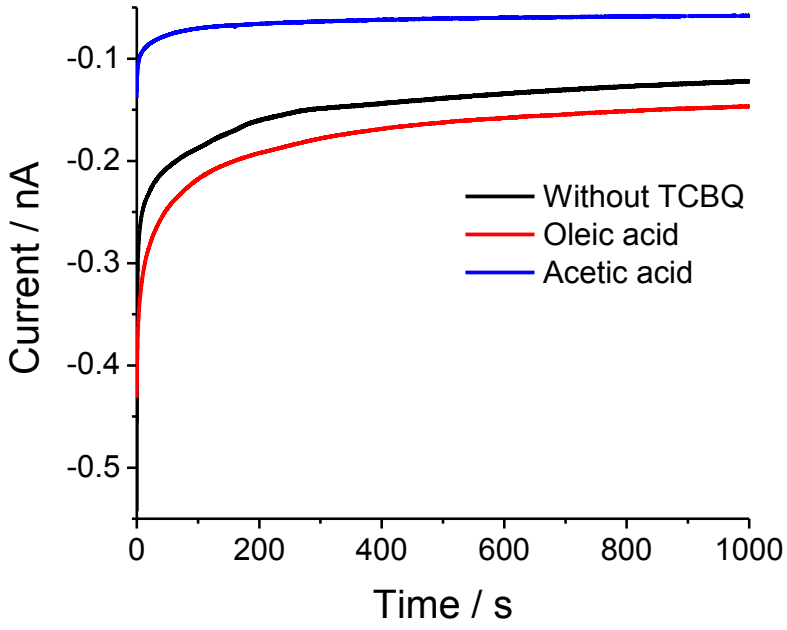

Figure 2.4 *i-t* curves for toluene droplets (without TCBQ, 0.4 M ILPA), with 50 mM acetic acid and with 50 mM oleic acid with C- UME (radius 4.3 μm) at -0.5 V versus Ag/AgCl.

To confirm that the variation in i_{spike} is driven mostly by chemical effects rather than particle size and polydispersity, the average droplet diameter from size distributions obtained by DLS was determined thrice for each condition in Figure 2.3 (Table 2.2 and Figure 2.5). All droplets regardless of additive had an average diameter of 1.4 µm and a similar polydispersity index (PDI), which is a parameter of the size distribution rendered by the DLS instrument (Table 2.2 and Figure 2.5) This similarity is further validated by examining the experimental collision frequency, f_d, which ranges from 0.10 to 0.07 Hz (Table 2.2) and agrees well with the theoretical value (0.07 Hz) calculated using equation 2.5. The average value of ζ is -11 ± 5 mV when no acid is added and -9 ± 5 mV with acetic acid (Appendix). However, for the emulsion with oleic acid, (ζ) reaches -30 ± 6 mV, thus revealing some level of acid deprotonation driven by phase separation and despite the low apparent pH (Table 2.2). This result is consistent with the negative electrophoretic mobility observed in hexadecane droplets when loaded with oleic acid observed at pH 3-4.[55] Appropriately, during DLS measurements, TCBQ is in its neutral most hydrophobic state, which has negligible affinity for hydrogen bonding.

Table 2.2 Measured parameters for emulsions of TCBQ-Toluene in water

Additive	Size / µm[a]	ζ / mV[a]	f_d / Hz[b]	PDI[a]	pH
None	1.4 ± 0.5	-11± 5	0.10 ± 0.07	0.473	3.72 ± 0.03
Acetic	1.4 ± 0.6	-9 ± 5	0.07 ± 0.01	0.483	3.33 ± 0.03
Oleic	1.4 ± 0.6	-30 ± 6	0.07 ± 0.03	0.476	3.49 ± 0.04

[a] DLS, [b*] i-t* curve

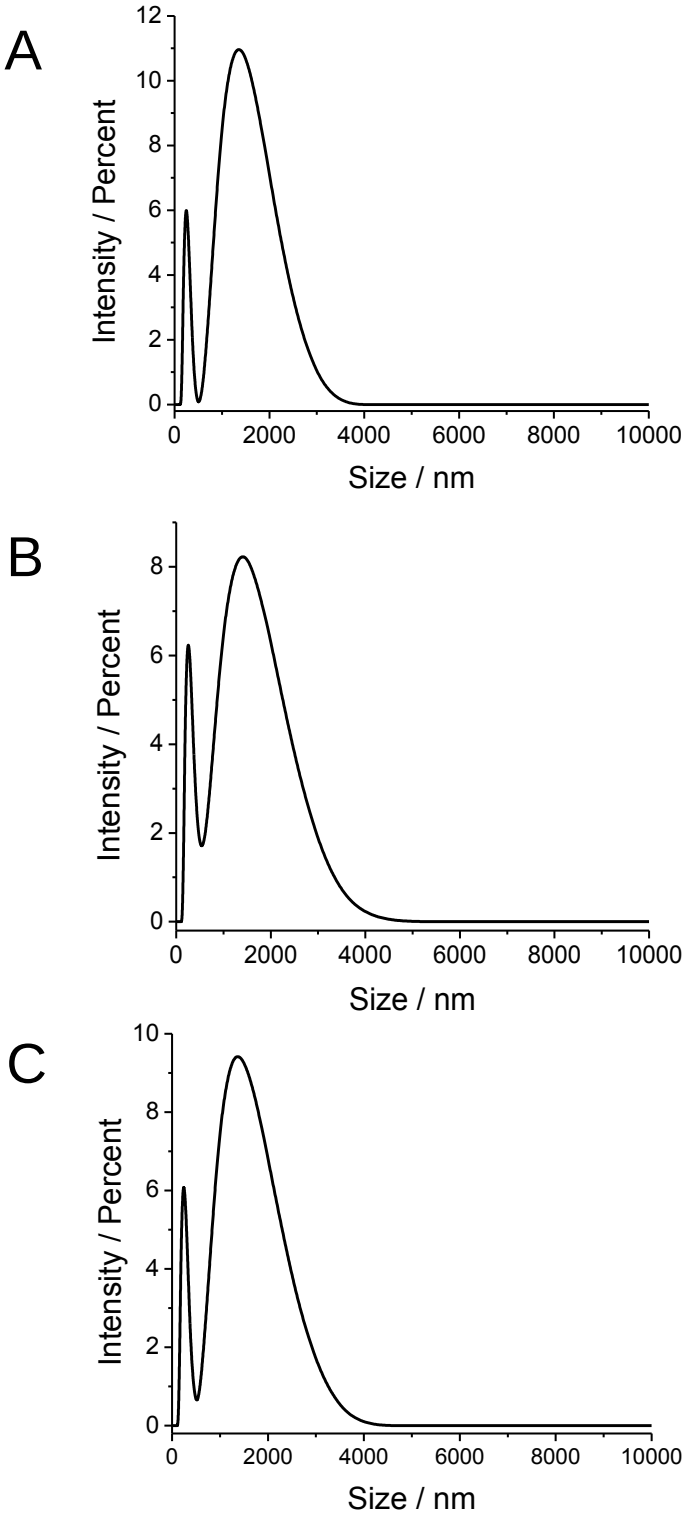

Figure 2.5 DLS measurements for emulsions A) no additives, B) 50 mM acetic acid and C) 50 mM oleic acid.

It is possible to determine the average current per droplet, i_{avg}, from each *i*-t curve of 1000 s recorded for an emulsion. Figure 2.6 shows plots of i_{avg} as a function of applied potential at the same concentration of additives as in Figure 2.1, so that every i_{avg} point is in turn the mean value from three *i-t* curves recorded at the same condition. The error bars are standard deviations of i_{avg} divided by the square root of spikes tallied from each *i-t* curve. Though not perfectly matched, each set of points resembles the steady state shape of the CVs obtained for TCBQ in homogeneous toluene (Figure 2.1).

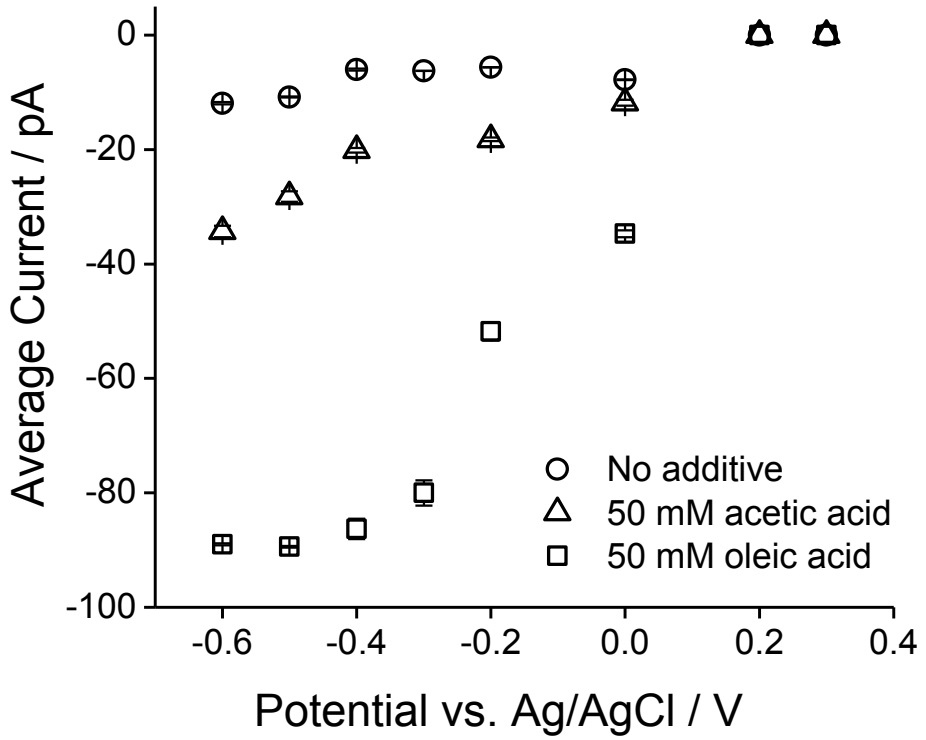

Figure 2.6 Average current per droplet (i_{avg}) as a function of potential.

This similarity is more evident when plotting the average charge per droplet, q_{avg}, after integrating the area of every spike (Figure 2.7). *i-t* curves for emulsions at different potential is shown in Appendix. *i-t* curves were performed thrice at each potential for all

emulsions. Between 0.3 and 0.2 V, no charge transfer occurs, but as negative potentials are surveyed, both i_{avg} and q_{avg} start rising indicating an increase in the reduction of TCBQ, until a leveling off appears at ~-0.4 V when the current and charge reach a plateau. The values of i_{avg} and q_{avg} for droplets without additive, display the same profile as the other two, but the scale of the graph makes it appear flat (Figure 2.8). The increase in i_{avg} and q_{avg} in the presence of acids, is interpreted as a positive in E equation 2.4 driven by hydrogen bonding, which translates into a higher current at same applied potential as observed in homogeneous toluene (Figure 2.1).

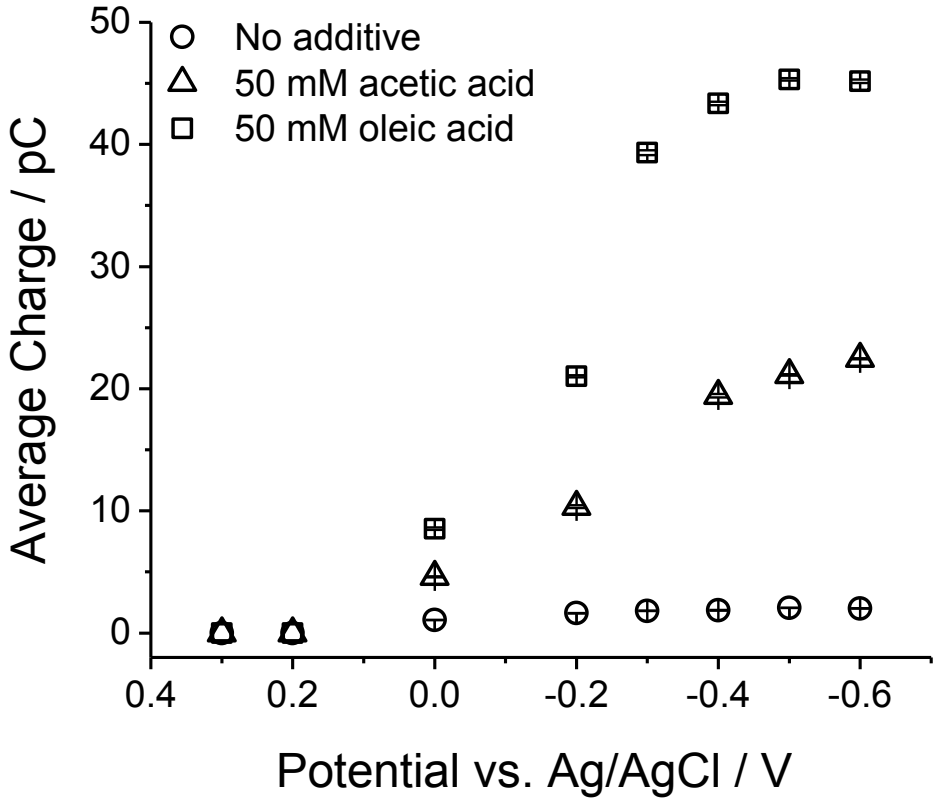

Figure 2.7 Average charge per droplet (q_{avg}) as a function of potential.

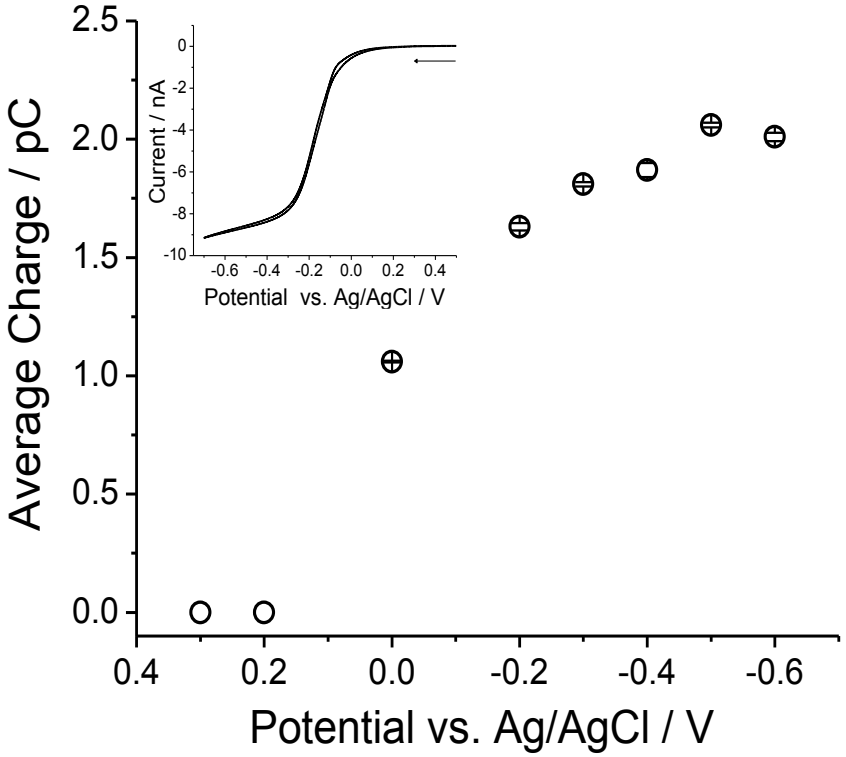

Figure 2.8 Average charge per droplet as a function of potential. The inset shows a CV response for 5.0 mM and 0.4 M ILPA in toluene with a C-UME at scan rate 20 mV/s.

Similarly, the effect is also facilitated through disproportionation assisted by hydrogen bonding as noted in homogeneous toluene and in previous reports for TCBQ in other aprotic solvents.[40] In the end, the reduction becomes easier as $TCBQ^{2-}$ is stabilized by hydrogen bonding with the HD molecules. However, in contrast to homogeneous toluene when adventitious water is present in one phase, oleic acid, is the one that displays the strongest shift and produces the highest current. We attribute this result to the enforced compartmentalization of oleic acid inside the droplet, while acetic acid is able to partition freely between the immiscible phases, given its solubility in water. In

other words, the water solvation of acetic acid prevails over the hydrogen bonding with $TCBQ^{2-}$ inside the toluene phase.

2.4 Conclusion

In summary, a few points emerge from this effort to extract mechanistic data from the organic-water interface using PCE in emulsions. First, besides providing single droplet characterization, PCE is also able to render ensemble average information about chemical effects across the interfacial boundary and despite droplet polydispersity. Therefore, PCE should be able to expand the scope of electrochemistry to obtain mechanistic and reactivity information in immiscible heterogeneous systems, for which other approaches may come up short. Finally, chemical effects driven by phase segregation such as the one described here, are commonplace in heterogeneous systems in which differences of polarity between phases exist, and thus ought to be considered in “on water” reactions and heterogeneous catalysis.

2.5 Reference

1. Breslow, R. Hydrophobic Effects on Simple Organic Reactions in Water. *Acc. Chem. Res*. **1991**, *24*, 159-164.

2. Rideout, D. C.; Breslow, R. Hydrophobic Acceleration of Diels-Alder Reaction. *J. Am. Chem. Soc.* **1980***, 102,* 7817-7818.

3. Narayan, S.; Muldoon, J.; Finn, M. G.; Fokin, V.V.; Kolb, H. C.; Sharpless, K. B. "On Water": Unique Reactivity of Organic Compounds in Aqueous Suspension. *Angew. Chem. Int. Ed.* **2005**, *44*, 3275-3279.

4. Beattie, J. K.; McErlean, C. S. P.; Phippen, C. B. W. The Mechanism of On-Water Catalysis. *Chem. Eur. J.* **2010**, *16,* 8972-8974.

5. Butler, R. N.; Coyne, A. G. Water: Nature's Reaction Enforcers Comparative Effects for Organic Synthesis "In-Water" and "On-Water". *Chem. Rev.* **2010**, *110,* 6302-6337.

6. Butler, R. N.; Coyne, A. G. Understanding "On-Water" Catalysis of Organic Reactions. Effects of H^+ and Li^+ Ions in the Aqueous Phase and Nonreacting Competitor H-Bond Acceptors in the Organic Phase: On H_2O versus on D_2O for Huisgen Cycloadditions. *J. Org. Chem.* **2015**, *80*, 1809-1817.

7. Guo, D.; Zhu, D.; Zhou, X.; Zhen, Bo. Accelerating the "On Water" Reaction: By Organic−Water Interfaceor By Hydrodynamic Effects?. *Langmuir* **2015**, *31*, 13759-13763.

8. Manna, A.; Kumar, A. Why Does Water Accelerate Organic Reactions under Heterogeneous Condition?. *J. Phys. Chem. A* **2013**, *117*, 2446-2454.

9. Mellouli, S.; Bousekkine, L.; Theerge, A. B.; Huck, W. T. S. Investigation of “On Water” Conditions Using a Biphasic Fluidic Platform. *Angew. Chem. Int. Ed.* **2012**, *51*, 7981-7984.

10. Shapiro, N.; Vigalok, A. Highly Efficient Organic Reactions “on Water”, “in Water”, and Both. *Angew. Chem. Int. Ed.* **2008**, *47*, 2849-2852.

11. Tiwari, S.; Kumar, A. Interfacial Reactivity of “on Water” Reactions in the Presence of Alcoholic Cosolvents. *J. Phys. Chem. A* **2009**, *113,* 13685-13693.

12. Zhang, H.–B.; Liu, L.; Chen, Y.-J.; Wang, D.; Li, C.-J. “On Water”-Promoted Direct Coupling of Indoles with 1,4-Benzoquinones without Catalyst. *Eur. J. Org. Chem.* **2006**, *2006, 869-873.*

13. Jung, J.; Marcus, R. A. On the Theory of Organic Catalysis “On Water”. *J. Am. Chem. Soc.* **2007***, 129,* 5492-5502.

14. Beare, K. D.; McErlean, C. S. P. Revitalizing the Aromatic Aza-Claisen Rearrangement: Implications for the Mechanism of ‘on-water’ catalysis. *Org. Biomol. Chem.* **2013**, *11*, 2452-2459.

15. Zuo, Y.-J.; Qu, J. How Does Aqueous Solubility of Organic Reactant Affect a Water-Promoted Reaction? *J. Org. Chem.* **2014**, *79*, 6832−6839.

16. Tandon, V. K.; Hasdesh, K. M. ‘On water’: Unprecedented Nucleophilic Substitution and Addition Reactions with 1,4-Quinones in Aqueous Suspension. *Tetrahedron Lett.* **2009**, *50*, 5896-5902.

17. Yu, J.-S.; Liu, Y.-L.; Tang, J.; Wang, X.; Zhou, J. Highly Efficient “On Water” Catalyst-Free Nucleophilic Addition Reactions Using Difluoroenoxysilanes: Dramatic Fluorine Effects. *Angew. Chem. Int. Ed.* **2014**, *53*, 9512-9516.

18. Chang, C.-R.; Huang, Z.-Q.; Li, J. The promotional Role of Water in Heterogeneous Catalysis: Mechanism Insights from Computational Modeling. *WIREs Comput. Mol. Sci.* **2016**, *6*, 679-693.

19. Davies, P. R. On the Role of Water in Heterogeneous Catalysis: A Tribute to Professor M. Wyn Roberts. *Top. Catal.* **2016**, *59*, 671-677.

20. Roberts, M. W. Low Energy Pathways and Precursor States in the Catalytic Oxidation of Water and Carbon Dioxide at Metal Surfaces and Comparisons with Ammonia Oxidation. *Catal. Lett.* **2014**, *144*, 767-776.

21. Mullen, G. M.; Zhang, L. E.; Evans, J.; Yan, T.; Henkelman, G.; Mullins, B.; Control of Selectivity in Allylic Alcohol Oxidation on Gold surfaces: the Role of Oxygen Adatoms and hydroxyl species. *Phys. Chem. Chem. Phys.* **2015**, *17*, 4730-4738.

22. Hibbitts, D. D.; Loveless, B. T.; Neurock, M.; Iglesia, E. Mechanistic Role of Water on the Rate and Selectivity of Fischer– Tropsch Synthesis on Ruthenium Catalysts *Angew. Chem. Int. Ed.* **2013**, *52*, 12273-12278.

23. Deng, H. J.; Dick, E.; Kummer, S.; Kragl, U.; Strauss, S. H.; Bard, A. J. Probing Ion Transfer across Liquid–Liquid Interfaces by Monitoring Collisions of Single Femtoliter Oil Droplets on Ultramicroelectrodes. *Anal. Chem.* **2016**, *88*, 7754-7761.

24. Dick, J. E.; Lebegue, E.; Strawsine, A.; Bard, A. J. Millisecond Coulometry via Zeptoliter Droplet Collisions on an Ultramicroelectrode. *Electroanalysis* **2016**, *28*, 1-8.

25. Kim, B. K.; Boika, A.; Kim, J.; Dick, J. E.; Bard, A. J. Characterizing Emulsions by Observation of Single Droplet Collisions-Attoliter Electrochemical Reactors. *J. Am. Chem. Soc.* **2014,** *136*, 4849−4852.

26. Kim, B. K.; Kim, J.; Bard, A. J.; Electrochemistry of a Single Attoliter Emulsion Droplet in Collisions. *J. Am. Chem. Soc.* **2015**, *137*, 2343-2349.

27. Li, Y.; Deng, H.; Dick, J. E.; Bard, A. J. Analyzing Benzene and Cyclohexane Emulsion Droplet Collisions on Ultramicroelectrodes. *Anal. Chem.* **2015,** *87*, 11013-11021.

28. Acevedo, O.; Armacost, K. Claisen Rearrangements: Insight into Solvent Effects and “on Water” Reactivity from QM/MM Simulations. *J. Am. Chem. Soc.* 2010, *132*, 1966-1975.

29. Cheng, W.; Compton, R. G. Oxygen Reduction Mediated by Single Nanodroplets Containing Attomoles of Vitamin B_{12}: Electrocatalytic Nano-Impacts Method. *Angew. Chem. Int. Ed.* **2015,** *54*, 7082-7085.

30. Cheng, W.; Compton, R. G. Quantifying the Electrocatalytic Turnover of Vitamin B_{12}-Mediated Dehalogenation on Single Soft Nanoparticles. *Angew. Chem. Int. Ed.* **2016**, *55*, 2545-2549.

31. Zhang, H.; Sepunaru, L.; Sokolov, S. V.; Laborda, E. C.; Batchelor-McAuley, Compton, R. G. Electrochemistry of Single Droplets of Inverse (Water-in-Oil) Emulsions. *Phys. Chem. Chem. Phys.* **2017**, *19*, 15662-15666.

32. Kwon, S. J.; Zhou, H. F.; Fan, F. R.; Vorobyev, V.; Zhang, B. Stochastic Electrochemistry with Electrocatalytic Nanoparticles at Inert Ultramicroelectrodes--Theory and Experiments. *Phys. Chem. Chem. Phys.* **2011**, *13*, 5394-5402.

33. Sokolov, S. V.; Eloul, S.; Katelhon, E.; Batchelor-McAuley, C.; Compton, R. G. Electrode–particle impacts: a users guide *Phys. Chem. Chem. Phys.* 2017, *19*, 28-43.

34. Dick, J. E.; Renault, C.; Bard, A. J. Observation of Single-Protein and DNA Macromolecule Collisions on Ultramicroelectrodes. *J. Am. Chem. Soc.* **2015**, *137*, 8376-8379.

35. Dick, J. E.; A. Boika, H. A.; Upton, J. W.; Bard, A. J. Enzymatically Enhanced Collisions on Ultramicroelectrodes for Specific and Rapid Detection of Individual Viruses. *Proc. Natl. Acad. Sci. U.S.A.* 2015, *112*, 5303-5308.

36. Sepunaru, L.; Sokolov, S. V.; Holter, J.; Young, N. P.; Compton, R. G. Electrochemical Red Blood Cell Counting: One at a Time. *Angew. Chem. Int. Ed.* **2016**, *55*, 9768-9771.

37. Dick, J. E. Electrochemical detection of single cancer and healthy cell collisions on a microelectrode. *Chem. Commun.*, **2016**, *52*, 10906-10909.

38. Xiao, X.; Bard, A. J. Observing Single Nanoparticle Collisions at an Ultramicroelectrode by Electrocatalytic Amplification. *J. Am. Chem. Soc.* **2007,** *129*, 9610-9612.

39. Lebègue, E.; Anderson, C. M.; Dick, J. E.; Webb, L. J.; Bard, A. J. Electrochemical Detection of Single Phospholipid Vesicle Collisions at a Pt Ultramicroelectrode. *Langmuir* **2015,** *31*, 11734-11739.

40. Gupta, N.; Linschitz, H. Hydrogen-Bonding and Protonation Effects in Electrochemistry of Quinones in Aprotic Solvents. *J. Am. Chem. Soc.* **1997***, 119,* 6384-6391.

41. Quan, M.; Sanchez, D.; WasylKim, M. F.; Smith, D. K. Voltammetry of Quinones in Unbuffered Aqueous Solution: Reassessing the Roles of Proton Transfer and Hydrogen

Bonding in the Aqueous Electrochemistry of Quinones. *J. Am. Chem. Soc.* **2007***, 129,* 12847-12856.

42. Tessensohn, M. E.; Hirao, H.; Webster, R. D. Electrochemical Properties of Phenols and Quinones in Organic Solvents are Strongly Influenced by Hydrogen-Bonding with Water. *J. Phys. Chem. C* **2013**, *117*, 1081-1090.

43. Tessensohn, M. E. Webster, R. D. Using Voltammetry to Measure Hydrogen-Bonding Interactions in Non-Aqueous Solvents: A Mini-Review. *Electrochem. Commun.* **2016**, *62*, 38-43.

44. Hui, Y.; Chng, E. L. K.; Chng, C. Y.; Poh, L. H. L.; Webster, R. D. Hydrogen-Bonding Interactions between Water and the One- and Two-Electron-Reduced Forms of Vitamin K_1: Applying Quinone Electrochemistry To Determine the Moisture Content of Non-Aqueous Solvents *J. Am. Chem. Soc.* **2009**, *131*, 1523-1534.

45. Alligrant, T. M.; Alvarez, J. C. The Role of Intermolecular Hydrogen Bonding and Proton Transfer in Proton-Coupled Electron Transfer. *J. Phys. Chem. C* **2011**, *115*, 10797-10805.

46. Alligrant, T. M.; Hackett, J. C.; Alvarez, J. C. Acid/Base and Hydrogen Bonding Effects on the Proton-Coupled Electron Transfer of Quinones and Hydroquinones in Acetonitrile: Mechanistic Investigation by Voltammetry, ^{1}H NMR and Computation. *Electrochim. Acta* **2010**, *55,* 6507-6516.

47. Garza, J.; Vargas, R.; Gomez, M.; Gonzalez, I.; Gonzalez, F. J. Theoretical and Electrochemical Study of the Quinone−Benzoic Acid Adduct Linked by Hydrogen Bonds *J. Phys. Chem. A* **2003**, *107*, 11161-11168.

48. Hui, Y.; Chng, E. L. K.; Chua, L. P.-L.; Liu, W. Z.; Webster, R. D. Voltammetric Method for Determining the Trace Moisture Content of Organic Solvents Based on Hydrogen-Bonding Interactions with Quinones. *Anal. Chem.* **2010,** *82*, 1928-1934.

49. Peover, M. E.; Davis, J. D. The Influence of Ion-Association on the Polarograpgy of Quinones Dimethylformamide. *J. Electroanal. Chem.* **1963**, *6*, 46-53.

50. Danis, L.; Polcari, D.; Kwan, A.; Michelle, S.; Mauzeroll, J. Fabrication of Carbon, Gold, Platinum, Silver, and Mercury Ultramicroelectrodes with Controlled Geometry. *Anal. Chem.* **2015**, *87*, 2565−2569.

51. Bard, A. J.; Faulkner, L.R. *Electrochemical Methods: Fundamentals and Applications*. 2nd ed.; Willy, New York, **2001**.

52. Ojani, R.; Raoof, J. B.; Zamani, S.; Electrochemical Behavior of Chloranil Chemically Modified Carbon Paste Electrode. Application to the Electrocatalytic Determination of Ascorbic Acid. *Electroanalysis* **2005**, *17*, 1740-1745.

53. Kanicky, J. R.; Shah, D. O. Effect of Degree, Type, and Position of Unsaturation on the pK_a of Long-Chain Fatty Acids. *J. Colloid Interface Sci.* **2002**, *256*, 201-207.

54. Kanicky, J. R.; Poniatowski, A. F.; Metha, N. R.; Shah, D. O. *Langmuir* **2000**, *16*, 172-177.

55. Roger, K.; Cabane, B. Why Are Hydrophobic/Water Interfaces Negatively Charged? *Angew. Chem. Int. Ed.* **2012**, *51*, 5625-5628.

2.6 Appendix

Calculation for Concentration of Emulsion Droplets loaded with TCBQ

Average droplet volume = $\frac{4}{3}\pi r^3$

$= \frac{4}{3} X \frac{22}{7} X (719.3 X 10^{-9})^3$ m^3

= 1.560 X 10^{-18} m^3

= 1.560 X 10^{-18} X 1000 L

= 1.560 X10^{-15} L

Volume of toluene used = 0.1 mL

= 0.1 X 10^{-3} L

Number of droplets = (0.1 X 10^{-3} L) / (1.560 X10^{-15} L)

= 6.410 X 10^{10}

Moles of droplets = (6.410 X 10^{10}) / (6.023 X 10^{23})

= 1.06 X 10^{-13} mol

Total water used = 5 mL

= 5 X 10^{-3} L

Concentration of emulsion droplets = (1.06 X 10^{-13}) /(5 X 10^{-3}) M

= 21.2 pM

Total Concentration of TCBQ based on Average Droplet Size of Emulsion

Average charge at -0.4 V = 1.87 pC [From Figure 2.7]

Moles = charge / nF

= (1.87 X 10^{-12}) / (96487 X 2)

= 9.69 X 10^{-18} mol

Average droplet volume = $\frac{4}{3}\pi r^3$

$= \frac{4}{3} X \frac{22}{7} X (719.3 X 10^{-9})^3$ m^3

= 1.560 X 10^{-18} m^3

= 1.560 X 10^{-18} X 1000 L

= 1.560 X10^{-15} L

Concentration of TCBQ = 9.69 X 10^{-18} mol / 1.560 X10^{-15} L

= 6.20 mM

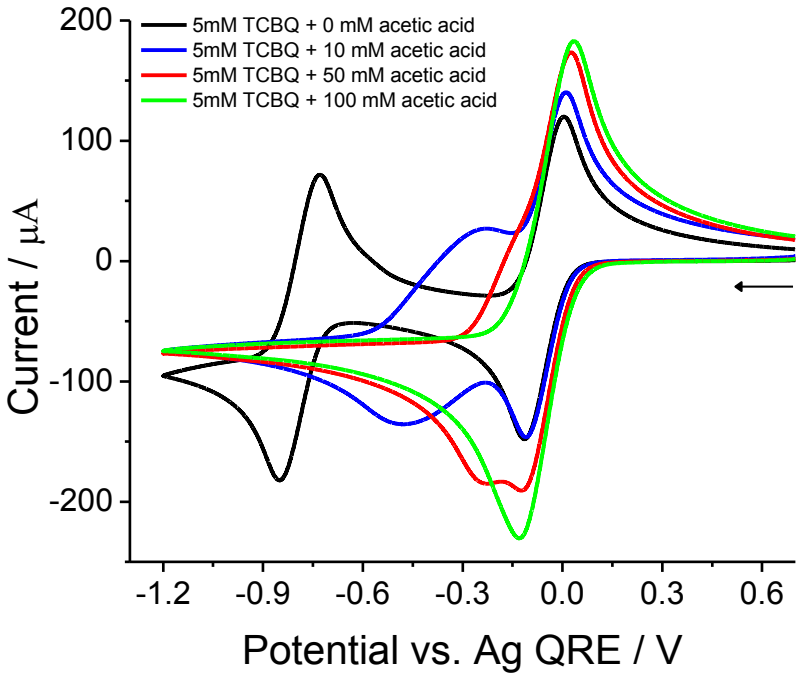

Figure 1A Cyclic voltammograms of TCBQ and 100 mM TBAP at different concentrations of acetic acid in CH_3CN on glassy carbon (dia. 3 mm) electrode. Scan rate = 100 mV/s.

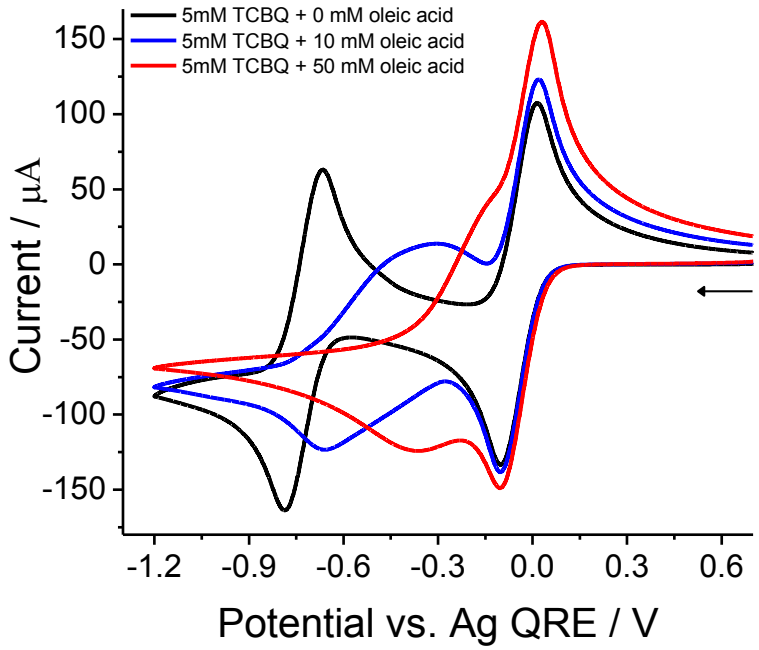

Figure 1B Cyclic voltammograms of TCBQ and 100 mM TBAP at different concentrations of oleic acid in CH_3CN on glassy carbon (dia. 3 mm) electrode. Scan rate = 100 mV/s.

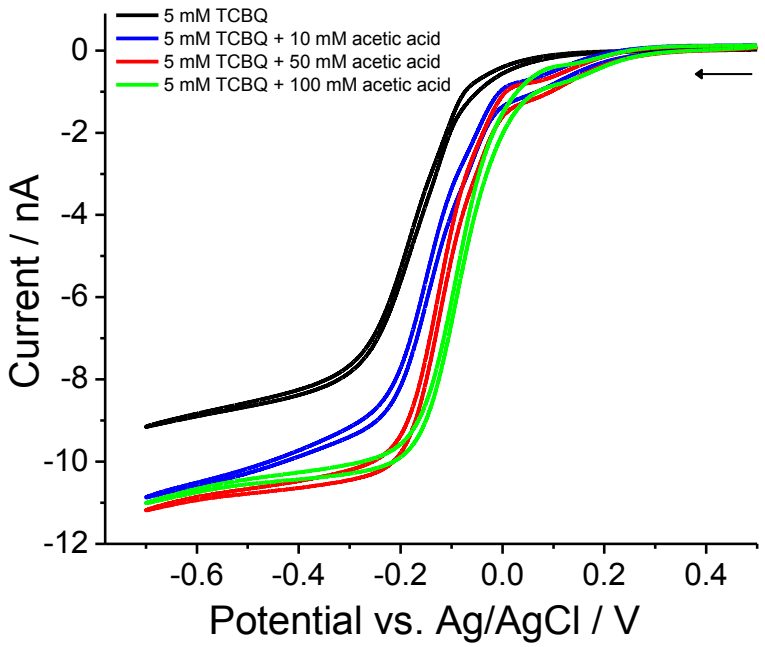

Figure 2A Cyclic voltammograms of TCBQ and 0.4 M ILPA at different concentrations of acetic acid in toluene on C UME (radius 4.3 μm). Scan rate = 20 mV/s.

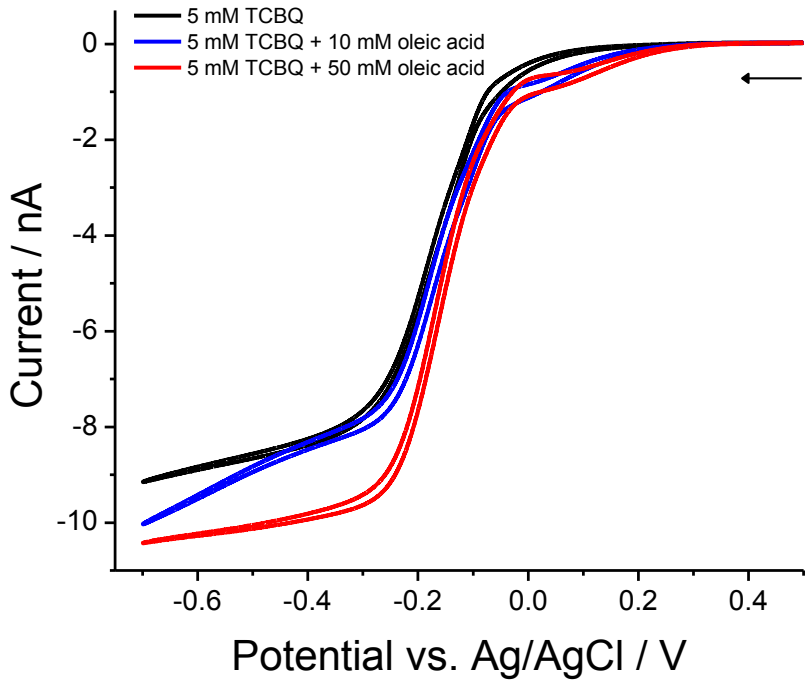

Figure 2B Cyclic voltammograms of TCBQ and 0.4 M ILPA at different concentrations of oleic acid in toluene on C-UME (radius 4.3 μm). Scan rate = 20 mV/s.

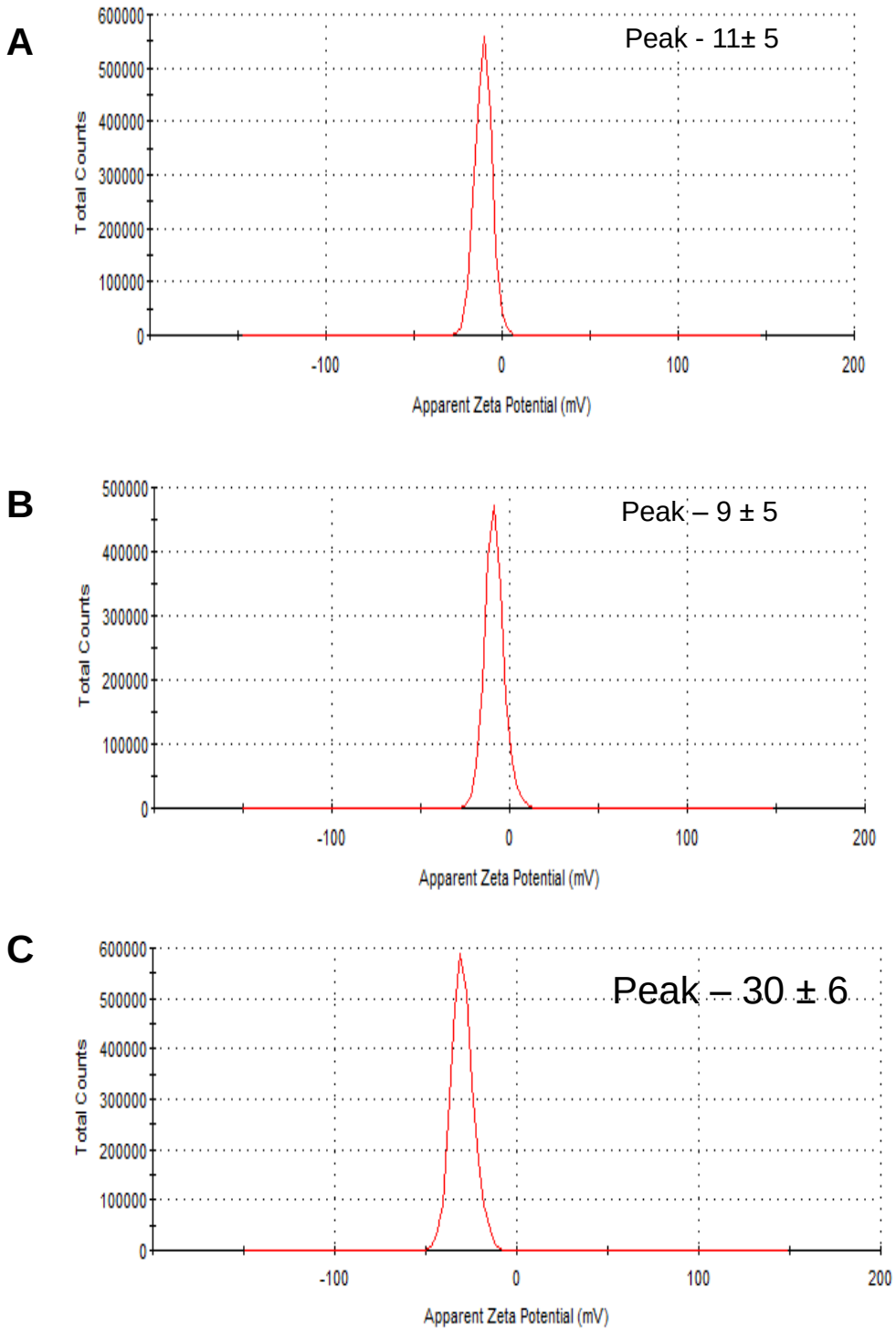

Figure 3 Zeta potential measurement data for emulsions (A) only TCBQ (no additives), (B) with 50 mM acetic acid and (C) with 50 mM oleic acid.

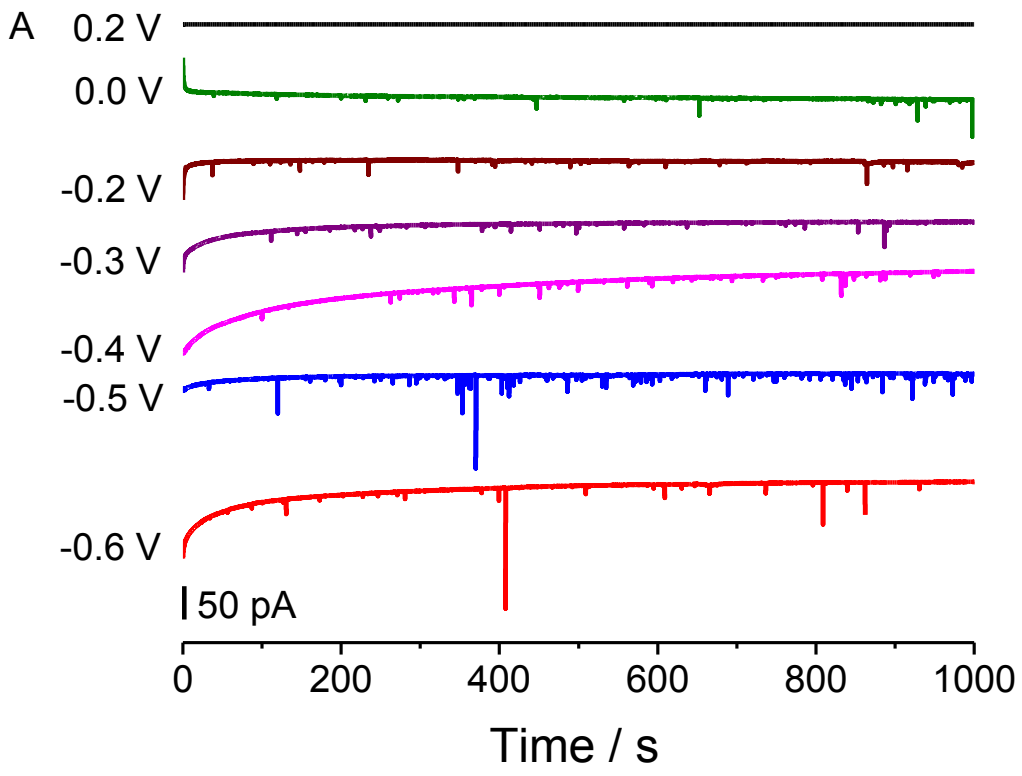

Figure 4A Amperometric *i-t* curves of TCBQ emulsion droplet on C UME (radius 4.3 µm) at different potentials versus Ag/AgCl.

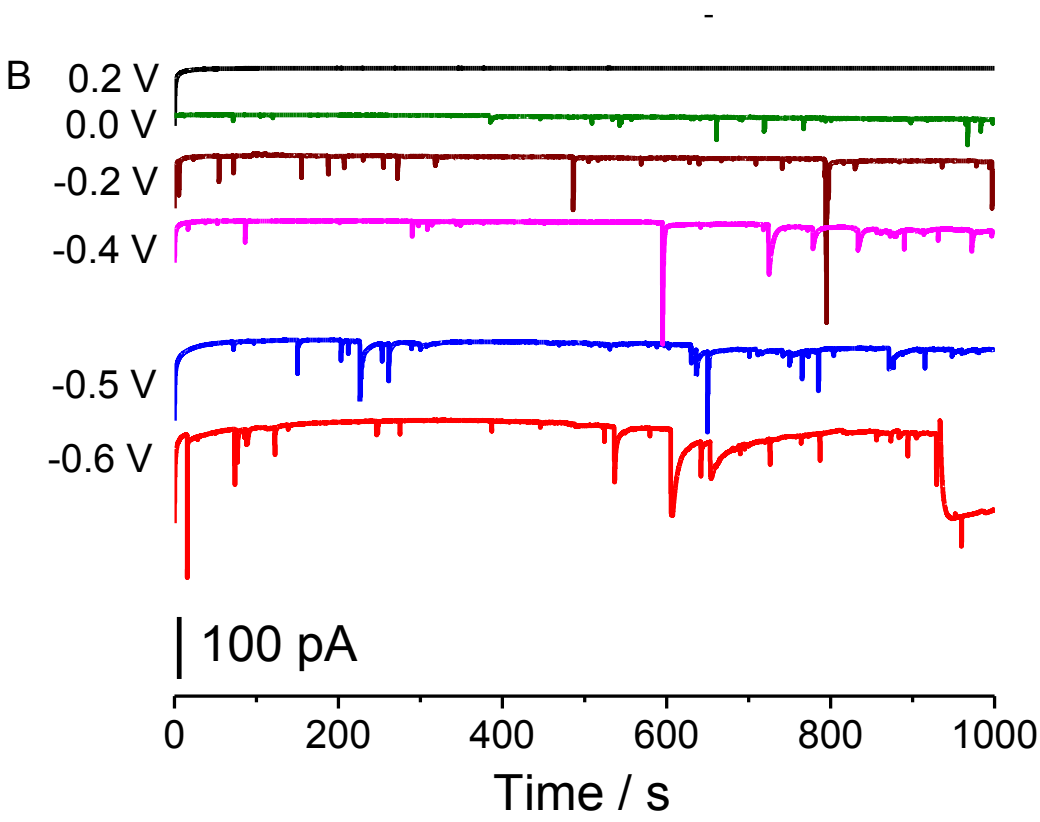

Figure 4B Amperometric *i-t* curves of TCBQ emulsion droplet with 50 mM acetic acid on C fiber UME (radius 4.3 µm) at different potentials versus Ag/AgCl.

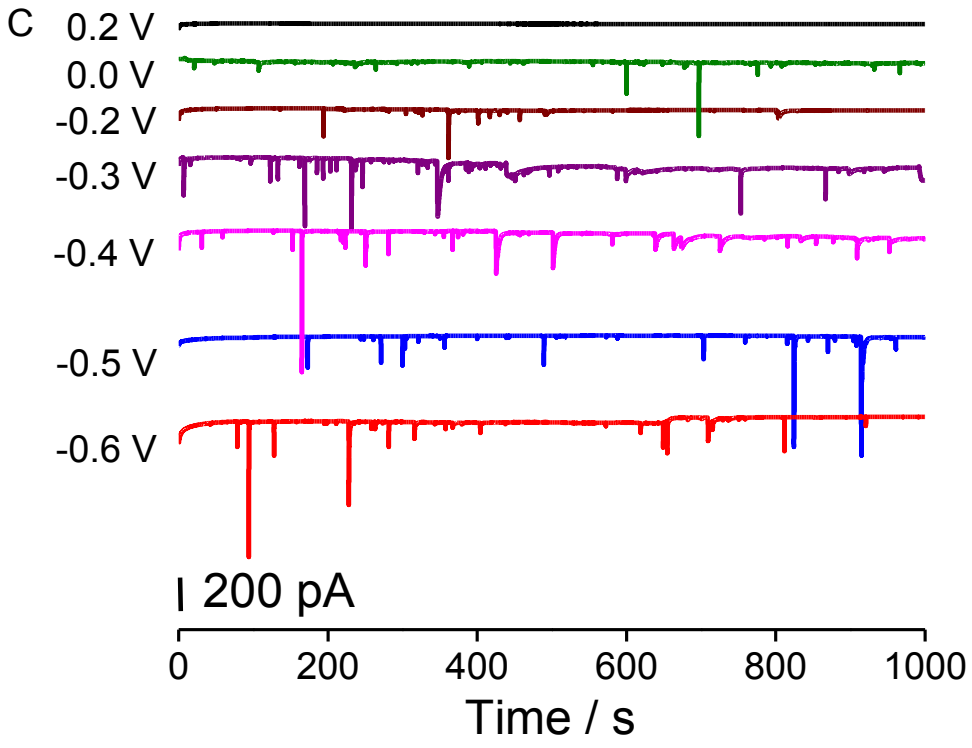

Figure 4C Amperometric *i-t* curves of TCBQ emulsion droplet with 50 mM oleic acid on C UME (radius 4.3 µm) at different potentials versus Ag/AgCl.

Chapter 3

Study the Effects of Electrolyte and Surfactant on Emulsion Droplets Size and Stability by Monitoring Electrochemical reactions

3.1 Introduction

Emulsions tend to minimize stability by separating the phases. Research on emulsion stability has been growing fast over the last decade because of the dynamic nature of the liquid-liquid interface. Several groups have worked with different types of electrolytes and surfactants to investigate the effect on the emulsions stability and size.[1-6] Burgess[1] and Saunder[2] studied the effect of NaCl and $MgSO_4$ on water/oil emulsions and observed that emulsion droplet size increased due to “salting out” effect and retardation of surfactant adsorption at water-oil interface. In contrast, experimental work by Solans[3] indicated that droplet size decreases by varying electrolyte concentration with the development of osmotic gradient and reduction of oil-water interfacial tension. In addition to the electrolyte effect, the nature of surfactants[4] exhibited critical control over the emulsion size. Goloub[4] reported that cationic surfactants have more influence on decreasing droplet size compared to nonionic and anionic ones. Contradictory findings were observed by Li,[5] who found that nonionic surfactants have more impact than the anionic surfactants on droplet size. The chemical structure of surfactants also showed an important role on the electrochemistry of some electroactive molecules. For example, anionic surfactants strongly interact with $Os(bpy)_3^{2+}$, thus reducing the intensity of its oxidation peak.[6] On the other hand, cationic

surfactants interact weakly whereas nonionic surfactants have no interaction with $Os(bpy)_3^{2+}$.

The details above illustrate that the role of electrolyte and surfactant in controlling size and stability of emulsion droplets is more nuanced and complicated. Moreover, interactions between surfactant molecules and electroactive species are still not completely understood in emulsion droplet systems. For instance, it is not known how the species inside and outside the droplet in emulsion systems, affect the electrochemical properties of trapped redox molecules and stability of emulsions. To address this problem, it is important to develop a model system for a better understanding of the basic research across the oil-water interface. The gathered knowledge could be employed for applications in food industry, petroleum chemistry, and biosensors.

In this work, our goal is to understand the factors that control the size and stability of emulsion droplets by electrochemical interrogation using the particle collision method. Herein, toluene droplets containing ferrocene (Fc) are used as a model for the systematic study of variables that impact interfacial tension at the oil-water interface. In addition, we also investigate the mediated oxidation of L-cysteine by the oxidized Fc inside the droplet. Here the goal is to prove that Fc inside the toluene droplet can act as a rely of electrons for a species outside (cysteine) that cannot be solubilized in the droplet. Direct oxidation of cysteine is very slow at most conventional electrodes[7-9] and requires high overpotential at which electron transfer process can occur.

3.2 Experimental Section

3.2.1 Reagents and Materials

Ferrocene (Fluka, 98%), tetrabutylammonium hexafluorophosphate (Aldrich, 98%). sodium chloride (NaCl, Aldrich, 99.9%), trihexyltetradecylphosphonium bis(trifluoromethylsulfonyl)amide (IL, Sigma-Aldrich, ≥95.0%), L-cysteine (Aldrich, 97%), acetonitrile (Acros, 99.9%), toluene (Fisher, 99.5%), triton X-100 (Sigma) were used as received without further purification. All working solutions were made up using water of resistivity 18.2 MΩ cm (Millipore).

3.2.2 Instrumentation

All electrochemical measurements were performed at room temperature using a potentiostat CHI model 660C (CH Instruments, Austin, TX) equipped with a standard three-electrode cell placed in a faradic cage. A nitrogen atmosphere was maintained inside the electrochemical cell during experiments**.**

For voltammetric measurements, the working electrode was a gold (Au) microdisk of 25 μm - diameter, otherwise known as an ultramicroelectrode (UME). A Pt wire was used as a counter electrode and a silver (Ag) wire coated with silver chloride served as a quasi-reference electrode (QRE) in all experiments. Before each voltammetric experiment, Au UME was polished with 0.05 μm alumina mixed with deionized water (DI) on a cleaning pad (Lake Bluff, Illinois) and rinsed with DI water between experiments. All working solutions were deoxygenated with nitrogen. The same working, counter and reference electrodes were used as mentioned earlier for particle collisions electrochemistry experiments.

3.2.3 Emulsions Preparation

The toluene/water emulsions were prepared by using similar procedure that described in chapter 1. During the preparation, 20 mM (1.9 mg) ferrocene and 400 mM (145 µL) ionic liquid were mixed into 355 µL of toluene in a vial. After that, 100 µL of this toluene mixture were transferred to 5 mL of DI water. Finally, the solution was mixed vigorously for 20 s in a vortex mixer (Vortex Genie 2^{TM}, Fisher, Waltham MA) and sonicated for 5 min at room temperature. As prepared emulsion showed stability up to 16 h. Here, ionic liquid served as both supporting electrolyte and emulsifier.

Other toluene emulsions were also prepared with sodium chloride (NaCl), surfactant (triton X-100) and without ionic liquid. Like NaCl, triton X-100 was dissolved into water during emulsion preparation.

3.2.4 Droplet Size Measurement

The size of emulsion droplets were measured by Dynamic Light Scattering (DLS) instrument (Zetasizer Nano ZS, Malvern Instrument, Malvern, U.K.) at a scattering angle of 173 º with each measurement being an average of 12 runs. The light source was a laser beam operating at 633 nm. Around 2.5 mL volume of each sample was used to DLS measurements.

3.3 Results and Discussion

3.3.1 Electrochemical oxidation of Ferrocene

Cyclic voltammetry was carried out to demonstrate the electrochemical oxidation of 5 mM Fc on a 25 µm Au electrode in acetonitrile solution containing 0.1 M tetrabutylammonium hexafluorophosphate ($TBAPF_6$) that served as supporting

electrolyte. Voltammogram shows a sigmoidal wave for one electron electrochemical oxidation of ferrocene molecule (Figure 3.1) at a scan rate of 20 mV/s. From the starting potential of zero, the oxidation of Fc starts at approximately +0.2 V versus Ag QRE and exhibits a steady state current of around +0.45 V that agreed with previous report.[1] In order to ensure complete oxidation of Fc to Fc^+, we had applied a constant potential of +0.5 V to study the single collision experiments.

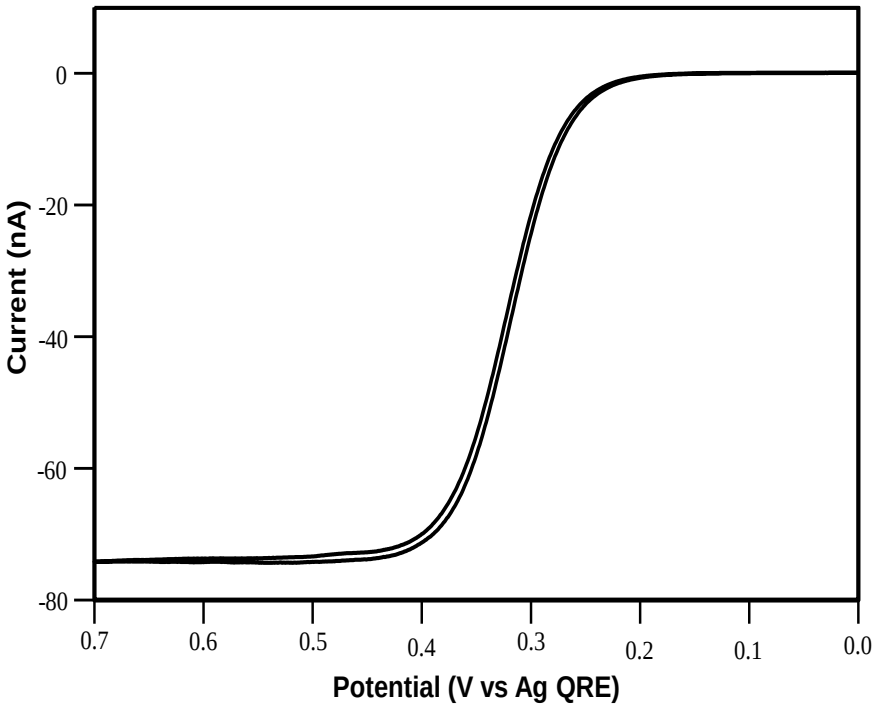

Figure 3.1 CV of 5 mM Fc and 0.1 M $TBAPF_6$ in acetonitrile on Au UME (dia. 25 μm) at a scan rate 20 mV/s.

3.3.2 Collision Experiments of Fc Emulsion Droplets

Amperometric *i-t* curves were recorded to monitor the collision of Fc droplets on Au UME at the applied potential of +0.5 V. Figure 3.2 shows many spikes type of current which were attributed to the electrolysis of Fc inside the droplets. It is presumed that oxidation of Fc to Fc^+ results in removal of Fc^+ ion from the toluene droplet into the

water to maintain charge neutrality. In reality, each current spike represents individual droplet collision on the electrode surface. The number of current spikes is also associated with diffusion of emulsion droplets to the Au UME as shown in Figure 3.2. The diffusion coefficient of a spherical emulsion droplet (D_{ems}) was calculated by the Stokes−Einstein equation 3.1.

$$D_{ems} = \frac{k_B T}{6\pi\eta r_{ems}} \quad \ldots\ldots\ldots\ldots\ldots\ldots\ldots (3.1)$$

Where, k_B = Boltzmann constant, T = temperature in kelvin, η = viscosity of water at 25 °C (8.90 X 10^{-4} Pa.s), and r_{ems} = radius of an emulsion droplet. By using this equation, the diffusion coefficient was 4.8 × 10^{-9} cm^2/s for a 1200 nm diameter emulsion droplet, which is comparable to previously reported value (8.2 × 10^{-9} cm^2/s for 600 nm diameter emulsion droplet).[10]

Furthermore, droplet size of the emulsion can also be estimated from the current time (*i-t*) curve. The amount of charge transferred during electrolysis of Fc in each droplet was determined by integrating individual current spike versus time. The droplet diameter (d_{drop}) was calculated using equation 3.2.[10]

$$d_{drop} = 2\sqrt[3]{\frac{3Q}{4\pi FnC_{redox}}} \quad \ldots\ldots\ldots\ldots\ldots\ldots (3.2)$$

Where, Q = integrated charge in coulomb, F = Faraday's constant (96487 C/mole e), n = number of electrons involved in redox reaction (1 e^-) and C_{redox} = concentration of redox molecules in dispersed phase (20 mM). It was assumed that all spherical toluene droplets contain 20 mM of Fc and all the Fc molecules in each droplet were completely

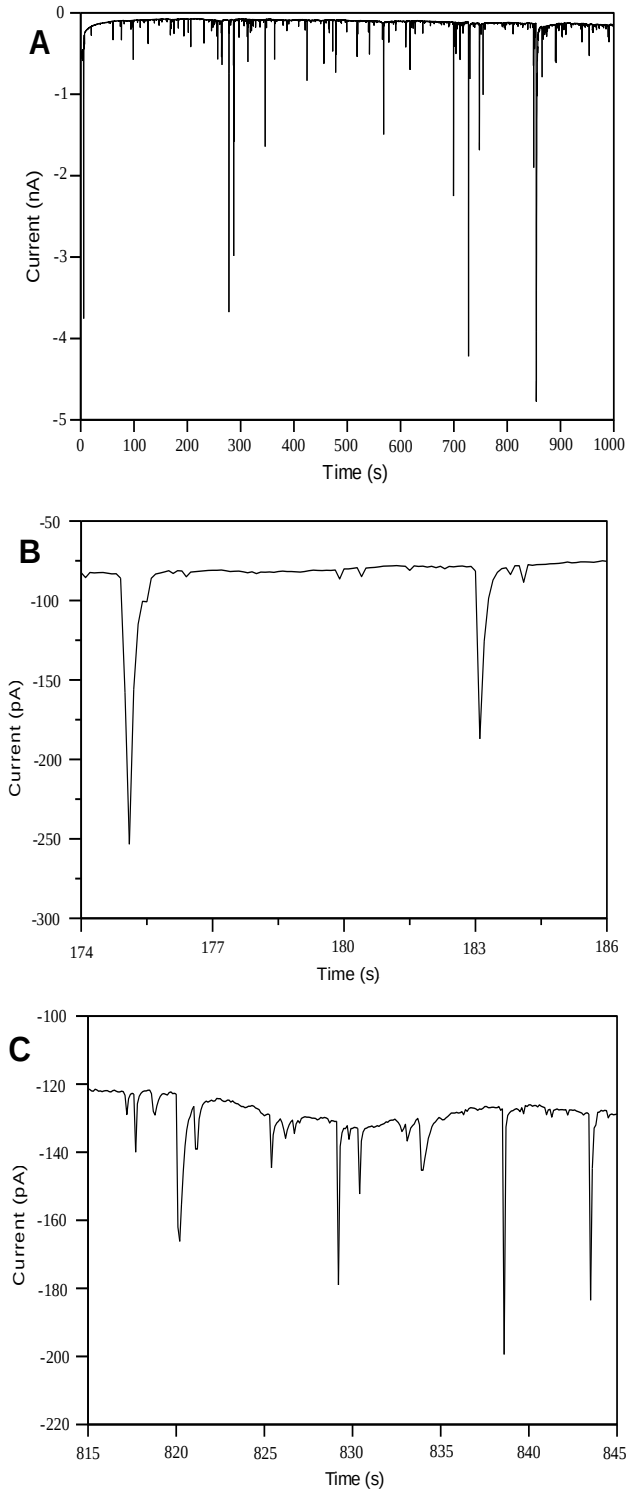

Figure 3.2 (A) Amperometric *i-t* curve for single collision events of toluene droplet loaded with Fc at 25 µm Au UME. UME potential vs Ag QRE: +0.5 V. (B, C) represents magnified *i-t* curves at different time intervals.

electrolyzed during single collision event. The droplet size distribution is presented in Figure 3.3. The size dispersity ranges from 800 to 6000 nm, indicating polydispersity of the droplets. Average diameter of droplet was around 1600 nm. Due to the variation in experimental conditions (such as sonication power and sonication time), a deviation in the result was observed from Bard's group.[10] DLS experiments were performed to compare the experimental size distribution data. In DLS, two peaks were observed for sizes of droplets and the values were 285 nm and 2085 nm. The discrepancy between electrochemical and DLS values can be ascribed to the difference in operating principle (charge transfer vs light scattering) of these methods and polydispersity of emulsions.[11] Although the droplets size distribution was not homogeneous, the emulsion showed stability up to 16 h, after which a white sedimentation started to form at the bottom of the vial.

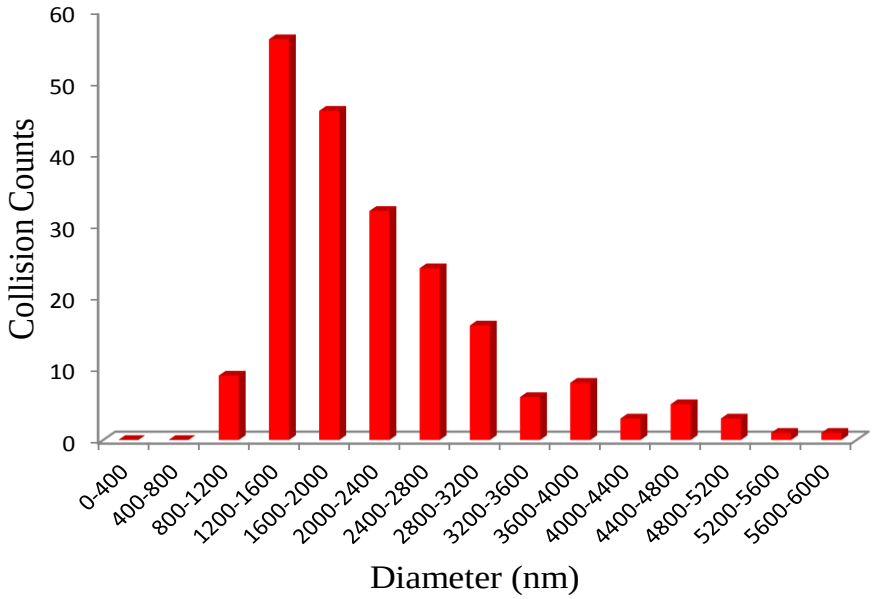

Figure 3.3 Droplet size distributions from equation 3.2.

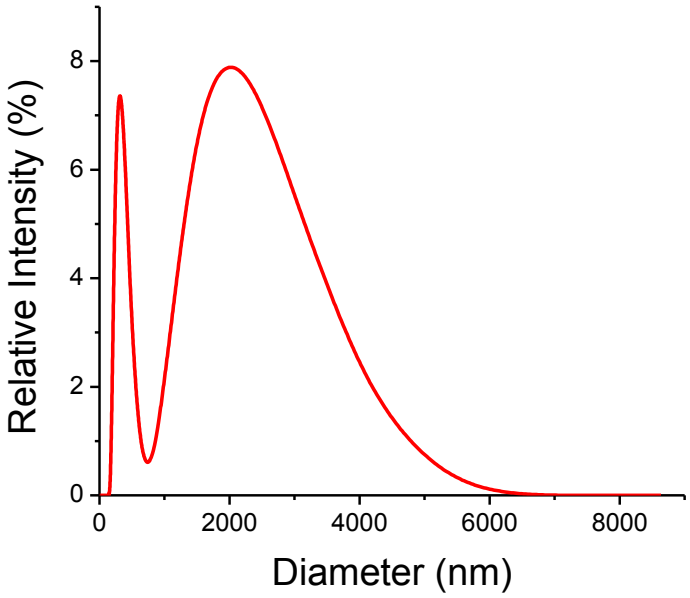

Figure 3.4 Droplet size distributions of emulsions by DLS.

3.3.3 Effect of the Electrolyte on Toluene-Water Emulsion Droplets

The influence of the electrolyte, NaCl was investigated on the physical properties of emulsions. In this study, emulsions were prepared as described earlier except 0.1 M NaCl aqueous solution was used as a continuous phase instead of neat water. Figure 3.5 shows current-time (*i-t*) curve for collision experiments of the emulsion droplets in the presence of NaCl that was recorded under same experimental conditions. The corresponding size distribution of emulsion droplets was obtained by applying equation 3.2 (Figure 3.6). The result exhibits a broad size distribution ranging from 1500 to 9000 nm in the presence of NaCl. This was expected due to the presence of higher concentration of NaCl.[1,12] The larger size droplets were observed as a result of increased interfacial tension during emulsification.

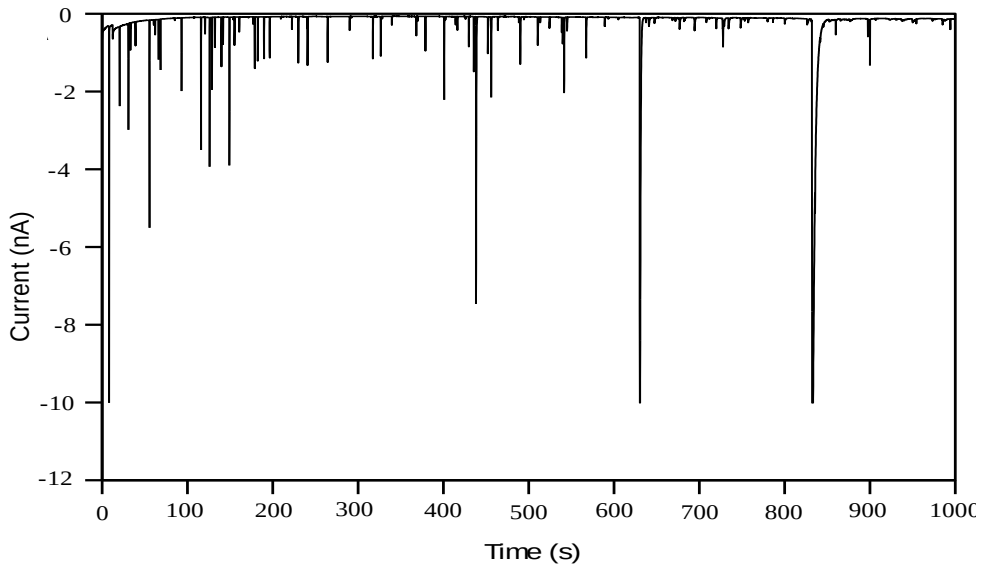

Figure 3.5 *i-t* curve of emulsion droplets (20 mM Fc + 400 mM IL + 0.1 M NaCl) collided on 25 µm Au UME vs Ag QRE: +0.5 V.

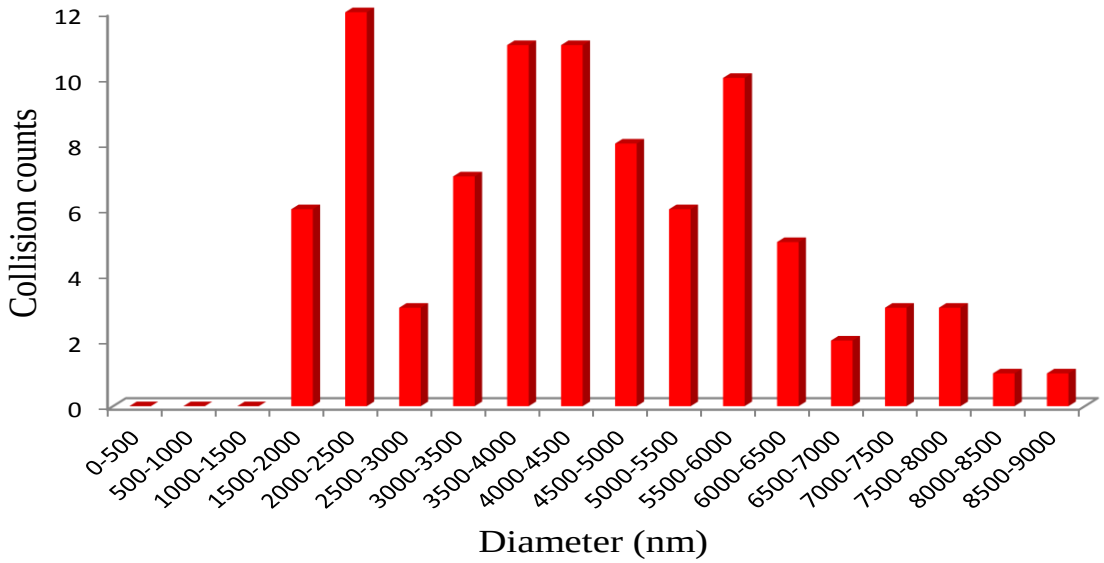

Figure 3.6 Electrochemical size distributions of emulsion droplets (20 mM Fc + 400 mM IL + 0.1 M NaCl).

Moreover, the stability of the emulsion was monitored over time and it started to become less cloudy within 30 minute. To observe the electrochemical response over

time, an amperometric *i-t* curve was recorded after 1 h under similar experimental conditions and no spike was observed at that time (Figure 3.7). This result implies that the stability of the emulsion was less than 1 h. This phenomenon can be explained by previously measured zeta potential data that showed negative charge on the surface[10] of the droplet. This negative charge caused an electrostatic interaction between the droplet and positive ion of the electrolyte resulting in aggregation of emulsion droplets. Further studies are needed to understand the influence of other electrolytes such as KCl to tune the size and increase the stability of droplets.

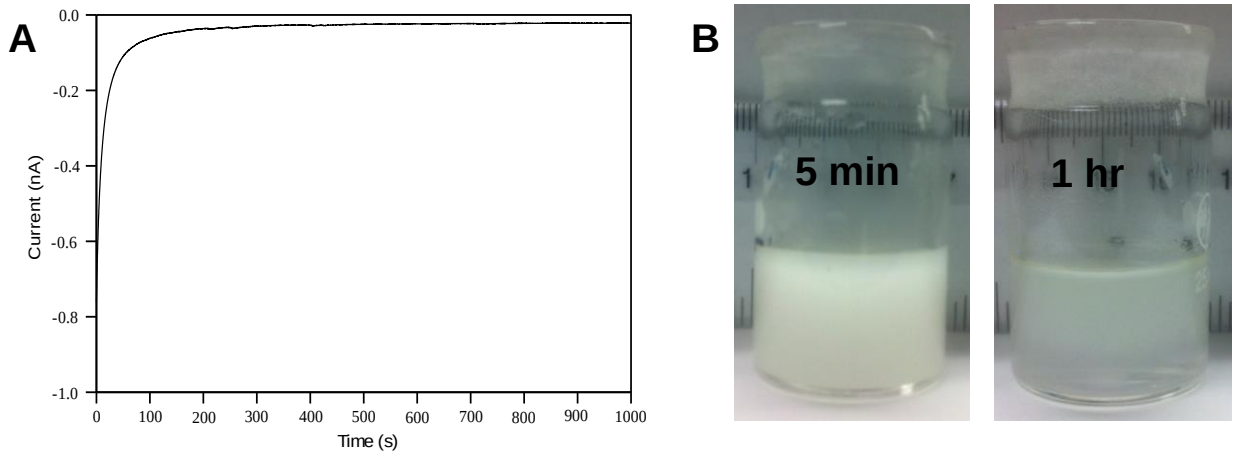

Figure 3.7 (A) Amperometric *i-t* curve of emulsion droplets (20 mM Fc + 400 mM IL + 0.1 M NaCl) after 1 h on 25 µm Au UME vs Ag QRE: +0.5 V and (B) Stability of emulsion as a function of time.

3.3.4 Influence of the Surfactant on Droplets Size and Stability

Toluene in water emulsions was prepared without adding ionic liquid to understand the mechanism and effect of the surfactant on the emulsification process, specifically on the droplet size and stability. Different concentrations (0.4 mM and 0.6 mM) of the nonionic surfactant (triton X-100) were used to prepare the emulsions and its effect was examined. Figure 3.8A displays the responses of these emulsions on

amperometric studies. It is clearly shown that no spike was found on the *i-t* curve although both emulsions were stable for 2 days. Similar finding was observed in 3.8 B even the concentration of Fc was increased from 20 to 40 mM. These results suggest that the ionic liquid plays an important role to observe spike on collision experiments.

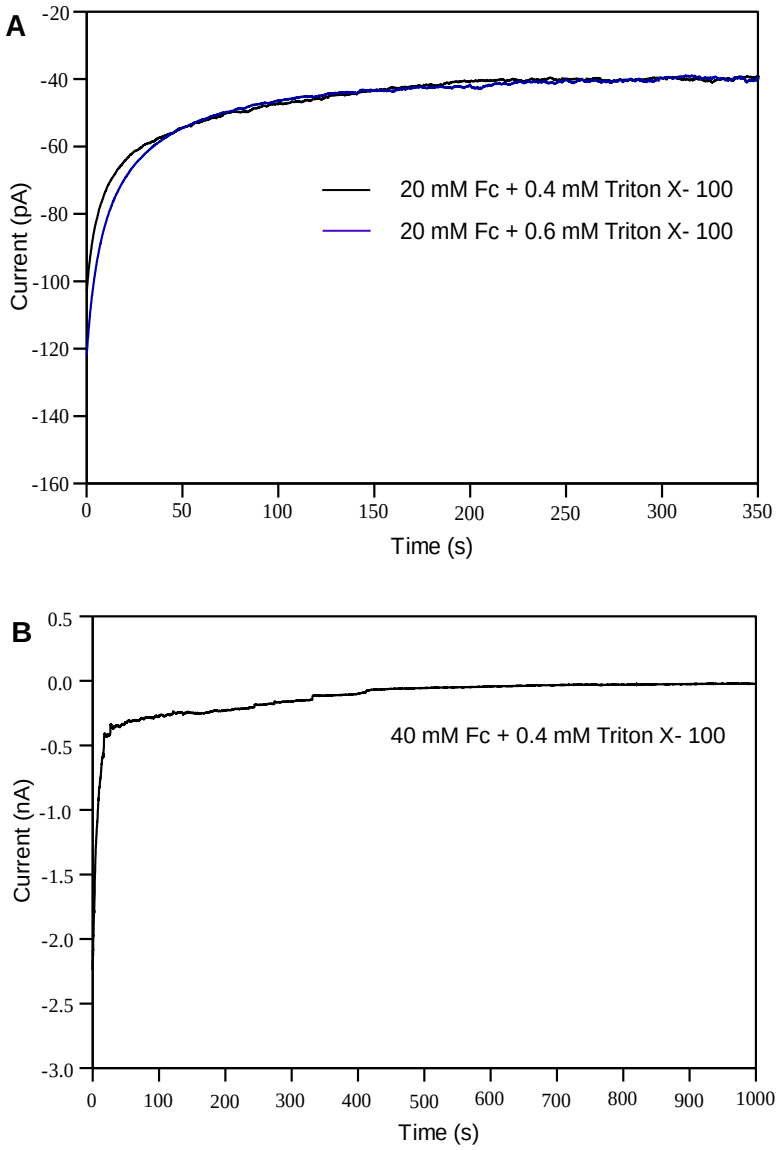

Figure 3.8 *i-t* curve of emulsion droplets without ionic liquid (A) at 20 mM of ferrocene in different concentration of triton X-100 and (B) at 40 mM of ferrocene in presence of 0.4 mM triton X-100.

To investigate the role of the ionic liquid, several emulsions were prepared by using various concentrations of IL in the presence of 0.4 mM triton X-100. The collision study was monitored for emulsion droplets containing Fc to observe the current spikes that are shown in Figure 3.9. The number of collisions were insignificant at the minimum concentration of IL (300 mM) whereas at the higher concentration (400 mM), a collision frequency of 0.22 Hz was observed (Figure 3.10). This implies that the ionic liquid acts as an emulsifier and a supporting electrolyte to ensure enough conductivity.

In the present study, one target was to control the size and stability of emulsion droplets that should be observed with the surfactant introduction in aqueous phase during emulsion preparation. Figure 3.10 represents the chronoamperometric *i-t* curve recorded for emulsion droplets in the presence of triton X-100 (0.4 mM) along with 400 mM ionic liquid and the droplet size distribution is presented in Figure 3.10D. Promising results were obtained at 0.4 mM of triton X-100 incorporation in water. In this case, both the droplets size (800 to 1200 nm) and distribution became smaller and narrower, respectively compared to that of using only ionic liquid. This indicates that surfactant reduced the surface tension on the toluene-water droplet interface. This fact may be explained either by coadsorption of the surfactant and ionic liquid or complete removal of the ionic liquid on the droplet surface. Additional studies are required to understand this phenomenon.

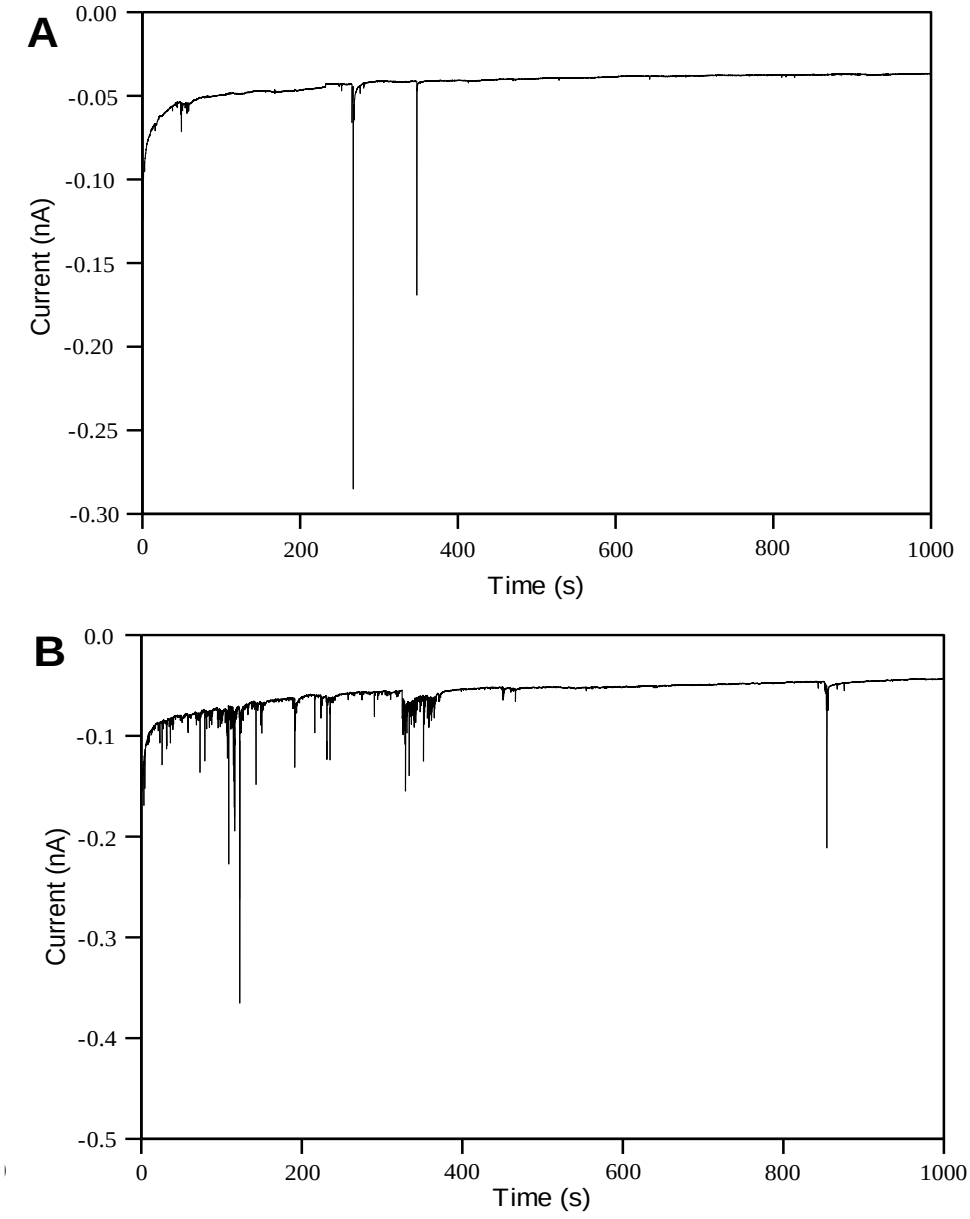

Figure 3.9 Amperometric *i-t* curve of emulsion droplets (20 mM Fc + 0.4 mM triton X-100) at (A) 300 mM IL and (B) 350 mM IL.

Another interesting feature was observed regarding the shape of the current spikes detected for these emulsion droplets. Here, instead of the expected 'peak' shape current, we observed symmetrical and sharp current spikes with fast decay time ranging between 0.3 to 0.6 s (Figure 3.10B-C). This short decay time suggests a rapid

electrolysis process. These observations are in good agreement with previous work done by Lebègue and Bard who observed the effect of triton X-100 on vesicle collisions at Pt UME surface.[5] However, this electrolysis mechanism is not completely understood yet and seems more complicated. More research is needed for mechanistic study of the Fc oxidation in the presence of the surfactant.

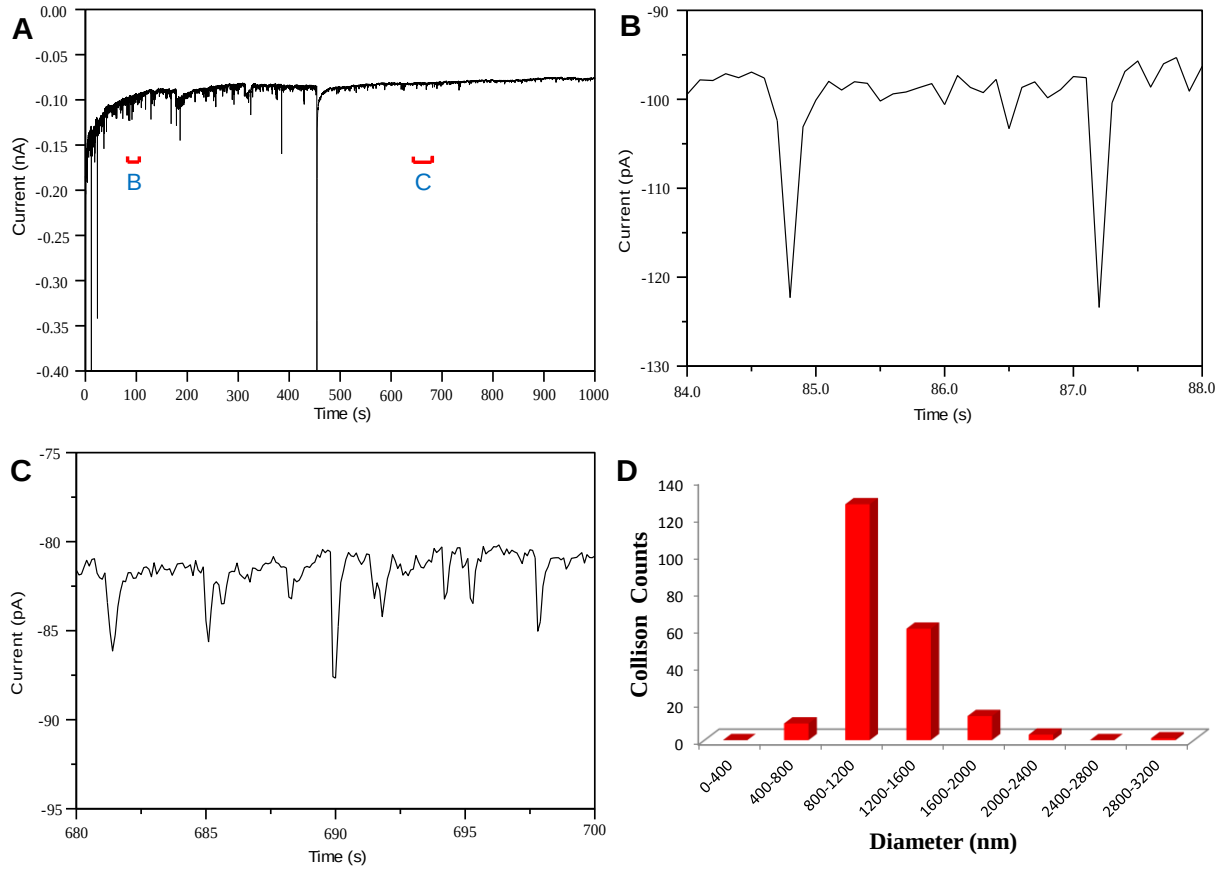

Figure 3.10 (A) Amperometric *i-t* curve for single collision of toluene droplets loaded with Fc in presence of triton X-100 at 25 µm Au UME. UME potential vs Ag QRE: +0.5 V. (B, C) represents magnified *i-t* curves at different time intervals. (D) Droplet size distribution from equation 3.2.

3.3.5 Collision Experiments of the Toluene (Fc + IL)/water Emulsion Droplets

3.3.5.1 Electrochemical oxidation of L-cysteine in 0.1M NaCl aqueous solution

Cyclic voltammetry was employed for investigating the electrochemical oxidation of L-cysteine on a 25 μm Au electrode in 0.1 M aqueous solution of NaCl. Electrochemical oxidation of cysteine starts around +0.5 V shown in voltammogram (Figure 3.11) at a scan rate of 10 mV/s. This implies that direct oxidation of cysteine is sluggish due to slow electron transfer process on electrode surface. Hence, if we apply a potential around +0.5 V, we can selectively oxidize Fc inside the toluene droplets during the collision experiments.

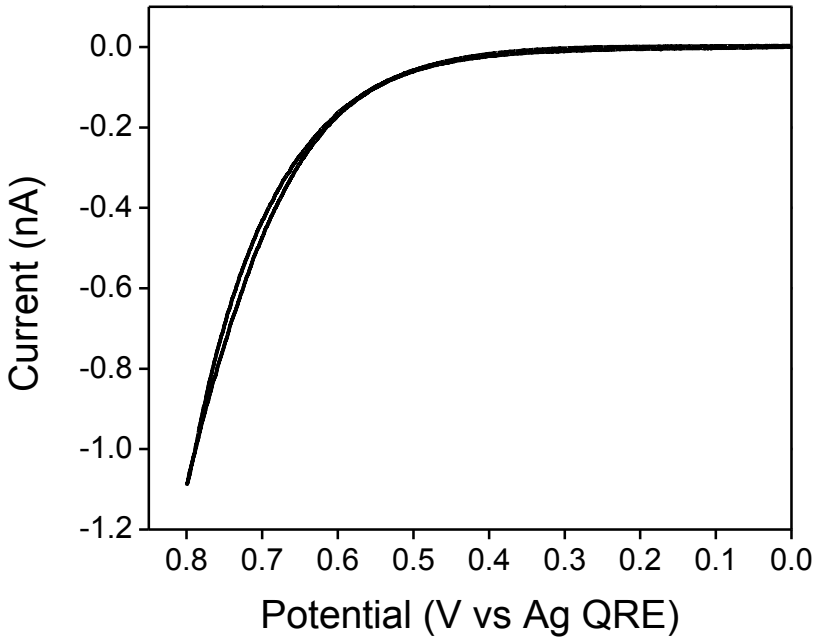

Figure 3.11 CV of 5 mM L-cysteine in 0.1 M NaCl aqueous solution on Au UME (dia. 25 μm) at a scan rate 10 mV/s.

3.3.5.2 Collision Experiments of the Toluene (Fc + IL)/water Emulsion Droplets in the presence of L-cysteine

Amperometric *i-t* curve was measured to monitor the collision of Fc droplets on Au UME at the applied potential of +0.5 V at different concentrations of cysteine solution. During *i-t* curve measurement, different concentrations of cysteine solutions (50 µM, 100 µM, 300 µM, 500 µM) were injected into the emulsion at an interval of 200 s. Figure 3.12 shows with increasing the concentration of cysteine, number of spikes which were attributed to the electrolysis of Fc inside the droplets were decreasing. No spikes were observed at 500 µM of cysteine. To understand this phenomenon, further investigation is ongoing.

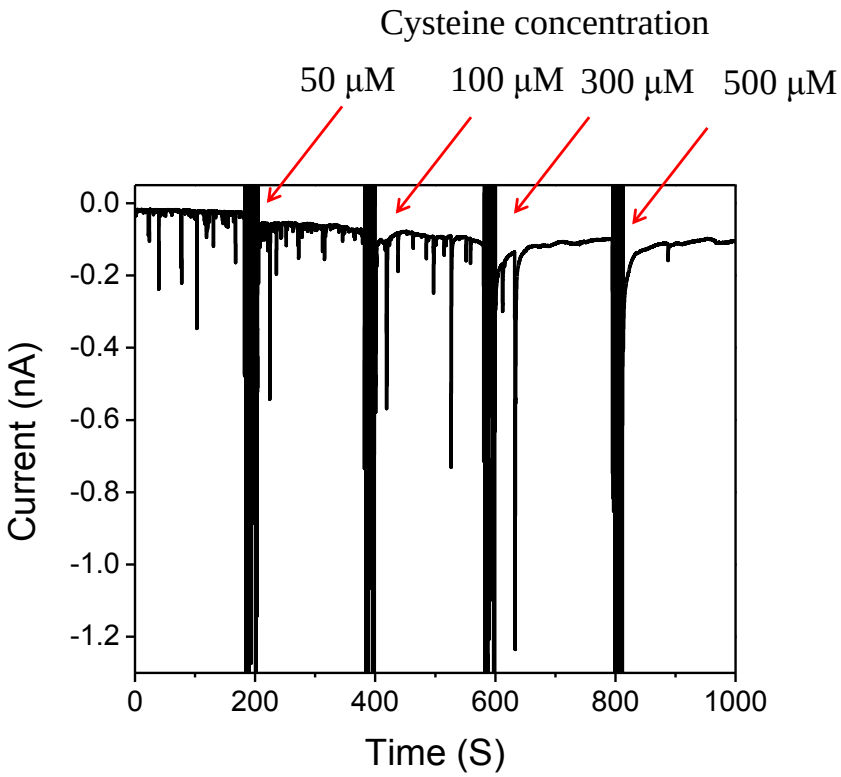

Figure 3.12 Amperometric *i-t* curve for single collision of toluene droplets loaded with Fc in the presence of different concentrations of L-cysteine on 25 µm Au UME. The UME potential was +0.5 V vs Ag QRE.

3.4 Conclusion

We investigated the electrochemical oxidation of Fc in the toluene emulsion droplets by particle collisions electrochemistry. We observed that droplet size was increased in the presence of NaCl in aqueous phase and the stability of the emulsion was decreased. Although the stability of emulsions were increased due to the presence of the surfactant, triton X-100, but no oxidative spikes were observed without ionic liquid in particle collisions experiments. This result concluded that ionic liquid plays a critical role to observe spikes in the experiments. Both surfactant and ionic liquid may have combined effects to reduce the droplets size while surfactant was dissolved into water. We further extended our study to investigate mediated oxidation of cysteine by electrochemically generated Fc^+ in the emulsion droplets. The *i-t* curve exhibited that individual collision responses were becoming less with increasing the concentration of cysteine. A systematic study is needed to understand this phenomenon clearly.

3.5 References

1. Opawale, F. O.; Burgess, J. D. Influence of Interfacial Properties of Lipophilic Surfactants on Water-in-Oil Emulsion Stability. *J. Colloid Interface Sci.* **1998,** *197*, 142-150.

2. Kent, P.; Saunders, B. R. The Role of Added Electrolyte in the Stabilization of Inverse Emulsions. *J. Colloid Interface Sci.* **2001,** *242*, 437-442.

3. Fornaguera, C.; Calder´o, G.; Solans, C. Electrolytes as a Tuning Parameter to Control Nanoemulsion and Nanoparticle size. *RSC Adv.* **2016,** *6*, 58203–58211.

4. Goloub, T.; Pugh, R. J., The Role of the Surfactant Head Group in the Emulsification Process: Single Surfactant Systems. *J. Colloid Interface Sci.* **2003**, *257*, 337-343.

5. Li, W.; Chen, H.; He, Z.; Han, C.; Liu, S.; Li, Y. Influence of Surfactant and Oil Composition on the Stability and Antibacterial Activity of Eugenol Nanoemulsions. *LWT - Food Sci. Technol.* **2015**, *62*, 39-47.

6. Ouyan, J.; Bard, A. J., Electrogenerated Chemiluminescence. 50. Electrochemistry and Electrogenerated Chemiluminescence of Micelle Solubilized $Os(bpy)_3^{2+}$. *Bull. Chem. Soc. Jpn.* **1998**, *61*, 17-24.

7. Raoof, J.-B.; Ojani, R.; Beitollahi, H. L-Cysteine Voltammetry at a Carbon Paste Electrode Bulk-Modified with Ferrocenedicarboxylic Acid. *Electroanalysis* **2007**, *19*, 1822-1830.

8. Lin, Q.; Lin, C.; Wu, H.; Batchelor-McAuley, C.; Compton, R. G. Catalytic Single-Particle Nano-Impacts: Theory and Experiment. Poly(vinylferrocene)-Modified Graphene Nanoplatelet Mediated L-Cysteine Oxidation. *J.Phys.Chem.C* **2016**, *120*, 20216-20223.

9. Nekrassova, O.; Allen, G. D.; Lawrence, N. S.; Jiang, Li.; Jones, T. G. J.; Compton, R. G. The Oxidation of Cysteine by Aqueous Ferrocyanide: A Kinetic Study Using Boron Doped Diamond Electrode Voltammetry. *Electroanalysis* **2002**, *14*, 1464-1469.

10. Kim, B. K.; Boika, A.; Kim, J.; Dick, J. E.; Bard, A. J. Characterizing Emulsions by Observation of Single Droplet Collisions-Attoliter Electrochemical Reactors. *J. Am.Chem. Soc.* **2014**, *136*, 4849-4852.

11. Deng, H.; Dick, J. E.; Kummer, S.; Kragl, U.; Strauss, S. H.; Bard, A. J. Probing Ion Transfer across Liquid–Liquid Interfaces by Monitoring Collisions of Single Femtoliter Oil Droplets on Ultramicroelectrodes. *Anal. Chem.* 2016, *88*, 7754-7761.

12. de Morais, J. M.; dos Santos, O. D. H.; Delicato, T.; da Rocha-Filho, P. A., Characterization and Evaluation of Electrolyte Influence on Canola Oil/Water Nano-Emulsion. *J. Dispersion Sci. Technol.* **2006,** *27*, 1009-1014.

13. Lebègue, E.; Anderson, C. M.; Dick, J. E.; Webb, L. J.; Bard, A. J., Electrochemical Detection of Single Phospholipid Vesicle Collisions at a Pt Ultramicroelectrode. *Langmuir* **2015,** *31*, 11734−11739.

Chapter 4

Conclusion and Future Work

In this dissertation, a new approach was demonstrated to study hydrogen bonding through heterogeneous toluene-water interface using Particle Collision Electrochemistry. It was observed that strong hydrogen bonding donor (acetic acid) has more mpact on hydrogen bonding with tetrachloro phenolate di-anion ($TCBQ^{2-}$) than weaker one (oleic acid) in bulk acetonitrile and toluene. However, the reversed trend was observed in toluene droplets containing TCBQ when studied by PCE. This suggested that hydrogen bonding takes place notably inside the droplets between $TCBQ^{2-}$ and oleic acid whereas acetic acid and $TCBQ^{2-}$ form significantly less hydrogen bonding inside the droplets due to their opposite preferential partition between the two phases in the emulsion. We believe that this unique procedure and the experimental studies reported here will help to understand the mechanism of diverse organic reactions occurring in microheterogeneous systems. In the future, the other factors will be investigated that control the chemical reactivity for reactions occuring in organic-water heteogeneous systems to understand the “on-water”catalysis mechanism. For this purpose, hydrophilc strong acid (hydrochloric acid) will be introduced into outside of the droplets (aqueous phase) and the effect will be will be studied by monitoring the electrochemistry across the droplet interface. Similarly, effect of hydrophobic strong acid (perfluorooctanoic acid) will be studied on quinonone reduction by introducing the acid inside the nonpolar toluene emulsion droplets. Futhermore, emulsions of toluene droplets will be prepared in perflurocarbons solvents to understand the influenece of

water on quinonone reduction behavior. Finally different oraganic reactions will be performed on emulsions droplet systems.

Dilip Kumar Paul

Phone: 804-588-8465 | Email: pauldk@vcu.edu
300 West Franklin Street, Apt: 701W, Richmond, VA 23220

Summary

Research focus was on preparation of emulsion to understand the structural elements at oil-water interface for different applications. Looking for an opportunity to utilize my technical skills in professional career.

Education

Jan 2014 - May 2018

Doctor of Philosophy

Research Area : **Electrochemistry and Nano Emulsion Chemistry**, GPA :**3.67/4.00**

Virginia Commonwealth University, Richmond, VA-23284

Thesis Title: *Redox Reactions at Oil-Water Interface by Particle Collision Electroanalysis.*

Aug 2012 - Dec 2013

Graduate Student

Research Area : **Nanoscience and Nanotechnology**, GPA :**4.00/4.00**

Jackson State University, Jackson, MS 39217
Transferred to Virginia Commonwealth University

July 2007 - June 2008

Master of Science

Research Area : **Inorganic and Analytical Chemistry**, GPA : **4.00/4.00**

University of Dhaka, Bangladesh

Thesis Title: *Studies of Guanine Compounds of Some Toxic Metals.*

July 2002 - June 2007

Bachelor of Science (Honors)

Research Area : **Chemistry**, GPA :**3.50/4.00**

University of Dhaka, Bangladesh

Undergraduate Project Title: *Preparation and Characterization of Saccharin Complexes of Silver(I) and Lead(II).*

Research Experience

Jan, 2014 - May 2018 **Virginia Commonwealth University**

- Investigated the electrochemical reactions across toluene-water interface by single particle collision on ultramicroelectrode.
- Developed a new general methodology for photoinduced electron transfer heterobinuclear system for O_2 activation.
- Collaborated with a research group from Department of Chemistry to investigate electrochemical properties of functionalized thioureas compounds.
- Based on the preliminary research and consultation on various proposals resulting in $200,000 Fund from Petroleum Research.

Aug, 2012 - Dec 2013 **Jackson State University**

- Designed a new long-range two-photon scattering (TPS) spectroscopy rulers using gold nano-antenna separated by a bifunctional rigid double strand DNA molecule.

July 2007 - June 2008

- Developed a synthetic protocol for several compounds of guanine with toxic metals (M = Cr(VI), As(III), As(V), Ag(I), Cd(II) Hg(II) and Pb(II)) in aqueous acid medium that can be a good candidate for antagonist.

Jan 2007 - May 2007

- Developed a new synthetic strategy of saccharin complexes of Ag(I) and Pb(II).

Teaching Experience

Jan 2014 - May 2018 **Teaching Assistant**, Virginia Commonwealth University

- Performed laboratory sessions weekly for Quantitative Analysis and General Chemistry laboratory.
- Assists undergraduate students with their weekly lab reports.
- Review session was held to help out the students in undergraduate Inorganic courses.
- Through discussion on the class lectures were covered during review sessions.

Jan 2010 - June 2012 **Faculty**, Mastermind School, Dhaka, Bangladesh

- Prepared and delivered lectures to college students on Inorganic, Organic and Analytical Chemistry
- Assigned and graded exams, quizzes and group activities.
- Maintained student attendance records and grades.
- Held office hours for advising and assist undergraduate students

Technical Expertise

Spectroscopy: Nuclear magnetic resonance spectroscopy (NMR)
Electron paramagnetic resonance Spectroscopy (EPR)
Infrared spectroscopy (IR), Fourier transform IR (FTIR)
UV/Vis Spectroscopy, Photoluminescence spectroscopy
Transient Absorption Spectrophotometer

Microscopy: Transmission electron microscopy (TEM)

Instrument: Cyclic voltammetry (CHI instrument), Gas chromatography (GC), Dynamic Light Scattering (DLS), Carbon, hydrogen, nitrogen and sulfur analyzer (CHNS)

Scholarships

- James V. Quagliano Fellowship in Chemistry (2016)

Selected Publications

1. Paul, D. K; Meng, K.; Omanovic, D.; Alvarez, J. C. Reversal of Hydrogen Bonding Equilibria due to Micro-Confinement of Immiscible Phases in Toluene-Water Emulsions Studied by Particle Collision Electrochemistry submitted to **ChemElectroChem**.

2. Franklin, C; Zavalij, P.; Diamond, C; Groth, A.; LeBron, D.; Paul, D.; Alvarez, J.; Sidorov, V.A Controlled Cyclization of Functionalized Thioureas and Unprecedented Termolecular Decyclization of Iminothiazolidinones. ***J. Org. Chem.*** under reveiw.

3. Sinha, S. S.; Paul, D. K.; Kanchanapally, R.; Pramanik, A.; Chavva, R. S.; Viraka Nellore, B. P.; Jones, S. J.; Ray, P. C. Long-range Two-Photon Scattering Spectroscopy Ruler for Screening Prostate Cancer Cells. ***Chem. Sci.,*** 2015, *6*, 2411−2418.

4. Shaikh, A. A.; Paul, D. K.; Rahman, M. S.; Bakshi, P. K. Interactions of Guanine with Cr(VI), Ag(I), Cd(II) and Hg(II) in Acidic Aqueous Medium. ***J. Bangladesh Chem. Soc.,*** 2011, *24*, 106-114**.**

5. Paul, D. K.; Shaikh, A. A.; Bakshi, P. K. Preparation and Characterization of Saccharinato Complexes of Silver(I) and Lead(II). ***J. Bangladesh Chem. Soc.,*** 2009, *22*, 98-104.

Conferences Presentations

1. Paul, D.; Alvarez, J. Study of electrochemical reactions across oil-water interface by single particle collision. 254th ACS National Meeting & Exposition, Washington, DC, USA, August 20-24, ANYL-160, 2017.

2. Paul, D. K.; Alvarez, J. C. Single Particle Collisions – A Pathfinder to Understand the Molecular Effect on Emulsion Droplets by Electrochemical Reactions. *3rd ADSE Young Researchers Conference September 16, 2017.*

REFERENCES

1. **Dr. Julio C. Alvarez**

Associate Professor and Director of Graduate Studies
Chemistry Department
Virginia Commonwealth University
1001 West Main Street
Office: Oliver Hall 4025, Richmond, VA, 23284
Tel 804 828 3521
Fax 804 828 8599
Email: jcalvarez2@vcu.edu

2. Dr. Maryanne M. Collinson

Professor
Chemistry Department
Virginia Commonwealth University
1001 West Main Street
Office: Temple 4429, Richmond, VA, 23284
Tel 804 828 7509
Email: mmcollinson@vcu.edu

3. Dr. Matthew C. T. Hartman

Associate Professor
Chemistry Department
Virginia Commonwealth University
1001 West Main Street
Office: Oliver Hall 3048, Richmond, VA, 23284
Tel 804 828 7513
Email: mchartman@vcu.edu

4. Dr. Joseph Reiner

Assistant Professor
Physics Department
Virginia Commonwealth University
701 W. Grace Street.
Office 2406
Tel 804 828 7079
Email: jereiner@vcu.edu